Topological Band Theory

Tristan.W

December 30, 2025

Contents

1 Review: Basic Band Theory in Optical Lattices

1.1 Optical-lattice realization and the basic single-particle model

Standing-wave potential and scales. A typical optical lattice in 1D is created by counter-propagating lasers forming a standing wave, producing a periodic potential

$$V_{\text{lat}}(x) = V_0 \cos^2(k_0 x), \tag{1}$$

with lattice spacing $a = \pi/k_0$. The single-particle Hamiltonian is

$$\hat{H}_0 = -\frac{\hbar^2}{2m}\partial_x^2 + V_{\text{lat}}(x), \tag{2}$$

and similarly in higher dimensions with separable forms such as $V_{\text{lat}}(\boldsymbol{r}) = \sum_{\mu=x,y,z} V_\mu \cos^2(k_0 r_\mu)$ for a cubic lattice.

Recoil energy and dimensionless lattice depth. It is convenient to measure energies in units of the recoil energy

$$E_R = \frac{\hbar^2 k_0^2}{2m}, \tag{3}$$

and parametrize the depth as $V_0 = \alpha E_R$ (or $V_\mu = \alpha_\mu E_R$). This isolates the key control knob α, which continuously interpolates between the free-particle limit $\alpha \to 0$ and the deep-lattice (tight-binding) limit $\alpha \gg 1$.

A periodic potential endows the spectrum with a band structure $\mathcal{E}_m(k)$, where k is a quasi-momentum defined modulo reciprocal lattice vectors, and m is the band index.

1.2 Bloch theorem, Brillouin zone, quasi-momentum, and bands

Bloch theorem and Bloch functions.

In free space ,$V_{\text{lat}}(x) = 0$, so $\hat{H}_0 = -\hbar^2\partial_x^2/(2m)$ is invariant under *continuous* translations, so the momentum k is a good quantum number and the eigenstates are plane waves e^{ikx}.

In a lattice, continuous translation symmetry is broken, so k is no longer a strictly conserved quantum number. What remains is the *discrete* translation symmetry by one lattice spacing a: $V_{\text{lat}}(x + a) = V_{\text{lat}}(x)$. This residual symmetry implies that $\hat{H}_0$ commutes with the lattice translation operator $\hat{T}_a$ defined by $(\hat{T}_a\psi)(x) = \psi(x + a)$. Therefore, the eigenstates of $\hat{H}_0$ can be chosen to be simultaneous eigenstates of $\hat{T}_a$, and the $\hat{T}_a$-eigenvalue naturally defines the *quasi-momentum* k.

Bloch's theorem states that the single-particle eigenstates can be written as

$$\psi_{mk}(x) = e^{ikx} u_{mk}(x), \qquad u_{mk}(x + a) = u_{mk}(x), \tag{4}$$

where k is the quasi-momentum and m labels bands, the discrete family of eigenvalues at fixed k.

Proof sketch of Bloch theorem (1D)

Consider the single-particle Hamiltonian

$$\hat{H}_0 = -\frac{\hbar^2}{2m}\frac{d^2}{dx^2} + V_{\text{lat}}(x), \qquad V_{\text{lat}}(x + a) = V_{\text{lat}}(x). \tag{5}$$

Define the lattice translation operator $\hat{T}_a$ by its action on wave functions:

$$(\hat{T}_a\psi)(x) \equiv \psi(x+a). \tag{6}$$

Because the potential is periodic, $\hat{H}_0$ is invariant under translation by a:

$$\hat{T}_a\hat{H}_0\hat{T}_a^{-1} = \hat{H}_0, \qquad \text{equivalently} \qquad [\hat{H}_0, \hat{T}_a] = 0. \tag{7}$$

Hence $\hat{H}_0$ and $\hat{T}_a$ can be simultaneously diagonalized. Let $\psi(x)$ be a common eigenstate:

$$\hat{H}_0\psi = E\psi, \qquad \hat{T}_a\psi = \lambda\psi, \tag{8}$$

so $\psi(x+a) = \lambda\psi(x)$.

Step 1: constrain λ to be a phase. $\hat{T}_a$ is unitary (it preserves the inner product), so all its eigenvalues satisfy $|\lambda| = 1$. Therefore we can write

$$\lambda = e^{ika} \tag{9}$$

for some real k, defined modulo $2\pi/a$ because $e^{i(k+2\pi/a)a} = e^{ika}$.

Step 2: construct a periodic part. Define

$$u_k(x) \equiv e^{-ikx}\psi(x). \tag{10}$$

Then

$$u_k(x+a) = e^{-ik(x+a)}\psi(x+a) = e^{-ik(x+a)}e^{ika}\psi(x) = e^{-ikx}\psi(x) = u_k(x), \tag{11}$$

so $u_k(x)$ is periodic with period a. Therefore the eigenstate can be written as

$$\psi_k(x) = e^{ikx}u_k(x), \qquad u_k(x+a) = u_k(x), \tag{12}$$

which is precisely the Bloch form.

■ **Remark on band index m.**
Fix a quasi-momentum k. Plugging the Bloch form $\psi_k(x) = e^{ikx}u_k(x)$ into the Schrödinger equation $\hat{H}_0\psi = E\psi$ gives an eigenvalue problem for the periodic function u_k:

$$\left[\frac{1}{2m}\Big(-i\hbar\partial_x + \hbar k\Big)^2 + V_{\text{lat}}(x)\right]u_k(x) = E(k)\,u_k(x), \qquad u_k(x+a) = u_k(x). \tag{13}$$

Here the operator

$$\hat{H}(k) \equiv \frac{1}{2m}\Big(-i\hbar\partial_x + \hbar k\Big)^2 + V_{\text{lat}}(x) \tag{14}$$

acts on the Hilbert space of a-periodic functions.
Since $\hat{H}(k)$ is a Hermitian differential operator defined on a compact domain[a], it admits a countable set of real eigenvalues. These eigenvalues can be ordered as

$$E_0(k) \le E_1(k) \le E_2(k) \le \cdots, \qquad E_m(k) \to +\infty \ \ (m \to \infty), \tag{15}$$

with corresponding orthonormal eigenfunctions $u_{mk}(x)$. The set $\{u_{mk}(x)\}$ forms a complete orthonormal basis of the Hilbert space $L^2([0,a])$ subject to periodic boundary conditions.

[a] Compact refers to periodic boundary conditions

Reciprocal lattice and Brillouin zone.

The quasi-momentum k emerges as the phase of the lattice translation eigenvalue: $\hat{T}_a\psi = e^{ika}\psi$. Since $e^{i(k+2\pi n/a)a} = e^{ika}$ for any integer n, the label k is only meaningful *modulo* $2\pi/a$. This is the origin of the reciprocal lattice and the Brillouin zone construction. Specifically, it suffices to restrict the crystal momentum to an interval of width $\Delta k = 2\pi/a$, known as the Brillouin zone, with all other momenta identified modulo reciprocal lattice vectors $G = 2nk_0$.

A complementary (and often more practical) viewpoint is to expand the periodic part $u_{mk}(x)$ into Fourier modes compatible with the lattice period:

$$u_{mk}(x) = \sum_{n\in\mathbb{Z}} u_n^m(k)\, e^{iG_n x}, \qquad G_n \equiv \frac{2\pi n}{a}.$$

Then the Bloch wave becomes a superposition of plane waves whose physical momenta differ by reciprocal lattice vectors:

$$\psi_{mk}(x) = \sum_n u_n^m(k)\, e^{i(k+G_n)x}.$$

This motivates calling $\{G_n\}$ the reciprocal lattice. In the notation used earlier, one may write

$$G = 2nk_0, \qquad k_0 \equiv \frac{\pi}{a}, \qquad n \in \mathbb{Z}. \tag{16}$$

Because k and $k + G$ correspond to the same translation eigenvalue e^{ika}, they describe the same Bloch sector:

$$k \sim k + G. \tag{17}$$

Therefore, in 1D the quasi-momentum space is topologically a circle S^1 (an interval with endpoints identified). A standard choice of the first Brillouin zone (BZ) is

$$k \in [-k_0, k_0], \tag{18}$$

with endpoints identified.

Higher-dimensional Bloch theorem, reciprocal lattice, and the Brillouin zone

Bravais lattice and translation symmetry. In d dimensions, a Bravais lattice is the set

$$\Lambda = \{\mathbf{R} = n_1\mathbf{a}_1 + \cdots + n_d\mathbf{a}_d \mid n_i \in \mathbb{Z}\},$$

with primitive vectors $\{\mathbf{a}_i\}$. A lattice-periodic potential satisfies

$$V_{\text{lat}}(\mathbf{r} + \mathbf{R}) = V_{\text{lat}}(\mathbf{r}), \qquad \forall\, \mathbf{R} \in \Lambda.$$

Define translation operators $(\hat{T}_\mathbf{R}\psi)(\mathbf{r}) = \psi(\mathbf{r} + \mathbf{R})$. Then $[\hat{H}_0, \hat{T}_\mathbf{R}] = 0$ for all $\mathbf{R} \in \Lambda$, and the $\hat{T}_\mathbf{R}$ form an Abelian group: $\hat{T}_\mathbf{R}\hat{T}_{\mathbf{R}'} = \hat{T}_{\mathbf{R}+\mathbf{R}'}$.

Bloch Theorem. Because the $\hat{T}_\mathbf{R}$ commute, we can choose ψ such that

$$\hat{T}_\mathbf{R}\psi(\mathbf{r}) = \psi(\mathbf{r} + \mathbf{R}) = \lambda(\mathbf{R})\,\psi(\mathbf{r}).$$

Unitarity implies $|\lambda(\mathbf{R})| = 1$. The group property forces $\lambda(\mathbf{R} + \mathbf{R}') = \lambda(\mathbf{R})\lambda(\mathbf{R}')$, whose general solution is

$$\lambda(\mathbf{R}) = e^{i\mathbf{k}\cdot\mathbf{R}}$$

for some real vector $\mathbf{k}$ (defined modulo reciprocal lattice vectors; see below). Define $u_\mathbf{k}(\mathbf{r}) \equiv e^{-i\mathbf{k}\cdot\mathbf{r}}\psi(\mathbf{r})$. Then

$$u_\mathbf{k}(\mathbf{r} + \mathbf{R}) = e^{-i\mathbf{k}\cdot(\mathbf{r}+\mathbf{R})}\psi(\mathbf{r} + \mathbf{R}) = e^{-i\mathbf{k}\cdot\mathbf{r}}\psi(\mathbf{r}) = u_\mathbf{k}(\mathbf{r}),$$

so $u_{\mathbf{k}}$ is lattice-periodic. Hence Bloch theorem:

$$\psi_{m\mathbf{k}}(\mathbf{r}) = e^{i\mathbf{k}\cdot\mathbf{r}} u_{m\mathbf{k}}(\mathbf{r}), \qquad u_{m\mathbf{k}}(\mathbf{r}+\mathbf{R}) = u_{m\mathbf{k}}(\mathbf{r}). \tag{19}$$

For each fixed $\mathbf{k}$, solving $\hat{H}_0\psi_k = E\psi_k$ within a unit cell with Bloch boundary conditions yields discrete eigenvalues $\{E_m(\mathbf{k})\}$ (band index m).

Reciprocal lattice and k-identification. The reciprocal lattice Λ^* is defined as the set of vectors $\mathbf{G}$ satisfying

$$e^{i\mathbf{G}\cdot\mathbf{R}} = 1 \quad \forall\, \mathbf{R} \in \Lambda,$$

equivalently

$$\mathbf{G} = m_1\mathbf{b}_1 + \cdots + m_d\mathbf{b}_d, \quad m_i \in \mathbb{Z}. \qquad \text{satisfying} \quad \mathbf{a}_i \cdot \mathbf{b}_j = 2\pi\delta_{ij}$$

Then $\mathbf{k}$ and $\mathbf{k}+\mathbf{G}$ give the same translation eigenvalues:

$$e^{i(\mathbf{k}+\mathbf{G})\cdot\mathbf{R}} = e^{i\mathbf{k}\cdot\mathbf{R}} e^{i\mathbf{G}\cdot\mathbf{R}} = e^{i\mathbf{k}\cdot\mathbf{R}},$$

so they label the same Bloch sector. Thus quasi-momentum lives on the quotient space

$$\mathbf{k} \in \mathbb{R}^d/\Lambda^*,$$

which is a d-torus T^d (a higher-dimensional generalization of the S^1 in 1D).

Brillouin zone. A Brillouin zone is any fundamental domain of $\mathbb{R}^d/\Lambda^*$. The standard *first Brillouin zone* is the Wigner–Seitz cell of the reciprocal lattice: the set of $\mathbf{k}$ points closer to $\mathbf{0}$ than to any other reciprocal lattice point. Any two $\mathbf{k}$ differing by $\mathbf{G} \in \Lambda^*$ are identified, i.e. opposite faces of the chosen BZ are glued according to $\mathbf{k} \sim \mathbf{k}+\mathbf{G}$.

Useful formulas for reciprocal lattices in 2D and 3D

■ **2D: primitive vectors $\mathbf{a}_1, \mathbf{a}_2$.** Define the (signed) unit-cell area

$$A \equiv \hat{\mathbf{z}} \cdot (\mathbf{a}_1 \times \mathbf{a}_2),$$

where $\hat{\mathbf{z}}$ is the unit normal (choose orientation so $A > 0$ for convenience). Then the reciprocal primitive vectors $\mathbf{b}_1, \mathbf{b}_2$ satisfying $\mathbf{a}_i \cdot \mathbf{b}_j = 2\pi\delta_{ij}$ are

$$\mathbf{b}_1 = \frac{2\pi}{A}(\hat{\mathbf{z}} \times \mathbf{a}_2), \qquad \mathbf{b}_2 = \frac{2\pi}{A}(\mathbf{a}_1 \times \hat{\mathbf{z}}). \tag{20}$$

Equivalently, in components (with $\mathbf{a}_1 = (a_{1x}, a_{1y})$, $\mathbf{a}_2 = (a_{2x}, a_{2y})$):

$$A = a_{1x}a_{2y} - a_{1y}a_{2x}, \qquad \mathbf{b}_1 = \frac{2\pi}{A}(a_{2y}, -a_{2x}), \quad \mathbf{b}_2 = \frac{2\pi}{A}(-a_{1y}, a_{1x}).$$

■ **3D: primitive vectors $\mathbf{a}_1, \mathbf{a}_2, \mathbf{a}_3$.** Define the unit-cell volume

$$V \equiv \mathbf{a}_1 \cdot (\mathbf{a}_2 \times \mathbf{a}_3).$$

Then the reciprocal primitive vectors $\mathbf{b}_1, \mathbf{b}_2, \mathbf{b}_3$ are

$$\mathbf{b}_1 = 2\pi\,\frac{\mathbf{a}_2 \times \mathbf{a}_3}{V}, \qquad \mathbf{b}_2 = 2\pi\,\frac{\mathbf{a}_3 \times \mathbf{a}_1}{V}, \qquad \mathbf{b}_3 = 2\pi\,\frac{\mathbf{a}_1 \times \mathbf{a}_2}{V}. \tag{21}$$

These automatically satisfy $\mathbf{a}_i \cdot \mathbf{b}_j = 2\pi\delta_{ij}$, and any reciprocal lattice vector is $\mathbf{G} = m_1\mathbf{b}_1 + m_2\mathbf{b}_2 + m_3\mathbf{b}_3$ with $m_i \in \mathbb{Z}$.

Solving the Bloch eigenproblem by plane-wave expansion.

Because $u_{mk}(x)$ is periodic, it admits a Fourier expansion over reciprocal lattice vectors:

$$u_{mk}(x) = \sum_G u_G^m(k)\, e^{iGx}. \tag{22}$$

Equivalently, the Bloch state is expanded as a superposition of plane waves:

$$\psi_{mk}(x) = \sum_G u_G^m(k)\, e^{i(k+G)x}. \tag{23}$$

Insert this into $\hat{H}_0\psi = \mathcal{E}\psi$. Using orthogonality of plane waves, one obtains a matrix eigenvalue problem

$$\sum_{G'} H_{G,G'}(k)\, u_{G'}^m(k) = \mathcal{E}_m(k)\, u_G^m(k), \tag{24}$$

where

$$H_{G,G'}(k) = \frac{\hbar^2(k+G)^2}{2m}\,\delta_{G,G'} + V_{G-G'}. \tag{25}$$

Here V_q are Fourier components of the periodic potential, defined by $V_{\text{lat}}(x) = \sum_G V_G e^{iGx}$.

From the Bloch ansatz to a (truncated) plane-wave matrix problem

Step 1: Fourier-expand the periodic part. Because $u_{mk}(x+a) = u_{mk}(x)$, it has a Fourier series on the reciprocal lattice:

$$u_{mk}(x) = \sum_G u_G^m(k)\, e^{iGx}, \qquad G = \frac{2\pi}{a}n\ (n \in \mathbb{Z}). \tag{26}$$

Then the Bloch state is a superposition of plane waves at momenta $k+G$:

$$\psi_{mk}(x) = e^{ikx}u_{mk}(x) = \sum_G u_G^m(k)\, e^{i(k+G)x}. \tag{27}$$

Step 2: write the potential in Fourier modes. Expand the periodic lattice potential as

$$V_{\text{lat}}(x) = \sum_Q V_Q\, e^{iQx}, \qquad Q = G \quad \text{, i.e. } Q \in \text{Reciprocal lattice}. \tag{28}$$

(Here V_Q are complex in general, but for a real potential one has $V_{-Q} = V_Q^*$.)

Step 3: substitute into $\hat{H}_0\psi = \mathcal{E}\psi$ and project. Let

$$\hat{H}_0 = -\frac{\hbar^2}{2m}\partial_x^2 + V_{\text{lat}}(x).$$

For the kinetic term,acting on a plane wave gives

$$-\frac{\hbar^2}{2m}\partial_x^2\, e^{i(k+G)x} = \frac{\hbar^2(k+G)^2}{2m}\, e^{i(k+G)x},$$

so

$$-\frac{\hbar^2}{2m}\partial_x^2\,\psi_{mk}(x) = \sum_G \frac{\hbar^2(k+G)^2}{2m}\, u_G^m(k)\, e^{i(k+G)x}. \tag{29}$$

For the potential term,

$$V_{\text{lat}}(x)\psi_{mk}(x) = \left(\sum_Q V_Q e^{iQx}\right)\left(\sum_{G'} u^m_{G'}(k) e^{i(k+G')x}\right)$$
$$= \sum_{Q,G'} V_Q\, u^m_{G'}(k)\, e^{i(k+G'+Q)x}. \tag{30}$$

Relabel $G \equiv G' + Q$ (so $Q = G - G'$) to collect the coefficient of $e^{i(k+G)x}$:

$$V_{\text{lat}}(x)\psi_{mk}(x) = \sum_G \left(\sum_{G'} V_{G-G'}\, u^m_{G'}(k)\right) e^{i(k+G)x}. \tag{31}$$

Putting kinetic+potential together and comparing with $\mathcal{E}_m(k)\psi_{mk}(x)$, the coefficient of each basis function $e^{i(k+G)x}$ must match, yielding

$$\sum_{G'} \left[\frac{\hbar^2(k+G)^2}{2m}\delta_{G,G'} + V_{G-G'}\right] u^m_{G'}(k) = \mathcal{E}_m(k)\, u^m_G(k). \tag{32}$$

This is precisely the matrix eigenvalue problem

$$\sum_{G'} H_{G,G'}(k)\, u^m_{G'}(k) = \mathcal{E}_m(k)\, u^m_G(k), \qquad H_{G,G'}(k) = \frac{\hbar^2(k+G)^2}{2m}\delta_{G,G'} + V_{G-G'}. \tag{33}$$

■ **Intuitive matrix form (infinite-dimensional).**
Order the reciprocal vectors as $\ldots, -2G_0, -G_0, 0, G_0, 2G_0, \ldots$ with $G_0 \equiv 2\pi/a$. Define the coefficient column vector

$$\boldsymbol{u}^m(k) = \left(\ldots, u^m_{-2G_0}(k), u^m_{-G_0}(k), u^m_0(k), u^m_{G_0}(k), u^m_{2G_0}(k), \ldots\right)^{\mathsf{T}}.$$

Then

$$H(k)\,\boldsymbol{u}^m(k) = \mathcal{E}_m(k)\,\boldsymbol{u}^m(k),$$

where $H(k)$ has a diagonal kinetic part and an off-diagonal convolution structure from the potential:

$$H(k) = \underbrace{\begin{pmatrix} \ddots & & & & \\ & \frac{\hbar^2(k-G_0)^2}{2m} & & & \\ & & \frac{\hbar^2k^2}{2m} & & \\ & & & \frac{\hbar^2(k+G_0)^2}{2m} & \\ & & & & \ddots \end{pmatrix}}_{\text{kinetic}} + \underbrace{\begin{pmatrix} \ddots & \vdots & \vdots & \vdots & \\ \cdots & V_0 & V_{-G_0} & V_{-2G_0} & \cdots \\ \cdots & V_{G_0} & V_0 & V_{-G_0} & \cdots \\ \cdots & V_{2G_0} & V_{G_0} & V_0 & \cdots \\ & \vdots & \vdots & \vdots & \ddots \end{pmatrix}}_{\text{potential coupling } (V_{G-G'})}.$$

Practically we do reasonabel truncations to $H(k)$.

Truncation logic

One truncates to $|G| \le G_{\max}$, i.e. keeps a finite set of plane waves $\{k+G\}$. This is controlled because the kinetic energy grows as $\hbar^2(k+G)^2/(2m) \sim G^2$, so high-$|G|$ modes are separated by large energy denominators. In the weak-lattice limit, couplings $V_{G-G'}$ are small, so the

admixture of large-$|G|$ components is suppressed perturbatively.
Suppose the energy scale of the low-energy physics is E_{low}. Using perturbative theory, the typical weight of a high G component $\sim \frac{V_{G-G'}}{E_{\text{low}}-E_G}$, which is small when $V_{G-G'}$ is small (Weak-lattice limit) and E_G is large.
In the deep-lattice limit, the plane-wave basis becomes inefficient because a localized function can only be constructed from a superposition of many plane waves. In this regime, the Wannier basis becomes natural .

Band dispersion and group velocity. For each band m, the dispersion relation $\mathcal{E}_m(k)$ defines a semiclassical group velocity

$$v_m(k) = \frac{1}{\hbar}\frac{\partial \mathcal{E}_m(k)}{\partial k}. \tag{34}$$

A crucial lattice effect is that $\mathcal{E}_m(k)$ is periodic in k (BZ periodicity), hence $v_m(k)$ is also periodic.

In higher dimensions, the band dispersion $\mathcal{E}_m(\mathbf{k})$ gives rise to a vector-valued group velocity

$$\mathbf{v}_m(\mathbf{k}) = \frac{1}{\hbar}\nabla_{\mathbf{k}}\mathcal{E}_m(\mathbf{k}). \tag{35}$$

Similarly, $\mathbf{v}_m(\mathbf{k})$ is periodic in $\mathbf{k}$.

1.3 Weak-lattice limit: free-particle (nearly-free) treatment

Free particle as the unperturbed problem (viewed through band language). At $\alpha \to 0$, $V_{\text{lat}} \to 0$, the eigenstates are plane waves $|p\rangle \equiv e^{ipx}$ with

$$\epsilon(p) = \frac{\hbar^2 p^2}{2m}. \tag{36}$$

To make contact with band theory, fix a quasi-momentum $k \in [-k_0, k_0]$ (with $k_0 \equiv \pi/a$) and decompose the free momentum as

$$p = k + G, \qquad G = 2nk_0 \ (n \in \mathbb{Z}). \tag{37}$$

Then for each fixed k one obtains an infinite set of *free* "bands"

$$\epsilon_n^{(0)}(k) \equiv \epsilon(k + 2nk_0) = \frac{\hbar^2(k + 2nk_0)^2}{2m}, \tag{38}$$

i.e. a family of parabolas folded into the first Brillouin zone. Turning on a weak periodic potential mixes these folded branches and opens gaps at their crossings.

Perturbative analysis in the plane-wave basis. Write the periodic potential as a Fourier series over reciprocal lattice vectors,

$$V_{\text{lat}}(x) = \sum_G V_G\, e^{iGx}, \qquad V_{-G} = V_G^* \ \text{(for real } V_{\text{lat}}). \tag{39}$$

For a fixed quasi-momentum k, it is natural to use the plane-wave basis $\{|k + G\rangle\}_G$, because the lattice Hamiltonian preserves quasi-momentum and only couples momenta that differ by reciprocal vectors. The matrix elements of the single-particle Hamiltonian $\hat{H}_0 = \frac{\hat{p}^2}{2m} + V_{\text{lat}}(\hat{x})$ are

$$\langle k + G|\hat{H}_0|k + G'\rangle = \epsilon(k + G)\,\delta_{G,G'} + V_{G-G'}. \tag{40}$$

We now estimate the energy shift of the unperturbed state $|k + G_0\rangle$ assuming it is *non-degenerate* within the set $\{|k + G\rangle\}$. The first-order correction is

$$\delta\mathcal{E}^{(1)}(k + G_0) = \langle k + G_0|V_{\text{lat}}|k + G_0\rangle = V_0, \tag{41}$$

which is a k-independent overall shift (often absorbed into the energy zero). The leading k-dependent correction comes from second order:

$$\delta\mathcal{E}^{(2)}(k+G_0) = \sum_{G\neq G_0} \frac{\left|\langle k+G|V_{\text{lat}}|k+G_0\rangle\right|^2}{\epsilon(k+G_0)-\epsilon(k+G)} = \sum_{G\neq G_0} \frac{|V_{G-G_0}|^2}{\epsilon(k+G_0)-\epsilon(k+G)}. \tag{42}$$

In regions far away from degeneracy, this correction is arguably of order $O(V^2/E_R)$. A more detailed discussion can be found in the box below.

Degeneracy condition and two-level resummation.

Non-degenerate perturbation theory fails when there exists $G_1 \neq G_0$ such that

$$\epsilon(k+G_0) = \epsilon(k+G_1), \tag{43}$$

because the denominator in Eq. (42) vanishes. Intuitively, such degeneracy only happens in the center and the boundary of the 1st Brillouin zone. The proof is presented in the box below.

Near such a crossing, the correct leading description is obtained by diagonalizing the Hamiltonian in the (approximately) degenerate subspace spanned by $\{|k+G_0\rangle, |k+G_1\rangle\}$, yielding the explicit 2×2 effective Hamiltonian

$$H_{\text{eff}}(k) = \begin{pmatrix} \epsilon(k+G_0)+V_0 & V_{G_0-G_1} \\ V_{G_1-G_0} & \epsilon(k+G_1)+V_0 \end{pmatrix}. \tag{44}$$

Its eigenvalues are

$$\mathcal{E}_\pm(k) = V_0 + \frac{\epsilon(k+G_0)+\epsilon(k+G_1)}{2} \pm \sqrt{\left[\frac{\epsilon(k+G_0)-\epsilon(k+G_1)}{2}\right]^2 + |V_{G_0-G_1}|^2}. \tag{45}$$

At the exact degeneracy point where $\epsilon(k+G_0) = \epsilon(k+G_1)$, the splitting is *first order*:

$$\Delta_{\text{gap}} = 2|V_{G_0-G_1}|. \tag{46}$$

This is the precise sense in which the "dominant" modification of the dispersion occurs at crossings: the leading effect is $O(V)$ there, whereas away from crossings it is $O(V^2)$.

See Fig 1 for a graphical understanding.

Futher and Detailed Discussions

(i) Explicit BZ-edge calculation for the lowest crossing. Take $G_0 = 0$ and $G_1 = -2k_0$. The degeneracy condition $\epsilon(k) = \epsilon(k-2k_0)$ gives $k = \pm k_0$, i.e. the BZ edge. Write $k = k_0 + q$ with $|q| \ll k_0$. Then

$$\epsilon(k_0+q) - \epsilon(-k_0+q) = \frac{\hbar^2}{2m}\Big[(k_0+q)^2 - (-k_0+q)^2\Big] = \frac{2\hbar^2 k_0}{m}\, q,$$

so the detuning is linear in q. Diagonalizing Eq. (44) with $V_{G_0-G_1} = V_{2k_0}$ gives

$$\mathcal{E}_\pm(q) = V_0 + \frac{\epsilon(k_0+q)+\epsilon(-k_0+q)}{2} \pm \sqrt{\left(\frac{\hbar^2 k_0}{m}\, q\right)^2 + |V_{2k_0}|^2},$$

and hence the gap at $q = 0$ is $2|V_{2k_0}|$.

(ii) Why large-$|G|$ terms are perturbatively small in the second-order sum. In Eq. (42), the contribution from a state $|k+G\rangle$ scales as $|V_{G-G_0}|^2/\Delta E$, with

$$\Delta E = \epsilon(k+G_0) - \epsilon(k+G).$$

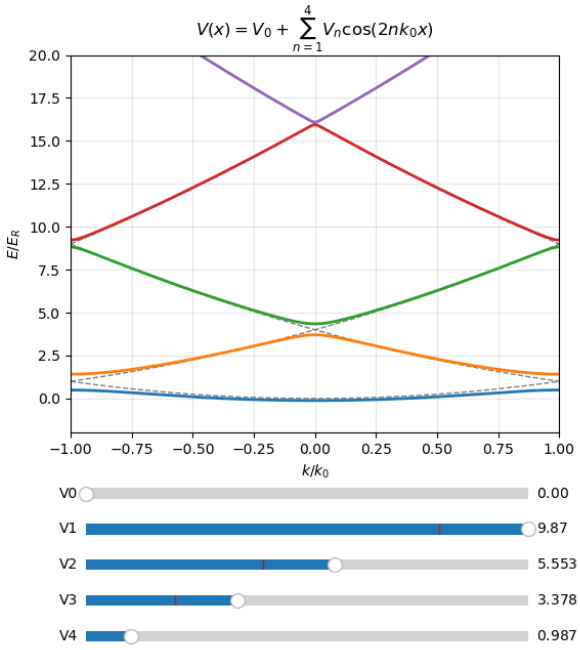

Figure 1: The folding of a quadratic potential and corrections in the weak-lattice limit

For fixed $k \in [-k_0, k_0]$ and large $|G| \sim 2|n|k_0$, one has $|\Delta E| \sim \hbar^2 G^2/(2m) \sim 4n^2 E_R$ (up to $O(n)$ corrections), so each term is suppressed at least as $1/n^2$ times the decay of $|V_{G-G_0}|^2$. For smooth lattice potentials the Fourier coefficients $|V_G|$ typically decay with $|G|$, making the sum rapidly convergent and the truncation to small $|G|$ controlled.

(iii) Comment: cosine lattice as the cleanest case. For $V_{\text{lat}}(x) = V\cos(2k_0x)$, the only nonzero Fourier components are $V_{\pm 2k_0} = V/2$. Thus, at the BZ edge the leading gap is entirely captured by the 2×2 problem; couplings to $|k \pm 4k_0\rangle$, $|k \pm 6k_0\rangle$, etc. can only arise via higher-order virtual processes and are additionally suppressed by powers of V/E_R.

(iv) Exact solution of the crossing condition in 1D. In 1D, the band crossings of the folded free spectrum are determined by the degeneracy condition

$$\epsilon(k + G_0) = \epsilon(k + G_1) \quad \Longleftrightarrow \quad (k + G_0)^2 = (k + G_1)^2, \tag{47}$$

with $G_0 \neq G_1$ reciprocal lattice vectors. Since every reciprocal vector has the form

$$G = 2nk_0, \qquad n \in \mathbb{Z}, \qquad k_0 \equiv \frac{\pi}{a}, \tag{48}$$

we write $G_0 = 2n_0k_0$ and $G_1 = 2n_1k_0$. Equation (47) then factorizes as

$$(k + G_0)^2 - (k + G_1)^2 = (G_0 - G_1)\Big(2k + G_0 + G_1\Big) = 0. \tag{49}$$

Because $G_0 \neq G_1$, the solution is uniquely

$$k = -\frac{G_0 + G_1}{2} = -(n_0 + n_1)k_0. \tag{50}$$

Suppose the quasi-momentum corresponding to k is denoted as k_{cross}, which lies in $[-k_0, k_0]$ and manifest an avoided crossing. Obviously it can only take value in $\{0, \pm k_0\}$:

$$k_{\text{cross}} \equiv -(n_0 + n_1)k_0 \pmod{2k_0} \in \{0, \pm k_0\}. \tag{51}$$

More explicitly:

- If $n_0 + n_1$ is even, then $k_{\text{cross}} \equiv 0$ (center of the BZ).
- If $n_0 + n_1$ is odd, then $k_{\text{cross}} \equiv \pm k_0$ (BZ edge; $-k_0$ and $+k_0$ are the same point).

Referring to Eq. (46), the size of the gap opened at the crossing between the unperturbed states labeled by (n_0, n_1) is

$$\Delta_{\text{gap}} = V_{2(n_0-n_1)k_0}, \tag{52}$$

where V_q denotes the q-th Fourier component of the periodic potential $V(x)$.
The corresponding unperturbed energy scale is (using Eq. (50))

$$\epsilon(k + G_0) \sim (n_0 - n_1)^2 k_0^2, \tag{53}$$

Therefore, the N-th band gap is controlled by the $2N$-th Fourier component of the periodic potential. [a]
The periodic potentials encountered in realistic systems typically do not contain significant high-frequency Fourier components. As a consequence, in the high-energy regime the spectrum of a weak lattice system becomes continuous, with no appreciable band gaps.

[a] To understand this point better, we leave a code and several pictures in Appendix B. Go and play with it!

1.4 Deep lattice: Wannier basis, harmonic approximation, and maximal localization

Wannier functions and gauge non-uniqueness. Given Bloch functions $\psi_{mk}(\boldsymbol{r})$, a Wannier function localized near lattice site $\boldsymbol{R}$ is defined by [1]

$$w_{m\boldsymbol{R}}(\boldsymbol{r}) = \frac{1}{\sqrt{N}} \sum_{k \in \text{BZ}} e^{-ik\cdot\boldsymbol{R}}\, \psi_{mk}(\boldsymbol{r}), \tag{54}$$

where N is the number of unit cells and the sum is over the discrete k-mesh. The construction is not unique because one may rephase Bloch states by a smooth k-dependent phase:

$$\tilde{\psi}_{mk}(\boldsymbol{r}) = e^{i\theta_m(k)} \psi_{mk}(\boldsymbol{r}), \tag{55}$$

with $\theta_m(k)$ periodic on the BZ. Different $\theta_m(k)$ produce Wannier functions with different shapes and localization properties.

Bloch–Wannier inverse transform, orthonormality, and completeness

Assume the Bloch states $\{\psi_{mk}\}$ are orthonormal in the crystal volume (Periodic boundary condition),

$$\int d^d r\, \psi^*_{mk}(\boldsymbol{r})\, \psi_{m'k'}(\boldsymbol{r}) = \delta_{mm'}\delta_{kk'}. \tag{56}$$

Then the definition of $w_{m\boldsymbol{R}}$ is a discrete Fourier transform in the lattice index $\boldsymbol{R}$. The inverse (Wannier $\to$ Bloch) transform is

$$\psi_{mk}(\boldsymbol{r}) = \frac{1}{\sqrt{N}} \sum_{\boldsymbol{R}} e^{ik\cdot\boldsymbol{R}}\, w_{m\boldsymbol{R}}(\boldsymbol{r}). \tag{57}$$

[1] Sometimes, the wannier wave function is also expressed as $w_m(\boldsymbol{r} - \boldsymbol{R}) = \frac{1}{\sqrt{N}} \sum_{k\in\text{BZ}} e^{-ik\cdot\boldsymbol{R}}\, \psi_{mk}(\boldsymbol{r})$ to emphasize its locality near $\boldsymbol{R}$.

Orthonormality. Using (56) and the definition of $w_{m\boldsymbol{R}}$,

$$\int d^d r\, w^*_{m\boldsymbol{R}}(\boldsymbol{r})\, w_{m'\boldsymbol{R}'}(\boldsymbol{r}) = \frac{1}{N}\sum_{k,k'} e^{ik\cdot\boldsymbol{R}} e^{-ik'\cdot\boldsymbol{R}'} \int d^d r\, \psi^*_{mk}(\boldsymbol{r})\psi_{m'k'}(\boldsymbol{r})$$
$$= \frac{1}{N}\sum_{k} e^{ik\cdot(\boldsymbol{R}-\boldsymbol{R}')}\, \delta_{mm'} = \delta_{mm'}\delta_{\boldsymbol{R},\boldsymbol{R}'}. \tag{58}$$

In the last step, we used the discrete orthogonality relation $\frac{1}{N}\sum_k e^{ik\cdot(\boldsymbol{R}'-\boldsymbol{R})} = \delta_{\boldsymbol{R},\boldsymbol{R}'}$.

Completeness within a chosen band subspace. For a fixed band m (or more generally, a set of bands), the Wannier functions span the same Hilbert subspace as the Bloch functions. This is expressed by the resolution of identity on that subspace:

$$\sum_{\boldsymbol{R}} |w_{m\boldsymbol{R}}\rangle\langle w_{m\boldsymbol{R}}| = \sum_{k\in \mathrm{BZ}} |\psi_{mk}\rangle\langle\psi_{mk}|. \tag{59}$$

Equivalently, in real space,

$$\sum_{\boldsymbol{R}} w_{m\boldsymbol{R}}(\boldsymbol{r})\, w^*_{m\boldsymbol{R}}(\boldsymbol{r}') = \sum_{k\in \mathrm{BZ}} \psi_{mk}(\boldsymbol{r})\, \psi^*_{mk}(\boldsymbol{r}'), \tag{60}$$

which is the projector kernel onto band m. Therefore, switching between Bloch and Wannier bases is a unitary change of basis inside the same band subspace.

Note on Gauge dependence. Under $\psi_{mk} \to e^{i\theta_m(k)}\psi_{mk}$, the inverse transform (57) remains valid, but the real-space shape of $w_{m\boldsymbol{R}}$ changes because the relative phases across k control interference in the Fourier sum. The orthonormality (58) and completeness (59) are unchanged, since the transformation is unitary in k-space.

Why maximal localization matters for lattice models.

If $w_{m\boldsymbol{R}}$ is sufficiently localized, then:

(i) kinetic energy is captured primarily by short-range hopping;

(ii) interactions are dominated by on-site terms. This yields the simplest effective lattice Hamiltonians (tight-binding and Hubbard types).

What controls Wannier localization?

For an isolated band in 1D, one can typically choose a smooth and periodic gauge $\theta(k)$, producing exponentially localized Wannier functions. Quantitatively, better localization is enabled by: (i) a larger band gap separating the target band from others (suppressing interband mixing under smooth gauges), and (ii) higher regularity/analyticity of ψ_{mk} as a function of k. In contrast, in 2D Chern bands (nonzero Chern number), there is a topological obstruction to choosing a globally smooth periodic gauge, and exponentially localized Wannier functions for a single isolated band cannot exist. This is the band-theoretic analogue of a topological obstruction rather than a dynamical limitation.

Harmonic approximation at deep minima. When the lattice is deep, expand $V_{\mathrm{lat}}(x)$ near a minimum x_i. Keeping quadratic terms gives an effective harmonic potential

$$\hat{H}_0 \approx -\frac{\hbar^2}{2m}\partial_x^2 + V_0 k_0^2 (x - x_i)^2. \tag{61}$$

With $V_0 = \alpha E_R$, the effective harmonic frequency and length scale are

$$\hbar\omega = 2\sqrt{\alpha}\, E_R, \qquad a_{\text{har}} = \sqrt{\frac{\hbar}{m\omega}} = \frac{1}{k_0\, \alpha^{1/4}}. \tag{62}$$

Local harmonic ground state as the zeroth-order Wannier envelope

Within the harmonic approximation around site x_i, the lowest local orbital is the harmonic-oscillator ground state

$$\phi_{0,i}(x) \equiv \phi_0(x - x_i) = \frac{1}{(\pi a_{\text{har}}^2)^{1/4}} \exp\left[-\frac{(x - x_i)^2}{2a_{\text{har}}^2}\right], \tag{63}$$

with energy $E_0^{(\text{har})} = \frac{1}{2}\hbar\omega$. This Gaussian gives a concrete "first guess" for the lowest-band Wannier function in the deep-lattice limit: one starts from $\phi_{0,i}$ at each site and then restores lattice orthogonality and translation symmetry by forming proper Bloch combinations and Fourier transforming back to Wannier functions.

From the harmonic approximation, we know the low energy excitations are of the order $\hbar\omega \propto \sqrt{V_0}$. This approximation only applies for low energy levels; when $n\hbar\omega$ is comparable with V_0, the quadratic expansion no longer holds. Thus, for a given lattice potential, the tight-binding approximation works for low-lying bands, and the free particle approximation works for high-energy bands.

In the tight-binding limit ($\alpha \gg 1$), the lowest-band maximally localized Wannier function $w_0(x - x_i)$ has an envelope close to a Gaussian of width a_{har}, while orthogonality between different sites enforces sign-changing oscillatory tails.

1.5 Band gap and metal/insulator: physical context and minimal classification

Condensed-matter motivation of "metal vs insulator". The language of metal/insulator originates in electronic condensed matter, where the operational distinction is about *low-temperature transport*: a metal can carry charge current under an arbitrarily small potential gradient, while an insulator cannot. In cold atoms, "charge transport" is usually not the primary probe, but the same band-theory logic remains a useful organizing principle because it classifies whether *adding/removing a particle* can be done at arbitrarily low energy.

Band gap and Charge gap. In band theory, a *band gap* is an energy window where the single-particle density of states (DOS) vanishes:

$$\rho(E) = 0 \qquad \text{for } E \in (E_1, E_2). \tag{64}$$

For fermions at $T = 0$, if the chemical potential μ lies inside such a window, then both particle and hole excitations cost finite energy: creating a particle excitation requires promoting to the bottom of the next band, while creating a hole excitation requires removing from the top of the filled band. Equivalently, changing the density costs finite energy. This finite energy cost is the *charge gap*,Δ_c.

A convenient many-body definition of the charge gap is

$$\Delta_c \equiv \Big[E_0(N+1) - E_0(N)\Big] - \Big[E_0(N) - E_0(N-1)\Big] = E_0(N+1) + E_0(N-1) - 2E_0(N), \tag{65}$$

where $E_0(N)$ is the ground-state energy with N particles. For a noninteracting band insulator, Δ_c reduces to the single-particle band gap between the highest occupied and lowest unoccupied states (up to finite-size effects).

Noninteracting filling criterion at $T = 0$. Consider noninteracting fermions at $T = 0$ with chemical potential μ.

- **Insulator:** If μ lies *in a band gap* (i.e. $\rho(\mu) = 0$), then the system has a finite charge gap $\Delta_c > 0$ and is an *insulator*: no arbitrarily low-energy particle/hole excitations exist at μ.
- **Metal:** If μ *crosses a band* (i.e. $\rho(\mu) \neq 0$), then $\Delta_c = 0$ and the state is *metallic*: there are gapless excitations at the Fermi surface (e.g. a free Fermi gas or a Fermi liquid).

Transport interpretation and the role of a potential gradient

A metal can respond to an infinitesimal potential gradient by carrying current because it has gapless charge excitations. An insulator has gapped charge excitations; therefore it cannot sustain a mass (or charge) current when the applied potential gradient is smaller than the charge gap scale. In cold atoms the current is a *mass current* (atoms are neutral), but the same logic applies at the level of low-energy excitations.

Different origins of the charge gap[2].
Insulators can be classified by *why* Δ_c is finite.

- **Band insulator:** Δ_c originates from band structure (the single-particle gap discussed in this chapter).
- **Mott insulator:** Δ_c originates from interactions (e.g. in the Hubbard model at commensurate filling, discussed later).

A band insulator can be further divided into *topologically trivial* and *topologically nontrivial* band insulators, depending on the topological invariants of the occupied band(s), as discussed in the topological band theory chapters later.

1.6 Tight-binding Model

Second quantize the single-particle Hamiltonian.
We first consider a *noninteracting* gas in a static optical lattice, i.e. we ignore all particle–particle interactions (contact interactions, long-range interactions, etc.). The starting point is therefore purely single-particle physics: a particle of mass m moving in a periodic potential $V_{\text{lat}}(\boldsymbol{r})$. Another key assumption is the deep lattice limit, *i.e.* the particles are strongly bound by the lattice potential.

To understand many-body systems, we need to build a second-quantized Hamiltonian that captures the key physics of such systems.

The key assumptions of Tight Binding Model:
(i) Ignore inter-particle interactions
(ii) Deep lattice limit

We start from the single particle Hamiltonian[3]:

$$H_{\text{sp}} = -\frac{\hbar^2\nabla^2}{2m} + V_{\text{lat}}(\boldsymbol{r}), \tag{66}$$

with $|V_{\text{lat}}|$ to be typically large.

[2] Disorder can also suppress transport and modify low-energy spectra (e.g. Anderson localization), but we do not include disorder effects here.

[3] The "first quantized" Hamiltonian

It's second quantized form[4] is:

$$\hat{H}_0 = \int d^d r\, \hat{\psi}^\dagger(\boldsymbol{r}) \left(-\frac{\hbar^2 \nabla^2}{2m} + V_{\text{lat}}(\boldsymbol{r}) \right) \hat{\psi}(\boldsymbol{r}). \tag{67}$$

If the reader is not familiar with techniques of second quantization, refer to Appendix A.

Single-band projection in the Wannier basis and the tight-binding Hamiltonian.

In the deep-lattice regime, we keep only the lowest band and expand the field operator as

$$\hat{\psi}(\boldsymbol{r}) \approx \sum_i \hat{b}_i\, w(\boldsymbol{r} - \boldsymbol{R}_i), \tag{68}$$

where $w(\boldsymbol{r} - \boldsymbol{R}_i)$ is the lowest-band[5] Wannier function centered at site $\boldsymbol{R}_i$, and $\hat{b}_i$ annihilates a particle on that site. Using Wannier orthonormality, $\int d^d r\, w^*(\boldsymbol{r} - \boldsymbol{R}_i) w(\boldsymbol{r} - \boldsymbol{R}_j) = \delta_{ij}$, one obtains the projected tight-binding kinetic Hamiltonian

$$\hat{H}_{\text{tb}} = \sum_{ij} \hat{b}_i^\dagger\, h_{ij}\, \hat{b}_j, \qquad h_{ij} = \int d^d r\, w^*(\boldsymbol{r} - \boldsymbol{R}_i) h_{\text{sp}}\, w(\boldsymbol{r} - \boldsymbol{R}_j), \tag{69}$$

with $h_{\text{sp}} \equiv -\hbar^2 \nabla^2/(2m) + V_{\text{lat}}(\boldsymbol{r})$. It is conventional to separate an on-site energy and define the *hopping* as

$$\varepsilon_0 \equiv h_{ii}, \qquad J_{ij} \equiv -h_{ij}\ (i \neq j), \tag{70}$$

so that

$$\hat{H}_{\text{tb}} = \varepsilon_0 \sum_i \hat{n}_i - \sum_{i \neq j} J_{ij} \hat{b}_i^\dagger \hat{b}_j, \qquad \hat{n}_i \equiv \hat{b}_i^\dagger \hat{b}_i. \tag{71}$$

Because w is exponentially localized in the tight-binding limit, J_{ij} decays rapidly with $|\boldsymbol{R}_i - \boldsymbol{R}_j|$. Keeping only nearest neighbors gives[6]:

$$\boxed{\hat{H}_{\text{tb}} = \varepsilon_0 \sum_i \hat{n}_i - J \sum_{\langle ij \rangle} \hat{b}_i^\dagger \hat{b}_j} \tag{72}$$

where $J \equiv J_{i,i+\boldsymbol{a}_\mu}$ for a nearest-neighbor displacement $\boldsymbol{a}_\mu$.

The Tight-binding dispersion from Lattice Fourier transform and .

For a translationally invariant Bravais lattice with N_s unit cells, define

$$\hat{b}_{\boldsymbol{k}} = \frac{1}{\sqrt{N_s}} \sum_i \hat{b}_i e^{-i\boldsymbol{k}\cdot\boldsymbol{R}_i}, \qquad \hat{b}_i = \frac{1}{\sqrt{N_s}} \sum_{\boldsymbol{k}} \hat{b}_{\boldsymbol{k}} e^{i\boldsymbol{k}\cdot\boldsymbol{R}_i}, \tag{73}$$

where $\boldsymbol{k}$ runs over the first Brillouin zone. Inserting this into (72), one finds a diagonal form in momentum space,

$$\hat{H}_{\text{tb}} = \sum_{\boldsymbol{k}} \mathcal{E}(\boldsymbol{k})\, \hat{b}_{\boldsymbol{k}}^\dagger \hat{b}_{\boldsymbol{k}}, \tag{74}$$

with the tight-binding dispersion

$$\mathcal{E}(\boldsymbol{k}) = \varepsilon_0 - 2J \sum_{\mu=1}^{d} \cos(\boldsymbol{k} \cdot \boldsymbol{a}_\mu). \tag{75}$$

[4] Eq. (67) is also referred to as a *continuum Hamiltonian*.

[5] Recall the general notation of the Wannier basis $w_{mR}(\boldsymbol{r}) \equiv w_m(\boldsymbol{r} - \boldsymbol{R})$. Now the band index m is no longer considered, and the expansion is realized with respect to the position index R.

[6] When refering to the tight-binding Hamiltonian, we usually assume the nearest-neighbor form, unless otherwise stated.

For a cubic lattice $\boldsymbol{a}_\mu = a\,\hat{\mu}$, this becomes

$$\mathcal{E}(\boldsymbol{k}) = \varepsilon_0 - 2J\Big[\cos(k_x a) + \cos(k_y a) + \cos(k_z a)\Big], \tag{76}$$

and in 1D,

$$\mathcal{E}(k) = \varepsilon_0 - 2J\cos(ka). \tag{77}$$

Derivation of $\mathcal{E}(\boldsymbol{k})$ from the (nearest-neighbor) tight-binding Hamiltonian

Start from $\hat{H}_{\text{kin}} = -J\sum_{\langle ij\rangle}\hat{b}_i^\dagger\hat{b}_j$. For a Bravais lattice, nearest neighbors can be written as $j = i + \boldsymbol{a}_\mu$ (and also $i - \boldsymbol{a}_\mu$). Using the Fourier transform,

$$\hat{b}_i^\dagger\hat{b}_{i+\boldsymbol{a}_\mu} = \frac{1}{N_s}\sum_{\boldsymbol{k},\boldsymbol{q}}\hat{b}_{\boldsymbol{k}}^\dagger\hat{b}_{\boldsymbol{q}}e^{-i\boldsymbol{k}\cdot\boldsymbol{R}_i}e^{i\boldsymbol{q}\cdot(\boldsymbol{R}_i+\boldsymbol{a}_\mu)} = \frac{1}{N_s}\sum_{\boldsymbol{k},\boldsymbol{q}}\hat{b}_{\boldsymbol{k}}^\dagger\hat{b}_{\boldsymbol{q}}e^{i(\boldsymbol{q}-\boldsymbol{k})\cdot\boldsymbol{R}_i}e^{i\boldsymbol{q}\cdot\boldsymbol{a}_\mu}.$$

Summing over sites gives $\sum_i e^{i(\boldsymbol{q}-\boldsymbol{k})\cdot\boldsymbol{R}_i} = N_s\,\delta_{\boldsymbol{k},\boldsymbol{q}}$, hence

$$\sum_i \hat{b}_i^\dagger\hat{b}_{i+\boldsymbol{a}_\mu} = \sum_{\boldsymbol{k}}\hat{b}_{\boldsymbol{k}}^\dagger\hat{b}_{\boldsymbol{k}}e^{i\boldsymbol{k}\cdot\boldsymbol{a}_\mu}.$$

Adding the Hermitian conjugate (the $-\boldsymbol{a}_\mu$ hop) produces $e^{i\boldsymbol{k}\cdot\boldsymbol{a}_\mu} + e^{-i\boldsymbol{k}\cdot\boldsymbol{a}_\mu} = 2\cos(\boldsymbol{k}\cdot\boldsymbol{a}_\mu)$, which yields $\mathcal{E}(\boldsymbol{k})$ in (75).

Group Velocity in Tight-binding Model. Because $\mathcal{E}(\boldsymbol{k})$ depends on $\boldsymbol{k}$ only through $\cos(\boldsymbol{k}\cdot\boldsymbol{a}_\mu)$, it is periodic under $\boldsymbol{k} \to \boldsymbol{k} + \boldsymbol{G}$ for any reciprocal lattice vector $\boldsymbol{G}$. The group velocity is

$$\boldsymbol{v}(\boldsymbol{k}) = \frac{1}{\hbar}\nabla_{\boldsymbol{k}}\mathcal{E}(\boldsymbol{k}) = \frac{2J}{\hbar}\sum_{\mu=1}^{d}\boldsymbol{a}_\mu\,\sin(\boldsymbol{k}\cdot\boldsymbol{a}_\mu), \tag{78}$$

which is also periodic in $\boldsymbol{k}$. In 1D, $v(k) = (2Ja/\hbar)\sin(ka)$, so $v(k) = 0$ at the band edges $k = 0$ and $k = \pm\pi/a$, consistent with standing-wave character at Brillouin-zone boundaries.

1.7 Hubbard model

Interacting continuum Hamiltonian: adding two-body collisions.

So far we considered only single-particle physics in the lattice potential. To describe a realistic cold-atom gas we must add interparticle interactions. The microscopic second-quantized Hamiltonian is

$$\hat{H} = \hat{H}_0 + \hat{H}_{\text{int}}, \qquad \hat{H}_0 = \int d^d r\,\hat{\psi}^\dagger(\boldsymbol{r})\left(-\frac{\hbar^2\nabla^2}{2m} + V_{\text{lat}}(\boldsymbol{r})\right)\hat{\psi}(\boldsymbol{r}). \tag{79}$$

A general number-conserving two-body interaction can be written as

$$\hat{H}_{\text{int}} = \frac{1}{2}\int d^d r\,d^d r'\;\hat{\psi}^\dagger(\boldsymbol{r})\hat{\psi}^\dagger(\boldsymbol{r}')\,U(\boldsymbol{r},\boldsymbol{r}')\,\hat{\psi}(\boldsymbol{r}')\hat{\psi}(\boldsymbol{r}), \tag{80}$$

where $U(\boldsymbol{r},\boldsymbol{r}')$ is the interaction kernel. For ultracold *bosons* in the dilute regime, short-range s-wave scattering is well captured by a contact interaction,

$$U(\boldsymbol{r},\boldsymbol{r}') = g\,\delta(\boldsymbol{r}-\boldsymbol{r}'), \qquad g = \frac{4\pi\hbar^2 a_s}{m}, \tag{81}$$

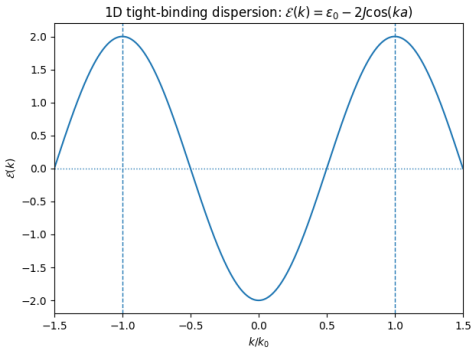

(a) 1D TB Dispersion

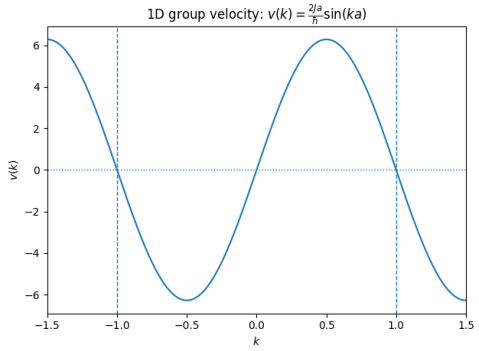

(b) 1D group velocity. In the center and the boundary of the Brillouin Zone, $v = 0$.

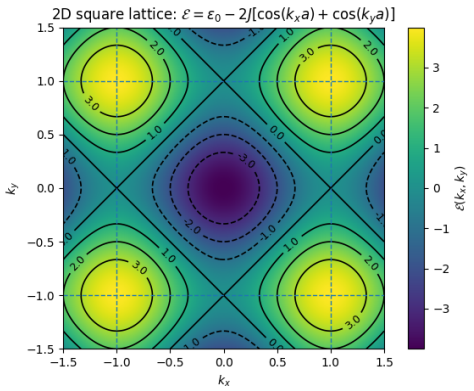

(c) 2D Square Lattice TB Dispersion

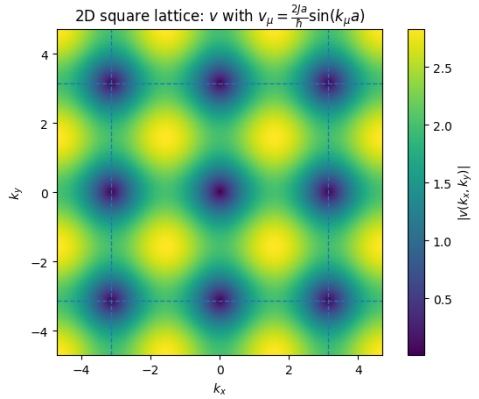

(d) 2D Square Lattice TB Group Velocities

Figure 2: Tight Binding Model: Dispersions and Group Velocities; ϵ_0 is set to be 0.

so that

$$\hat{H}_{\text{int}} = \frac{g}{2}\int d^d r\ \hat{\psi}^\dagger(\boldsymbol{r})\hat{\psi}^\dagger(\boldsymbol{r})\hat{\psi}(\boldsymbol{r})\hat{\psi}(\boldsymbol{r}). \tag{82}$$

Discrete-mode transform: Field-operator expansion in Wannier functions. To obtain a lattice model, expand the field operator in Wannier orbitals$w_{m\boldsymbol{R}}(\boldsymbol{r})$.

Introduce lattice annihilation operators $\hat{b}_{m,\boldsymbol{R}} = \int d^d r\, w^*_{m\boldsymbol{R}}(\boldsymbol{r})\hat{\psi}(\boldsymbol{r})$ and expand

$$\hat{\psi}(\boldsymbol{r}) = \sum_{m,\boldsymbol{R}} \hat{b}_{m,\boldsymbol{R}}\, w_{m\boldsymbol{R}}(\boldsymbol{r}), \qquad \hat{\psi}^\dagger(\boldsymbol{r}) = \sum_{m,\boldsymbol{R}} \hat{b}^\dagger_{m,\boldsymbol{R}}\, w^*_{m\boldsymbol{R}}(\boldsymbol{r}). \tag{83}$$

This is a *discrete change of basis* (a mode expansion): the continuum field is rewritten in terms of lattice-localized orbitals. No approximation has been made yet, as long as all relevant bands are retained.

Insert Eq. (83) into $\hat{H}_0$ and $\hat{H}_{\text{int}}$.

• For the one-body part one obtains

$$\hat{H}_0 = \sum_{m,m'}\sum_{\boldsymbol{R},\boldsymbol{R}'} h^{mm'}_{\boldsymbol{R}\boldsymbol{R}'}\, \hat{b}^\dagger_{m,\boldsymbol{R}}\hat{b}_{m',\boldsymbol{R}'}, \qquad h^{mm'}_{\boldsymbol{R}\boldsymbol{R}'} = \int d^d r\, w^*_{m\boldsymbol{R}}(\boldsymbol{r})\,[\frac{\hbar^2\nabla^2}{2m} + V_{\text{lat}}(\boldsymbol{r})]\, w_{m'\boldsymbol{R}'}(\boldsymbol{r}), \tag{84}$$

If w_m are constructed from Bloch eigenstates of band m, then band mixing is absent in $\hat{H}_0$ and $h^{mm'}_{\boldsymbol{R}\boldsymbol{R}'} \propto \delta_{mm'}$. It is then conventional to define on-site energies and hoppings within each band:

$$\varepsilon_m \equiv h^{mm}_{\boldsymbol{R}\boldsymbol{R}}, \qquad J^{(m)}_{\boldsymbol{R}\boldsymbol{R}'} \equiv -h^{mm}_{\boldsymbol{R}\boldsymbol{R}'} \quad (\boldsymbol{R} \neq \boldsymbol{R}'). \tag{85}$$

• For the interaction part, starting from the general kernel (80), the Wannier expansion gives

$$\hat{H}_{\text{int}} = \frac{1}{2} \sum_{m,m',n,n'} \sum_{\boldsymbol{R}_1,\boldsymbol{R}_2,\boldsymbol{R}_3,\boldsymbol{R}_4} U^{mm'nn'}_{\boldsymbol{R}_1\boldsymbol{R}_2\boldsymbol{R}_3\boldsymbol{R}_4}\, \hat{b}^\dagger_{m,\boldsymbol{R}_1} \hat{b}^\dagger_{m',\boldsymbol{R}_2} \hat{b}_{n,\boldsymbol{R}_3} \hat{b}_{n',\boldsymbol{R}_4}, \tag{86}$$

with matrix elements

$$U^{mm'nn'}_{\boldsymbol{R}_1\boldsymbol{R}_2\boldsymbol{R}_3\boldsymbol{R}_4} = \int d^d r\, d^d r'\; w^*_{m\boldsymbol{R}_1}(\boldsymbol{r})\, w^*_{m'\boldsymbol{R}_2}(\boldsymbol{r}')\, U(\boldsymbol{r},\boldsymbol{r}')\, w_{n\boldsymbol{R}_3}(\boldsymbol{r}')\, w_{n'\boldsymbol{R}_4}(\boldsymbol{r}). \tag{87}$$

In particular, for the contact interaction (82) one finds the familiar single-integral form

$$U^{mm'nn'}_{\boldsymbol{R}_1\boldsymbol{R}_2\boldsymbol{R}_3\boldsymbol{R}_4} = g \int d^d r\; w^*_{m\boldsymbol{R}_1}(\boldsymbol{r})\, w^*_{m'\boldsymbol{R}_2}(\boldsymbol{r})\, w_{n\boldsymbol{R}_3}(\boldsymbol{r})\, w_{n'\boldsymbol{R}_4}(\boldsymbol{r}). \tag{88}$$

To conclude, the Wannier expansion turns the continuum field theory into a *multi-band extended lattice model*: a quadratic hopping sector (84) plus a quartic interaction sector (86). All "exotic" lattice interaction processes (off-site density–density coupling, pair hopping, density-assisted tunneling, etc.) are contained in the general tensor $U^{mm'nn'}_{\boldsymbol{R}_1\boldsymbol{R}_2\boldsymbol{R}_3\boldsymbol{R}_4}$.

Controlled simplifications: From the multi-band lattice model to the single-band Bose–Hubbard model.

In the deep-lattice, weak-interaction regime, one typically makes the following controlled reductions:

- *Single-band projection.* Assume interaction and temperature scales are small compared with the band gap, so that higher-band occupation is negligible. Keep only the lowest band $m = 0$, and write $\hat{b}_{0,\boldsymbol{R}} \equiv \hat{b}_{\boldsymbol{R}}$, $w_{0\boldsymbol{R}} \equiv w_{\boldsymbol{R}}$.
- *Nearest-neighbor hopping.* Exponential localization of Wannier functions implies $J_{\boldsymbol{R}\boldsymbol{R}'}$ decays rapidly with $|\boldsymbol{R} - \boldsymbol{R}'|$. Keep only nearest neighbors: $J_{\boldsymbol{R},\boldsymbol{R}+\boldsymbol{a}_\mu} \equiv J$.
- *On-site interaction dominance.* For contact interactions, the leading matrix element is the on-site term $\boldsymbol{R}_1 = \boldsymbol{R}_2 = \boldsymbol{R}_3 = \boldsymbol{R}_4$. Off-site terms require overlap of Wannier tails and are exponentially suppressed in a deep lattice. Moreover, in the weak-scattering regime one often has an additional small parameter $\sim a_s/a_{\text{har}} \ll 1$ controlling corrections beyond the simplest on-site Hubbard term.

■ **Bose–Hubbard Model.**

Under these assumptions one obtains the single-band Bose–Hubbard Hamiltonian

$$\boxed{\hat{H}_{\text{BHM}} = -J \sum_{\langle ij \rangle} \hat{b}^\dagger_i \hat{b}_j + \frac{U}{2} \sum_i \hat{n}_i(\hat{n}_i - 1) - \mu \sum_i \hat{n}_i} \tag{89}$$

where $\hat{n}_i \equiv \hat{b}^\dagger_i \hat{b}_i$, μ is the chemical potential[7] and the on-site interaction is

$$U = g \int d^d r\, |w(\boldsymbol{r} - \boldsymbol{R}_i)|^4, \tag{90}$$

independent of i by translation invariance.

Equation (89) is the canonical lattice model capturing the competition between kinetic delocalization (J) and local interaction energy (U) in a deep optical lattice.

[7] The onsite energy ϵ_0 is absorbed into μ.

■ **Fermi–Hubbard model.**

We now specialize to a two-component ($\sigma = \uparrow, \downarrow$) Fermi gas in a deep optical lattice. After projecting to the lowest Wannier orbital on each site, the low-energy degrees of freedom are lattice fermions $\hat{c}_{i\sigma}$ that annihilate a spin-σ particle on site i. Keeping only nearest-neighbor tunneling and the dominant on-site interaction between opposite spins, one arrives at the single-band Fermi–Hubbard Hamiltonian

$$\hat{H}_{\mathrm{FHM}} = -J \sum_{\langle ij \rangle, \sigma} \hat{c}^{\dagger}_{i\sigma} \hat{c}_{j\sigma} + U \sum_{i} \hat{n}_{i\uparrow} \hat{n}_{i\downarrow} - \mu \sum_{i,\sigma} \hat{n}_{i\sigma}, \tag{91}$$

where $\hat{n}_{i\sigma} \equiv \hat{c}^{\dagger}_{i\sigma} \hat{c}_{i\sigma}$. The first term describes coherent hopping with amplitude J, while the second penalizes (or favors, if $U < 0$) double occupancy of a site by two opposite-spin fermions; same-spin contact interactions are absent due to Pauli exclusion. The chemical potential μ fixes the average filling, and at half filling the competition between tunneling and repulsion ($U > 0$) leads to the familiar Mott/antiferromagnetic physics in strong coupling.

2 Honeycomb Lattice and Dirac Semimetal

In a Bose condensate, "topology" typically refers to homotopy classes of maps from *real space* to the condensate order-parameter manifold (vortices, monopoles, skyrmions). In band theory, topology refers to maps from the *Brillouin zone (momentum space)* to the space of Bloch eigenstates (modulo a $U(1)$ phase gauge at each k). The mathematical language (homotopy, defects, winding) is parallel, but the physical objects being mapped and the meaning of singularities (gap closing points) are distinct.

2.1 Honeycomb geometry: Unit cell, Primitive vectors, Reciprocal lattice and Brillouin zone

Two-sublattice unit cell. The honeycomb lattice is not a Bravais lattice by itself: it is a triangular Bravais lattice with a two-site basis (sublattices A and B). The presence of two sites per unit cell is essential: it produces a two-component Bloch basis and enables a generic 2×2 Bloch Hamiltonian.

Primitive vectors. Let the nearest-neighbor bond length be a. A commonly used choice for triangular Bravais primitive vectors is

$$\boldsymbol{a}_1 = a\,(0,\, \sqrt{3}), \qquad \boldsymbol{a}_2 = a\left(\frac{3}{2}, -\frac{\sqrt{3}}{2}\right), \tag{92}$$

and define $\boldsymbol{a}_3 = -\boldsymbol{a}_1 - \boldsymbol{a}_2 = a\left(-\frac{3}{2}, -\frac{\sqrt{3}}{2}\right)$.

Reciprocal lattice. The reciprocal vectors $\boldsymbol{b}_i$ satisfy $\boldsymbol{a}_i \cdot \boldsymbol{b}_j = 2\pi\delta_{ij}$. One convenient choice is

$$\boldsymbol{b}_1 = \frac{2\pi}{a}\left(\frac{1}{3}, \frac{1}{\sqrt{3}}\right), \qquad \boldsymbol{b}_2 = \frac{2\pi}{a}\left(\frac{2}{3}, 0\right). \tag{93}$$

Brillouin zone. The first BZ, taken as the Wigner–Seitz cell of reciprocal lattice, is a hexagon. Two inequivalent corners can be taken as

$$\boldsymbol{K} = \frac{2\pi}{a}\left(0, \frac{2}{3\sqrt{3}}\right), \qquad \boldsymbol{K}' = \frac{2\pi}{a}\left(0, -\frac{2}{3\sqrt{3}}\right). \tag{94}$$

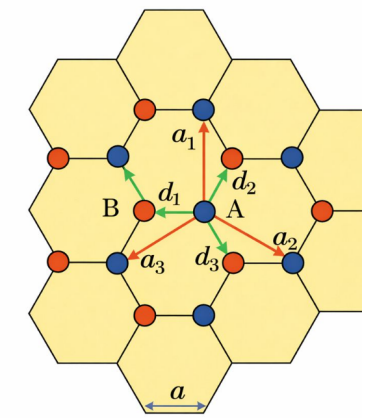

(a) Basic Settings of Honeycomb Lattice

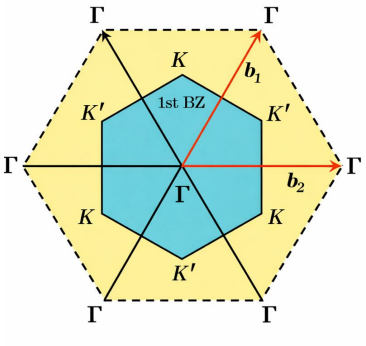

(b) The first Brillouin Zone of Honeycomb Lattice

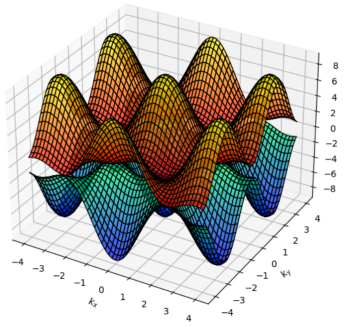

(c) Band Structure of Honeycomb NN Model. Near Dirac Points, the gap closes and there are linear dispersions.

Figure 3: Honeycomb Lattice

Experimental realization

A honeycomb optical lattice can be engineered by superposing multiple standing-wave laser fields with tunable relative phases/polarizations. Interference controls the positions and depths of potential minima, allowing a continuous interpolation among square-like, dimerized, and honeycomb configurations. For theory, the essential input is simply: the resulting low-energy tight-binding description has two sublattices per unit cell and (approximately) dominant nearest-neighbor hoppings.

2.2 Nearest-neighbor tight-binding Hamiltonian

Real-space model. Consider spinless fermions for the band-structure discussion [8]. With only nearest-neighbor hopping between A and B,

$$\hat{H}_{\mathrm{NN}} = -J_1 \sum_{\langle ij \rangle} \left(\hat{c}^\dagger_{B,j} \hat{c}_{A,i} + \mathrm{h.c.} \right). \tag{95}$$

This model is sometimes referred to as the "Honeycomb NN Model".

Dispersion and Eigenstates. By doing Lattice Fourier transformation, we get:

$$\hat{H}_{\mathrm{NN}} = \sum_{\boldsymbol{k}} \begin{pmatrix} \hat{c}^\dagger_A(\boldsymbol{k}) & \hat{c}^\dagger_B(\boldsymbol{k}) \end{pmatrix} H(\boldsymbol{k}) \begin{pmatrix} \hat{c}_A(\boldsymbol{k}) \\ \hat{c}_B(\boldsymbol{k}) \end{pmatrix}, \tag{96}$$

with the Bloch Hamiltonian

$$H(\boldsymbol{k}) = \begin{pmatrix} 0 & -J_1 f(\boldsymbol{k}) \\ -J_1 f^*(\boldsymbol{k}) & 0 \end{pmatrix}, \qquad f(\boldsymbol{k}) = \sum_{\ell=1}^{3} e^{i\boldsymbol{k}\cdot\boldsymbol{d}_\ell}. \tag{97}$$

Write $f(\boldsymbol{k}) = |f(\boldsymbol{k})| e^{i\varphi(\boldsymbol{k})}$. Then

$$E_\pm(\boldsymbol{k}) = \pm J_1 |f(\boldsymbol{k})|. \tag{98}$$

[8] spin can be appended as a degeneracy

The corresponding normalized eigenvectors can be chosen as

$$|u_+(\boldsymbol{k})\rangle = \frac{1}{\sqrt{2}}\begin{pmatrix}1\\ -e^{-i\varphi(\boldsymbol{k})}\end{pmatrix}, \qquad |u_-(\boldsymbol{k})\rangle = \frac{1}{\sqrt{2}}\begin{pmatrix}1\\ +e^{-i\varphi(\boldsymbol{k})}\end{pmatrix}, \tag{99}$$

up to a $U(1)$ phase at each $\boldsymbol{k}$.

Process supplement: explicit Fourier transform and $H(\boldsymbol{k})$

Choose Bravais lattice vectors $\boldsymbol{R}$ labeling unit cells. Within each unit cell define fermionic annihilation operators $\hat{c}_A(\boldsymbol{R})$ and $\hat{c}_B(\boldsymbol{R})$ acting on the two sublattices A and B.
We introduce the Fourier transforms

$$\hat{c}_A(\boldsymbol{R}) = \frac{1}{\sqrt{N}}\sum_{\boldsymbol{k}} \hat{c}_A(\boldsymbol{k})\, e^{i\boldsymbol{k}\cdot\boldsymbol{R}}, \qquad \hat{c}_B(\boldsymbol{R}) = \frac{1}{\sqrt{N}}\sum_{\boldsymbol{k}} \hat{c}_B(\boldsymbol{k})\, e^{i\boldsymbol{k}\cdot\boldsymbol{R}}, \tag{100}$$

where $\boldsymbol{k}$ runs over the first Brillouin zone and N is the number of unit cells.

Nearest-neighbor hopping connects an A-site at $\boldsymbol{R}$ to three B-sites located at $\boldsymbol{R} + \boldsymbol{d}_\ell$ ($\ell = 1, 2, 3$). A convenient and consistent choice of displacement vectors is

$$\boldsymbol{d}_1 = a(-1, 0), \quad \boldsymbol{d}_2 = a\left(\frac{1}{2}, \frac{\sqrt{3}}{2}\right), \quad \boldsymbol{d}_3 = a\left(\frac{1}{2}, -\frac{\sqrt{3}}{2}\right). \tag{101}$$

The nearest-neighbor tight-binding Hamiltonian is then

$$\hat{H}_{\mathrm{NN}} = -J_1 \sum_{\boldsymbol{R}}\sum_{\ell=1}^{3} \left(\hat{c}_B^\dagger(\boldsymbol{R} + \boldsymbol{d}_\ell)\, \hat{c}_A(\boldsymbol{R}) + \mathrm{h.c.}\right). \tag{102}$$

We now insert the Fourier representations explicitly. For the hopping term,

$$\begin{aligned}\hat{c}_B^\dagger(\boldsymbol{R} + \boldsymbol{d}_\ell)\hat{c}_A(\boldsymbol{R}) &= \left(\frac{1}{\sqrt{N}}\sum_{\boldsymbol{k}'} \hat{c}_B^\dagger(\boldsymbol{k}')\, e^{-i\boldsymbol{k}'\cdot(\boldsymbol{R}+\boldsymbol{d}_\ell)}\right)\left(\frac{1}{\sqrt{N}}\sum_{\boldsymbol{k}} \hat{c}_A(\boldsymbol{k})\, e^{i\boldsymbol{k}\cdot\boldsymbol{R}}\right)\\ &= \frac{1}{N}\sum_{\boldsymbol{k},\boldsymbol{k}'} \hat{c}_B^\dagger(\boldsymbol{k}')\hat{c}_A(\boldsymbol{k})\, e^{i(\boldsymbol{k}-\boldsymbol{k}')\cdot\boldsymbol{R}}\, e^{-i\boldsymbol{k}'\cdot\boldsymbol{d}_\ell}.\end{aligned} \tag{103}$$

Summing over all unit cells $\boldsymbol{R}$ gives

$$\sum_{\boldsymbol{R}} e^{i(\boldsymbol{k}-\boldsymbol{k}')\cdot\boldsymbol{R}} = N\,\delta_{\boldsymbol{k},\boldsymbol{k}'}, \tag{104}$$

which enforces crystal momentum conservation. Using this orthogonality relation, the Hamiltonian reduces to

$$\hat{H}_{\mathrm{NN}} = -J_1 \sum_{\boldsymbol{k}}\sum_{\ell=1}^{3} \left(e^{-i\boldsymbol{k}\cdot\boldsymbol{d}_\ell}\hat{c}_B^\dagger(\boldsymbol{k})\hat{c}_A(\boldsymbol{k}) + e^{i\boldsymbol{k}\cdot\boldsymbol{d}_\ell}\hat{c}_A^\dagger(\boldsymbol{k})\hat{c}_B(\boldsymbol{k})\right). \tag{105}$$

Introducing the *structure factor*

$$\boxed{f(\boldsymbol{k}) = \sum_{\ell=1}^{3} e^{i\boldsymbol{k}\cdot\boldsymbol{d}_\ell},} \tag{106}$$

the Hamiltonian can be written compactly as

$$\hat{H}_{\mathrm{NN}} = \sum_{\boldsymbol{k}} \begin{pmatrix}\hat{c}_A^\dagger(\boldsymbol{k}) & \hat{c}_B^\dagger(\boldsymbol{k})\end{pmatrix} H(\boldsymbol{k}) \begin{pmatrix}\hat{c}_A(\boldsymbol{k})\\ \hat{c}_B(\boldsymbol{k})\end{pmatrix}, \tag{107}$$

with the Bloch Hamiltonian

$$H(\boldsymbol{k}) = \begin{pmatrix} 0 & -J_1 f(\boldsymbol{k}) \\ -J_1 f^*(\boldsymbol{k}) & 0 \end{pmatrix}. \tag{108}$$

By construction, $f(\boldsymbol{k} + \boldsymbol{G}) = f(\boldsymbol{k})$ for any reciprocal lattice vector $\boldsymbol{G}$, so the Brillouin-zone periodicity $H(\boldsymbol{k} + \boldsymbol{G}) = H(\boldsymbol{k})$ is manifest.

Pauli-matrix expansion and the pseudo-spin language.

Because $H(\boldsymbol{k})$ is a 2×2 Hermitian matrix acting in the sublattice space (A, B), it admits a unique expansion in the Pauli-matrix basis,

$$H(\boldsymbol{k}) = E_0(\boldsymbol{k})\, I + \boldsymbol{B}(\boldsymbol{k}) \cdot \boldsymbol{\sigma}, \tag{109}$$

where I is the identity matrix, $\boldsymbol{\sigma} = (\sigma_x, \sigma_y, \sigma_z)$ are the Pauli matrices, and the real vector $\boldsymbol{B}(\boldsymbol{k})$ plays the role of an effective momentum-dependent Zeeman field acting on a pseudo-spin degree of freedom.

Why any 2×2 Hermitian matrix admits the Pauli expansion

The real vector space of 2×2 Hermitian matrices is four-dimensional. A convenient basis is $\{I, \sigma_x, \sigma_y, \sigma_z\}$. Therefore any Hermitian H can be written uniquely as $H = E_0 I + \sum_{i=x,y,z} B_i \sigma_i$ with real coefficients. In band problems with two internal components (here: sublattices A, B), this naturally defines a pseudo-spin-1/2 degree of freedom.

For the nearest-neighbor tight-binding model on the honeycomb lattice, the Hamiltonian is purely off-diagonal in the (A, B) basis. As a result,

$$E_0(\boldsymbol{k}) = 0, \qquad B_z(\boldsymbol{k}) = 0, \tag{110}$$

and the effective field $\boldsymbol{B}(\boldsymbol{k})$ lies entirely in the x–y plane:

$$B_x(\mathbf{k}) = -J_1\Big(1 + \cos(\mathbf{k} \cdot \mathbf{a}_3) + \cos(\mathbf{k} \cdot \mathbf{a}_2)\Big), \tag{111}$$

$$B_y(\mathbf{k}) = J_1\Big(\sin(\mathbf{k} \cdot \mathbf{a}_3) - \sin(\mathbf{k} \cdot \mathbf{a}_2)\Big), \tag{112}$$

In the pseudo-spin language, the Bloch Hamiltonian describes a two-level system in a momentum-dependent Zeeman field $\boldsymbol{B}(\boldsymbol{k})$. The energy eigenvalues are therefore

$$E_\pm(\boldsymbol{k}) = \pm|\boldsymbol{B}(\boldsymbol{k})|, \tag{113}$$

corresponding to pseudo-spins aligned parallel or antiparallel to the local field direction

$$\hat{\boldsymbol{B}}(\boldsymbol{k}) = \frac{\boldsymbol{B}(\boldsymbol{k})}{|\boldsymbol{B}(\boldsymbol{k})|}. \tag{114}$$

The associated eigenstates are completely determined by the orientation of this vector, i.e. by how the pseudo-spin winds in momentum space.

This pseudo-spin does *not* correspond to the real electron spin. Instead, it encodes the internal structure within each unit cell, namely the relative weight and phase between the two sublattice components of the Bloch wave function. Such a pseudo-spin description is only possible because the honeycomb lattice contains more than one site per unit cell; for a single-site Bravais lattice no analogous internal degree of freedom exists.

2.3 Dirac points: existence and linear dispersion from explicit expansion

Band touching occurs when $E_+(\boldsymbol{k}) = E_-(\boldsymbol{k}) = 0$, i.e. $f(\boldsymbol{k}) = 0$. For the honeycomb NN model, $f(\boldsymbol{K}) = f(\boldsymbol{K}') = 0$, hence the bands touch at $\boldsymbol{K}, \boldsymbol{K}'$.[9] These are the *Dirac points*.

Near $\boldsymbol{K}, \boldsymbol{K}'$, the honeycomb NN model realizes a 2D massless Dirac dispersion $E = \pm\hbar v_F|\boldsymbol{q}|$, hence the term "Dirac point". Equivalently, the Bloch Hamiltonian admits a *low-energy effective Dirac Hamiltonian* obtained by linearizing $H(\boldsymbol{k})$ around $\boldsymbol{K}$ or $\boldsymbol{K}'$.

$$H_{\text{eff}}^{(K)}(\boldsymbol{q}) \equiv H(\boldsymbol{K}+\boldsymbol{q}) \approx \hbar v_F \left(q_x \sigma_x + q_y \sigma_y\right), \tag{115}$$

$$H_{\text{eff}}^{(K')}(\boldsymbol{q}) \equiv H(\boldsymbol{K}'+\boldsymbol{q}) \approx \hbar v_F \left(q_x \sigma_x - q_y \sigma_y\right), \tag{116}$$

where $v_F = \frac{1}{\hbar}\frac{3}{2}J_1 a$. The detailed derivation can be found in the following box.

Process supplement: linearization near K and K', and the effective Dirac Hamiltonian

Let $\boldsymbol{k} = \boldsymbol{K} + \boldsymbol{q}$ with $|\boldsymbol{q}|a \ll 1$. Expand

$$f(\boldsymbol{K}+\boldsymbol{q}) = \sum_\ell e^{i(\boldsymbol{K}+\boldsymbol{q})\cdot\boldsymbol{d}_\ell} = \sum_\ell e^{i\boldsymbol{K}\cdot\boldsymbol{d}_\ell}\left(1 + i\boldsymbol{q}\cdot\boldsymbol{d}_\ell + \cdots\right). \tag{117}$$

Because $\sum_\ell e^{i\boldsymbol{K}\cdot\boldsymbol{d}_\ell} = f(\boldsymbol{K}) = 0$, the leading term is linear:

$$f(\boldsymbol{K}+\boldsymbol{q}) \approx i\sum_\ell e^{i\boldsymbol{K}\cdot\boldsymbol{d}_\ell}(\boldsymbol{q}\cdot\boldsymbol{d}_\ell). \tag{118}$$

Evaluating the geometric sum yields a complex linear form

$$f(\boldsymbol{K}+\boldsymbol{q}) \approx -\frac{3a}{2}\left(q_x - iq_y\right), \qquad f(\boldsymbol{K}'+\boldsymbol{q}) \approx -\frac{3a}{2}\left(q_x + iq_y\right), \tag{119}$$

up to convention-dependent rotations of (q_x, q_y). Therefore

$$E_\pm(\boldsymbol{K}+\boldsymbol{q}) \approx \pm\frac{3}{2}J_1 a\,|\boldsymbol{q}|. \tag{120}$$

More explicitly, substituting the linearized f into the Bloch Hamiltonian $H(\boldsymbol{k}) = \begin{pmatrix} 0 & -J_1 f(\boldsymbol{k}) \\ -J_1 f^*(\boldsymbol{k}) & 0 \end{pmatrix}$ gives the *effective* 2×2 Hamiltonian near each valley. Defining

$$v_F = \frac{1}{\hbar}\frac{3}{2}J_1 a, \tag{121}$$

one finds, to linear order in $\boldsymbol{q}$,

$$H_{\text{eff}}^{(K)}(\boldsymbol{q}) \equiv H(\boldsymbol{K}+\boldsymbol{q}) \approx \hbar v_F \left(q_x \sigma_x + q_y \sigma_y\right), \tag{122}$$

$$H_{\text{eff}}^{(K')}(\boldsymbol{q}) \equiv H(\boldsymbol{K}'+\boldsymbol{q}) \approx \hbar v_F \left(q_x \sigma_x - q_y \sigma_y\right), \tag{123}$$

where the relative sign between the two valleys is the standard "valley chirality" (it depends on the convention for $\boldsymbol{d}_\ell$ and the ordering of (A, B)). Diagonalizing either effective Hamiltonian yields

$$E_\pm(\boldsymbol{q}) = \pm\hbar v_F|\boldsymbol{q}|, \tag{124}$$

i.e. a massless Dirac cone.

[9] You can plug Eq. (94) into Eq. (106) to verify it.

2.4 Dirac semimetal and density of states at the Fermi level

Dirac semimetal at half-filling. If fermions are loaded so that (for each spin component[10]) the particle number equals the number of unit cells N_{uc}, then the lower band (which contains exactly N_{uc} Bloch states) is completely filled, while the upper band is empty. Because the two bands touch at $\boldsymbol{K}, \boldsymbol{K}'$, the Fermi energy sits at the touching energy, i.e. at the Dirac points.

Why "one particle per unit cell per spin" fills the lower band

General statement.
In a translationally invariant lattice with N_{uc} primitive unit cells, the Bloch theorem implies that *each energy band supplies exactly N_{uc} single-particle states in the first Brillouin zone* (per spin component). [a]

Explicit proof in two dimensions. Impose Born–von Karman periodic boundary conditions on a two-dimensional crystal with primitive lattice vectors $\boldsymbol{a}_1, \boldsymbol{a}_2$. Let the system contain N_1 and N_2 primitive unit cells along these directions, so that the total number of unit cells is $N_{\mathrm{uc}} = N_1 N_2$. The periodic boundary conditions require

$$e^{i\boldsymbol{k}\cdot\boldsymbol{L}_i} = 1, \qquad \boldsymbol{L}_i = N_i \boldsymbol{a}_i \ (i = 1, 2),$$

which quantizes crystal momentum as

$$\boldsymbol{k} = \frac{m_1}{N_1}\boldsymbol{b}_1 + \frac{m_2}{N_2}\boldsymbol{b}_2, \qquad m_i \in \{0, \ldots, N_i - 1\},$$

where the reciprocal lattice vectors satisfy $\boldsymbol{a}_i \cdot \boldsymbol{b}_j = 2\pi\delta_{ij}$. The allowed $\boldsymbol{k}$ points therefore form a uniform grid in reciprocal space with spacings $\Delta\boldsymbol{k}_1 = \boldsymbol{b}_1/N_1$ and $\Delta\boldsymbol{k}_2 = \boldsymbol{b}_2/N_2$. Each discrete $\boldsymbol{k}$ state occupies a reciprocal-space area

$$\Delta A_k = \left|\frac{\boldsymbol{b}_1}{N_1} \times \frac{\boldsymbol{b}_2}{N_2}\right| = \frac{|\boldsymbol{b}_1 \times \boldsymbol{b}_2|}{N_1 N_2} = \frac{A_{\mathrm{BZ}}}{N_{\mathrm{uc}}},$$

where $A_{\mathrm{BZ}} = |\boldsymbol{b}_1 \times \boldsymbol{b}_2|$ is the area of the first Brillouin zone. Hence,

$$\#(\boldsymbol{k}\text{-states in the 1st BZ}) = \frac{A_{\mathrm{BZ}}}{\Delta A_k} = N_{\mathrm{uc}}.$$

Since each band contributes one eigenstate at each allowed $\boldsymbol{k}$, each band contains exactly N_{uc} states (per spin).

Higher dimensions. The argument generalizes straightforwardly to arbitrary spatial dimension d: the allowed $\boldsymbol{k}$ points form a d-dimensional grid with elementary cell volume $V_{\mathrm{BZ}}/N_{\mathrm{uc}}$, where V_{BZ} is the volume of the first Brillouin zone. As a result, *each band always contains exactly N_{uc} states per spin*, independent of dimension or lattice geometry.

For the honeycomb lattice, the two bands touch only at isolated Dirac points; therefore, at filling "one particle per unit cell per spin", the Fermi "surface" collapses to these discrete points.

[a] Consequently, for a lattice with two sublattices (hence two bands per spin), filling N_{uc} fermions of a given spin component completely occupies the lower band.This is exactly the Honeycomb NN model.

The system is not a band insulator (no gap), but also differs from an ordinary metal. The extraordinary fact is that near the Dirac point, the density of states approximates 0. This is why

[10] Don't forget we didn't take spin degrees of freedom into account. Actually, spins only contribute to an extra degeneracy.

the phase is called a *Dirac semimetal*: gapless, but with vanishing DOS at the Fermi level.

Derivation of vanishing DOS at Dirac Points.

Near a Dirac point in 2D, $E = \hbar v_F |\boldsymbol{q}|$. The number of states with $|\boldsymbol{q}| < Q$ scales as area in $\boldsymbol{q}$-space:

$$N(E) \propto \int_{|\boldsymbol{q}|<Q} \frac{d^2q}{(2\pi)^2} \propto Q^2 \propto E^2. \tag{125}$$

Hence the density of states (per Dirac cone) behaves as

$$\rho(E) = \frac{dN}{dE} \propto |E|. \tag{126}$$

Therefore $\rho(E_F) = \rho(0) = 0$ when the Fermi energy lies exactly at the Dirac point.

Readers might want to exactly calculate the DOS. We start from the definition:

$$D(E) = \frac{1}{(2\pi)^2} \int_{\mathrm{BZ}} d^2k \, \delta(E - E(\boldsymbol{k})) \, . \tag{127}$$

Using the standard identity for changing variables with the δ-function, the two-dimensional area integral can be reduced to a line integral over the constant-energy contour $C_E = \{ \mathbf{k} : E_+(\mathbf{k}) = E \}$:

$$D(E) = \frac{1}{(2\pi)^2} \int_{C_E} \frac{dl}{|\nabla_{\mathbf{k}} E(\mathbf{k})|}. \tag{128}$$

So, to analytically calculate $D(E)$, you need to:

- find the constant-energy contour(s) (there may be more than one branch);
- compute the group velocity $|\nabla_{\mathbf{k}} E|$;
- perform the line integral along the entire curve.

An alternative and more convenient way is to do it numerically. The procedure is:

- Uniformly sample $\mathbf{k}$ points in the first Brillouin zone
- Evaluate the band energy $E(\mathbf{k})$ and perform energy binning

The result approximates Eq. (127). See Fig. 4a.

2.5 Dirac point as a topological defect: winding number and its locality

Phase factor $\psi(\boldsymbol{k})$ of Pseudo-spin. Recall the NN honeycomb Bloch Hamiltonian

$$H(\boldsymbol{k}) = \begin{pmatrix} 0 & -J_1 f(\boldsymbol{k}) \\ -J_1 f^*(\boldsymbol{k}) & 0 \end{pmatrix}, \qquad f(\boldsymbol{k}) = |f(\boldsymbol{k})| e^{i\varphi(\boldsymbol{k})}. \tag{129}$$

Comparing with the Pauli expansion $H(\boldsymbol{k}) = \boldsymbol{B}(\boldsymbol{k}) \cdot \boldsymbol{\sigma}$, one finds

$$H(\boldsymbol{k}) = -J_1 \Big[\mathrm{Re}\, f(\boldsymbol{k})\, \sigma_x - \mathrm{Im}\, f(\boldsymbol{k})\, \sigma_y \Big], \qquad B_x(\boldsymbol{k}) = -J_1 \mathrm{Re}\, f(\boldsymbol{k}), \quad B_y(\boldsymbol{k}) = +J_1 \mathrm{Im}\, f(\boldsymbol{k}), \quad B_z(\boldsymbol{k}) = 0. \tag{130}$$

Hence $|\boldsymbol{B}(\boldsymbol{k})| = J_1 |f(\boldsymbol{k})|$, and, more importantly, the in-plane direction of $\boldsymbol{B}(\boldsymbol{k})$ is locked to the phase of $f(\boldsymbol{k})$. Indeed,

$$B_x(\boldsymbol{k}) + iB_y(\boldsymbol{k}) = -J_1 f^*(\boldsymbol{k}) = J_1 |f(\boldsymbol{k})|\, e^{i\psi(\boldsymbol{k})}, \qquad \psi(\boldsymbol{k}) := \arg\Big(B_x + iB_y\Big) = \pi - \varphi(\boldsymbol{k}). \tag{131}$$

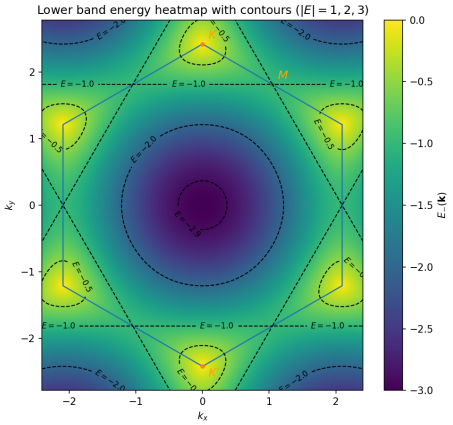

(a) Energy dispersion of the Honeycomb NN model. Set $a = 1$ and $J_1 = 1$. At Dirac points K and K', the energy vanishes, $E = 0$.

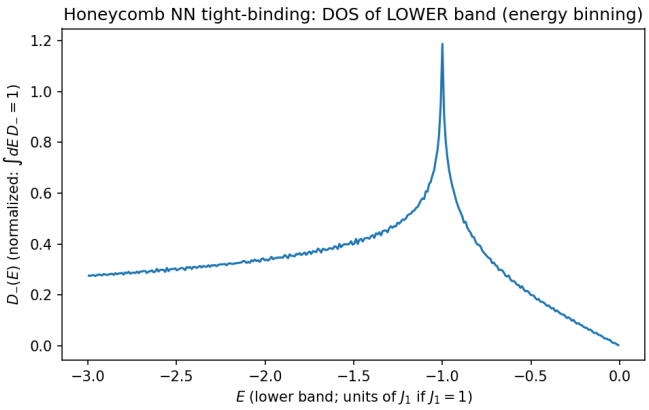

(b) Density of states $D(E)$ for the honeycomb NN model. It exhibits a logarithmic van Hove singularity at $E = \pm J_1$,*i.e.* at the M points of the Brillouin zone.

Figure 4: Honeycomb Lattice Density of States

Therefore the unit vector $\hat{\boldsymbol{B}}(\boldsymbol{k}) = \boldsymbol{B}(\boldsymbol{k})/|\boldsymbol{B}(\boldsymbol{k})|$ lies on the equator $S^1 \subset S^2$:

$$\hat{\boldsymbol{B}}(\boldsymbol{k}) = (\cos\psi(\boldsymbol{k}),\, \sin\psi(\boldsymbol{k}),\, 0). \tag{132}$$

Here $\psi(k)$ is the azimuthal angle of $\hat{\boldsymbol{B}}$ is the $x-y$ plane.

Closed loops avoiding $f(\boldsymbol{k}) = 0$ leads to $\Delta\psi = 2\pi w$.

The band touching points are precisely the zeros of $f(\boldsymbol{k})$ (equivalently $|\boldsymbol{B}(\boldsymbol{k})| = 0$), where the phase $\varphi(\boldsymbol{k})$ and the azimuthal angle $\psi(\boldsymbol{k})$ are ill-defined. Let C be a closed loop in the Brillouin zone that avoids these points, i.e. $f(\boldsymbol{k}) \neq 0$ for all $\boldsymbol{k} \in C$. Then $\psi(\boldsymbol{k})$ can be chosen continuously along C. Upon traversing the loop once, the direction $\hat{\boldsymbol{B}}(\boldsymbol{k}) \in S^1$ must return to itself, so the angle ψ can only change by an integer multiple of 2π:

$$\Delta\psi \equiv \oint_C d\psi = 2\pi w, \qquad w \in \mathbb{Z}. \tag{133}$$

This integer w is the winding number of the map $C \simeq S^1 \to S^1$ defined by $\boldsymbol{k} \mapsto \hat{\boldsymbol{B}}(\boldsymbol{k})$, equivalently by $\boldsymbol{k} \mapsto e^{i\varphi(\boldsymbol{k})}$. Note from Eq. (131) that $d\psi = -d\varphi$, so w can be computed using either angle, up to an overall sign convention.

Definition of the winding number.

Equation (133) motivates the standard definition

$$w(C) = \frac{1}{2\pi}\oint_C d\psi = \frac{1}{2\pi}\oint_C d\boldsymbol{k}\cdot\nabla_{\boldsymbol{k}}\psi(\boldsymbol{k}) = -\frac{1}{2\pi}\oint_C d\boldsymbol{k}\cdot\nabla_{\boldsymbol{k}}\varphi(\boldsymbol{k}). \tag{134}$$

This formula expresses w as the net number of times the in-plane pseudo-spin direction winds as one moves along C.

Equivalent expression in terms of $\hat{\boldsymbol{B}}$.

To eliminate the angular variable (and its branch-cut ambiguities), we derive $d\psi$ directly from (B_x, B_y). Write

$$B_x(\boldsymbol{k}) = \rho(\boldsymbol{k})\cos\psi(\boldsymbol{k}), \qquad B_y(\boldsymbol{k}) = \rho(\boldsymbol{k})\sin\psi(\boldsymbol{k}), \qquad \rho(\boldsymbol{k}) \equiv \sqrt{B_x^2(\boldsymbol{k}) + B_y^2(\boldsymbol{k})} = |\boldsymbol{B}(\boldsymbol{k})|. \tag{135}$$

Differentiating along the loop,

$$\begin{aligned} dB_x &= d\rho\cos\psi - \rho\sin\psi\, d\psi, \\ dB_y &= d\rho\sin\psi + \rho\cos\psi\, d\psi. \end{aligned} \tag{136}$$

Form the combination $B_x\, dB_y - B_y\, dB_x$:

$$\begin{aligned} B_x\, dB_y - B_y\, dB_x &= (\rho\cos\psi)(d\rho\sin\psi + \rho\cos\psi\, d\psi) - (\rho\sin\psi)(d\rho\cos\psi - \rho\sin\psi\, d\psi) \\ &= \rho^2(\cos^2\psi + \sin^2\psi)\, d\psi = \rho^2\, d\psi. \end{aligned} \tag{137}$$

Thus,

$$d\psi = \frac{B_x\, dB_y - B_y\, dB_x}{B_x^2 + B_y^2}. \tag{138}$$

Plugging this into Eq. (134) yields a manifestly gauge-free formula:

$$w(C) = \frac{1}{2\pi}\oint_C \frac{B_x\, dB_y - B_y\, dB_x}{B_x^2 + B_y^2}. \tag{139}$$

In the NN honeycomb model $B_z = 0$, so $\hat{B}_x^2 + \hat{B}_y^2 = 1$ and $\hat{B}_{x,y} = B_{x,y}/\sqrt{B_x^2 + B_y^2}$. Therefore Eq. (139) can be written purely in terms of the unit vector:

$$w(C) = \frac{1}{2\pi}\oint_C \left(\hat{B}_x\, d\hat{B}_y - \hat{B}_y\, d\hat{B}_x\right), \tag{140}$$

Since $\hat{B}$ is a functor of $\boldsymbol{k}$, one can write Eq. (140) as:

$$\boxed{w(C) = \frac{1}{2\pi}\oint_C \left[(\hat{\boldsymbol{B}}_x(k)\,\partial_k\hat{\boldsymbol{B}}_y(k) - \hat{\boldsymbol{B}}_y(k)\,\partial_k\hat{\boldsymbol{B}}_x(k)\right].} \tag{141}$$

The integrand is the oriented area form on the target circle S^1, and the integral counts how many times $\hat{\boldsymbol{B}}$ winds around the equator.

Berry connection and Berry phase: $\gamma_\pm(C) = \pm\pi\, w(C)$ in the equator case

Using the eigenvectors chosen earlier,

$$|u_+(\boldsymbol{k})\rangle = \frac{1}{\sqrt{2}}\begin{pmatrix} 1 \\ -e^{-i\varphi(k)} \end{pmatrix}, \qquad |u_-(\boldsymbol{k})\rangle = \frac{1}{\sqrt{2}}\begin{pmatrix} 1 \\ +e^{-i\varphi(k)} \end{pmatrix},$$

the Berry connection $\boldsymbol{A}_\pm(\boldsymbol{k}) = i\langle u_\pm(\boldsymbol{k})|\nabla_{\boldsymbol{k}} u_\pm(\boldsymbol{k})\rangle$ evaluates to

$$\boldsymbol{A}_+(\boldsymbol{k}) = \frac{1}{2}\nabla_k\varphi(\boldsymbol{k}), \qquad \boldsymbol{A}_-(\boldsymbol{k}) = -\frac{1}{2}\nabla_k\varphi(\boldsymbol{k}).$$

Hence the Berry phase acquired along a closed loop C is

$$\gamma_\pm(C) = \oint_C d\boldsymbol{k}\cdot\boldsymbol{A}_\pm(\boldsymbol{k}) = \pm\frac{1}{2}\oint_C d\boldsymbol{k}\cdot\nabla_k\varphi(\boldsymbol{k}) = \mp\pi\, w(C),$$

where the last equality uses $w(C) = -\frac{1}{2\pi}\oint_C d\boldsymbol{k}\cdot\nabla_k\varphi(\boldsymbol{k})$ from Eq. (134). Therefore, when $B_z = 0$ (pseudo-spin confined to the equator), the winding number controls the quantized Berry phase (modulo 2π gauge ambiguity): $\gamma_\pm(C) \in \pi\,\mathbb{Z}$ with $\gamma_\pm(C) = \pm\pi w(C)$ up to the fixed sign convention relating ψ and φ.

■ **If the loop does not enclose a Dirac point, why the winding is zero.**

If C can be continuously contracted to a point without crossing any band touching, then $\varphi(\boldsymbol{k})$ can be chosen continuously on the disk bounded by C. In that case $\oint_C d\varphi = 0$, hence $w(C) = 0$. Nonzero winding requires an obstruction to defining a single-valued phase inside the loop, which is precisely the presence of a singularity where $f(\boldsymbol{k}) = 0$, i.e. a Dirac point enclosed by C.

Weyl semimetal

In 3D two-band models, a generic Bloch Hamiltonian $H(\boldsymbol{k}) = \boldsymbol{B}(\boldsymbol{k}) \cdot \boldsymbol{\sigma}$ has three components. Solving $\boldsymbol{B}(\boldsymbol{k}) = 0$ is three equations in three variables (k_x, k_y, k_z), so isolated band-touching points are stable and generic; these are Weyl points. Topologically, one considers a closed 2D surface S^2 in momentum space enclosing the Weyl point, and the map $S^2 \to S^2$ (Bloch sphere) is classified by $\Pi_2(S^2) = \mathbb{Z}$, i.e. a Chern number. The Weyl point behaves as a monopole source of Berry curvature in momentum space.

2.6 Stability of Dirac points under perturbations

Perturbations that shift but do not gap the Dirac points. Generic small perturbations that preserve the condition $B_z(\boldsymbol{k}) = 0$ deform $B_x(\boldsymbol{k}), B_y(\boldsymbol{k})$ continuously. Dirac points are solutions to

$$B_x(\boldsymbol{k}) = 0, \qquad B_y(\boldsymbol{k}) = 0. \tag{142}$$

In 2D, this is two equations for two variables (k_x, k_y), so solutions typically persist under small deformations: the Dirac points move in the BZ and the Dirac velocity changes, but the gap remains closed.

How to gap: a $B_z(\boldsymbol{k})\sigma_z$ term. Adding a σ_z term makes gap opening generic, because simultaneously solving $B_x = B_y = B_z = 0$ is overconstrained in 2D. Thus an infinitesimal B_z term typically gaps the Dirac points. Physically, such a term must break a symmetry that forbids σ_z (e.g. inversion or time-reversal, depending on the microscopic realization).

Annihilation by merging. Dirac points come in pairs with opposite winding. A strong distortion can move them together until they merge and annihilate. Beyond that point, there is no band touching and a full gap opens, producing a semimetal-to-insulator transition.

Symmetry protection: why a mass term $B_z(\boldsymbol{k})\sigma_z$ can be forbidden

In the two-band (sublattice) form $H(\boldsymbol{k}) = B_x(\boldsymbol{k})\sigma_x + B_y(\boldsymbol{k})\sigma_y + B_z(\boldsymbol{k})\sigma_z$, a nonzero B_z acts as a *mass term* that generically gaps Dirac points. In many lattice realizations, however, $B_z(\boldsymbol{k}) \equiv 0$ is enforced by symmetry.

(i) Inversion $\mathcal{P}$. For a honeycomb inversion center at the plaquette center, $\mathcal{P}$ exchanges $A \leftrightarrow B$ and sends $\boldsymbol{k} \to -\boldsymbol{k}$, so in the sublattice basis it acts as[a]

$$\mathcal{P}: \quad H(\boldsymbol{k}) \;\mapsto\; \sigma_x H(-\boldsymbol{k})\, \sigma_x.$$

Requiring $\sigma_x H(-\boldsymbol{k})\sigma_x = H(\boldsymbol{k})$ implies the component constraints

$$B_x(\boldsymbol{k}) = B_x(-\boldsymbol{k}), \qquad B_y(\boldsymbol{k}) = -B_y(-\boldsymbol{k}), \qquad B_z(\boldsymbol{k}) = -B_z(-\boldsymbol{k}).$$

(ii) Time reversal $\mathcal{T}$ (spinless). For spinless bands, $\mathcal{T}$ acts by complex conjugation together with $\boldsymbol{k} \to -\boldsymbol{k}$. Using $\sigma_x^* = \sigma_x$, $\sigma_y^* = -\sigma_y$, $\sigma_z^* = \sigma_z$, the invariance condition

$$\mathcal{T}: \quad H(\boldsymbol{k}) \;\mapsto\; H^*(-\boldsymbol{k}) = H(\boldsymbol{k})$$

gives

$$B_x(\boldsymbol{k}) = B_x(-\boldsymbol{k}), \qquad B_y(\boldsymbol{k}) = -B_y(-\boldsymbol{k}), \qquad B_z(\boldsymbol{k}) = B_z(-\boldsymbol{k}).$$

Combining $\mathcal{P}$ and $\mathcal{T}$. Inversion forces B_z to be *odd* in $\boldsymbol{k}$, while time reversal forces B_z to be *even*. The only function that is both even and odd is zero, hence

$$B_z(\boldsymbol{k}) \equiv 0.$$

Therefore the Dirac semimetal is *symmetry-protected*: any perturbation that preserves both $\mathcal{P}$ and $\mathcal{T}$ cannot generate a σ_z mass term. Conversely, breaking either symmetry generically allows $B_z(\boldsymbol{k})\sigma_z$ and opens a gap (e.g. the Haldane-type mechanism).

[a] With the inversion center chosen at the center of a hexagonal plaquette, the inversion operation exchanges the two sublattices $A \leftrightarrow B$; in the (A, B) basis this swap is represented by σ_x.

3 SSH Model as a Topological Band Insulator

According to the last chapter, semimetal is characterized by topology tied to *gapless* points (defects) in momentum space. In contrast, a topological band insulator is fully gapped in the bulk; its topology is defined by the mapping from the *entire* Brillouin zone to the Bloch eigenstate manifold. This is the setting where bulk-edge correspondence and robust boundary modes are most transparent.

3.1 Model definition and physical picture

SSH Hamiltonian. The Su–Schrieffer–Heeger (SSH) model is a 1D chain with two sites per unit cell (sublattices A, B) and staggered hoppings:

$$\hat{H}_{\mathrm{SSH}} = -J_1 \sum_i \left(\hat{c}^\dagger_{A,i}\hat{c}_{B,i} + \mathrm{h.c.}\right) - J_2 \sum_i \left(\hat{c}^\dagger_{A,i+1}\hat{c}_{B,i} + \mathrm{h.c.}\right). \tag{143}$$

Historically, it models electrons in dimerized polyacetylene, where alternating bond strengths lead to two distinct insulating phases.

Two gapped phases and boundary sensitivity. Both $J_1 \neq J_2$ regimes are gapped in the bulk, but they differ by a topological invariant and (under appropriate symmetry) by the presence/absence of zero-energy edge modes in an open chain.

3.2 Momentum-space Hamiltonian, Brillouin zone, and Pauli form

Fourier transform. Let the unit-cell spacing be a (so the physical lattice spacing is $a/2$). Define

$$\hat{c}_{A,i} = \frac{1}{\sqrt{N}} \sum_k \hat{c}_A(k) e^{ikai}, \qquad \hat{c}_{B,i} = \frac{1}{\sqrt{N}} \sum_k \hat{c}_B(k) e^{ikai}. \tag{144}$$

Then

$$\hat{H}_{\mathrm{SSH}} = \sum_k \begin{pmatrix} \hat{c}^\dagger_A(k) & \hat{c}^\dagger_B(k) \end{pmatrix} H(k) \begin{pmatrix} \hat{c}_A(k) \\ \hat{c}_B(k) \end{pmatrix}, \tag{145}$$

with

$$H(k) = \begin{pmatrix} 0 & J_1 + J_2 e^{-ika} \\ J_1 + J_2 e^{ika} & 0 \end{pmatrix}. \tag{146}$$

Brillouin zone as a circle. The first BZ is $k \in [-\pi/a, \pi/a]$ with endpoints identified, hence topologically S^1. The Hamiltonian is periodic: $H(k + 2\pi/a) = H(k)$.

Pauli representation. Write

$$H(k) = B_x(k)\sigma_x + B_y(k)\sigma_y, \tag{147}$$

where

$$B_x(k) = J_1 + J_2\cos(ka), \qquad B_y(k) = J_2\sin(ka), \tag{148}$$

and $B_z(k) = 0$. The spectrum is

$$E_\pm(k) = \pm|\boldsymbol{B}(k)| = \pm\sqrt{B_x^2(k) + B_y^2(k)}. \tag{149}$$

See Fig 5 for a graphic understanding.

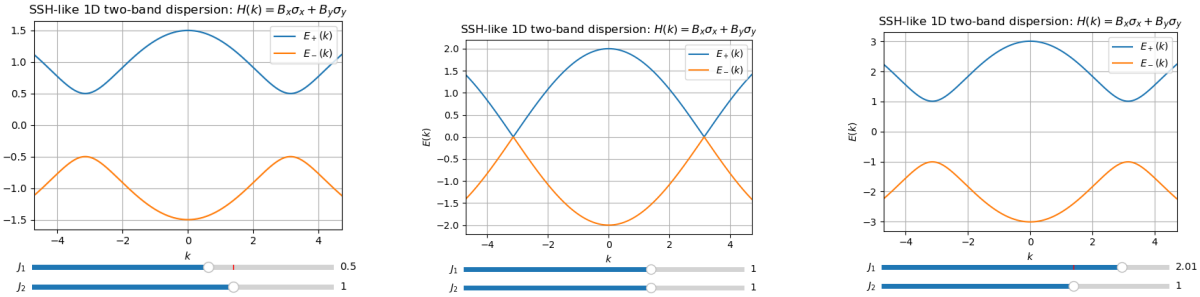

(a) $J_1 < J_2$ $(w = 0)$ (b) $J_1 = J_2$ (c) $J_1 > J_2$ $(w = 1)$

Figure 5: Energy Dispersion of SSH Model

3.3 Topology: winding number, phase transition, and why σ_z matters

Map $S^1_{\mathrm{BZ}} \to S^1_{\hat{\boldsymbol{B}}}$ and $\Pi_1(S^1) = \mathbb{Z}$. Because $B_z = 0$, $\hat{\boldsymbol{B}}(k) = \boldsymbol{B}(k)/|\boldsymbol{B}(k)|$ lies on a circle. Thus the gapped SSH Hamiltonian defines a map

$$k \in S^1_{\mathrm{BZ}} \longrightarrow \hat{\boldsymbol{B}}(k) \in S^1, \tag{150}$$

whose homotopy classification is $\Pi_1(S^1) = \mathbb{Z}$. The invariant is the winding number.

Winding number and its evaluation.

The derivation is similar to that in Sec 2.5. Let $q(k) = J_1 + J_2e^{-ika} = |q(k)|e^{-i\varphi(k)}$. Then

$$w = \frac{1}{2\pi}\int_{-\pi/a}^{\pi/a} dk\, \partial_k\varphi(k). \tag{151}$$

Geometrically, $\boldsymbol{B}(k) = (B_x, B_y)$ traces a circle of radius $|J_2|$ centered at $(J_1, 0)$.[11] If the origin lies inside the traced loop, $w = 1$; otherwise $w = 0$. This, for $J_1, J_2 > 0$,

$$w = \begin{cases} 0, & J_1 > J_2, \\ 1, & J_2 > J_1. \end{cases} \tag{152}$$

Topological phase transition and gap closing. If $J_1 \neq J_2$, then $|\boldsymbol{B}(k)| \neq 0$ for all k and the system is gapped. At the transition point $J_1 = J_2$, one finds $B_x = B_y = 0$ at $k = \pm\pi/a$, hence the bulk gap closes at the BZ edge.

[11] If you don't understand why, refer to Eq. (148). You should feel shamed and apologize to your high school math teacher for you sluggish response.

A σ_z term destroys the 1D winding classification

If a term $B_z(k)\sigma_z$ is allowed generically, then $\hat{\boldsymbol{B}}(k)$ lives on the full Bloch sphere S^2, and the relevant homotopy becomes $\Pi_1(S^2)$, which is trivial. Concretely, once $B_z \neq 0$ is permitted, one can continuously deform the loop $\hat{\boldsymbol{B}}(k)$ on S^2 to a point without closing the gap, connecting the two SSH phases. Thus, the nontrivial classification requires a symmetry that forbids B_z (often called **chiral/sublattice symmetry** in SSH, and also realizable via **time-reversal** + **inversion** in suitable settings).

Thus, the SSH model realizes two distinct gapped phases distinguished by a winding number; their boundary requires a gap closing at the transition $J_1 = J_2$, see Fig **??**. Bulk gap closure enables topology change.

3.4 Chiral Symmetry: the core protecting symmetry of the SSH model

A central structural feature of the SSH chain is the *chiral*(or *sublattice*) symmetry ,which enforces an energy spectrum symmetric about zero and underlies the existence of robust midgap edge states[12] in the topological phase.

In a higher-level perspective, the chiral symmetry is the symmetry that protects the SSH model (in $J_1 < J_2$ regime) as an SPT.

Definition of Chiral Symmetry. In the single-particle Hamiltonian language, *chiral symmetry* means that there exists a unitary operator Γ such that

$$\Gamma^2 = \mathbb{I}, \qquad \{\Gamma, H\} = 0,$$

i.e.,

$$\Gamma H \Gamma^{-1} = -H. \tag{153}$$

Chiral symmetry in the Pauli Pseudo-spin Description

In the Pauli Pseudo-spin description of a two-sublattice, two-band model, the single-particle Hamiltonian can be written as

$$H(k) = B_x(k)\,\sigma_x + B_y(k)\,\sigma_y + B_z(k)\,\sigma_z, \tag{154}$$

where the Pauli matrices act in the sublattice basis (A/B). The SSH model has a unitary operator $\Gamma = \sigma_z$ [a] such that

$$\Gamma^2 = \mathbb{I}, \qquad \{\Gamma, H(k)\} = 0, \tag{155}$$

Thus, Eq. (155) immediately forbids any term proportional to σ_z, because $\{\sigma_z, \sigma_z\} = 2\mathbb{I}$ while $\{\sigma_z, \sigma_{x,y}\} = 0$. Hence, chiral symmetry enforces the constraint

$$B_z(k) \equiv 0, \tag{156}$$

so that the Bloch vector $\boldsymbol{B}(k) = (B_x, B_y, B_z)$ is restricted to the equatorial plane.

[a] It assigns opposite "chiral charges" to the two sublattices

Paired Energy Eigenvalues. The spectral implication of Eq. (155) is extremely important. If $H(k)\,|u_k\rangle = E(k)\,|u_k\rangle$, then

$$H(k)\Big(\Gamma\,|u_k\rangle\Big) = -E(k)\Big(\Gamma\,|u_k\rangle\Big). \tag{157}$$

[12] If the chain is periodic, there is a gap between two bands when $J_1 \neq J_2$, with positive and negative energies respectively. Here "midgap" means the existence of *zero-energy states* within the band gap.

So: **All nonzero energies appear in $\pm E$ pairs**.

As shown in the next subsection, this mechanism allows for the existence of zero-energy states. They show up in open chains and appear as boundary-localized modes. Breaking chiral symmetry by allowing an on-site sublattice imbalance (a "mass" term) $m\sigma_z$ generically shifts such modes away from zero energy and removes the integer winding classification without requiring a bulk gap closing. In this precise sense, chiral symmetry is the minimal and canonical protecting symmetry for the SSH topological distinction and its associated robust edge physics.

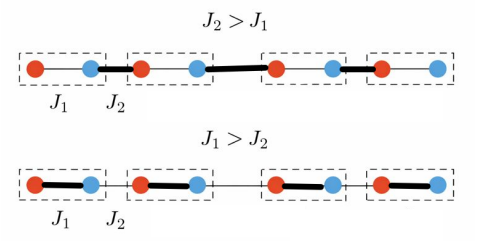

Figure 6: SSH Model, graphically presented in $J_1 < J_2$ (upper) and $J_1 > J_2$ (lower) regime. The bold line means stronger interactions.

3.5 Edge modes in an open chain

Readers may notice that Fig 5a and Fig 9b quite the same, though they have different winding numbers respectively. A natural question is:

"Why are they *physically* different?"

To answer this question, let's cut the periodic ring open, and see what topological physics happens in the boundary.

Open-boundary SSH Hamiltonian.

To expose boundary physics we now impose *open boundary conditions* (OBC) on a finite chain with N unit cells labeled by $i = 1, 2, \ldots, N$. The SSH Hamiltonian in real space is

$$\hat{H}_{\mathrm{SSH}}^{(\mathrm{OBC})} = -\sum_{i=1}^{N} \left(J_1 \, \hat{c}_{B,i}^{\dagger} \hat{c}_{A,i} + \mathrm{h.c.} \right) - \sum_{i=1}^{N-1} \left(J_2 \, \hat{c}_{A,i+1}^{\dagger} \hat{c}_{B,i} + \mathrm{h.c.} \right). \tag{158}$$

Compared with PBC, the inter-cell bond connecting B_N to A_1 is absent, and the two ends are physically distinct, see Fig 6.

Fly-by-Night analysis. Let us do a "Fly-by-Night" analysis[13].

- **Limit I: $J_2 \to 0$ with J_1 finite.** In this limit, particles are paired *within each unit cell*, and different unit cells decouple from each other. Each unit cell reduces to an independent two-orbital problem with an effective Hamiltonian

$$H_{\mathrm{pair}} \sim J_1 \, \hat{c}_A^{\dagger} \hat{c}_B + J_1^{*} \, \hat{c}_B^{\dagger} \hat{c}_A \sim \begin{pmatrix} 0 & J_1^{*} \\ J_1 & 0 \end{pmatrix},$$

  whose eigenvalues are $E = \pm |J_1|$. Therefore, the whole chain has a spectrum $E_{\pm} = \pm |J_1|$, each with N-fold degeneracy, where N is the number of unit cells. See Fig. 7a.

- **Limit II: $J_1 \to 0$ with J_2 finite.** In this limit, the leftmost A orbital and the rightmost B orbital are completely decoupled from the rest of the chain, while all other orbitals form

[13] This name comes from Anthony Zee. It means understanding a problem by making intuitive, back-of-the-envelope estimates and simplifying assumptions.

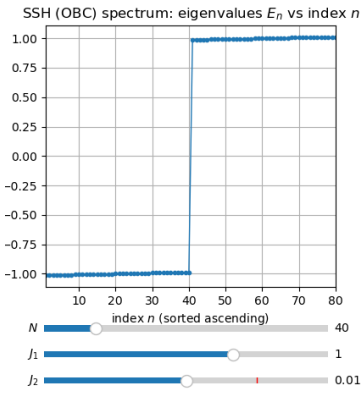

(a) J_1 finite, $J_2 = 0$. There are two degenerate energies $\pm|J_1|$

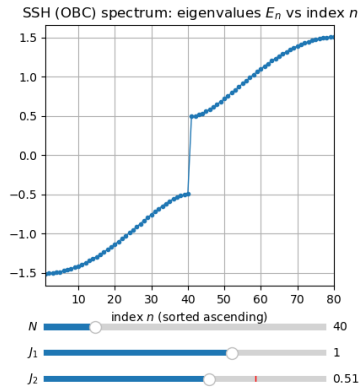

(b) $J_1 > J_2 \quad (w = 0)$. The system is gapped.

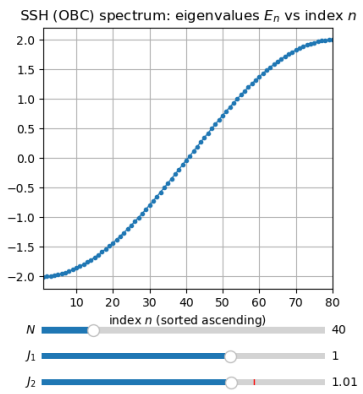

(c) $J_1 = J_2$. The system is gapless.

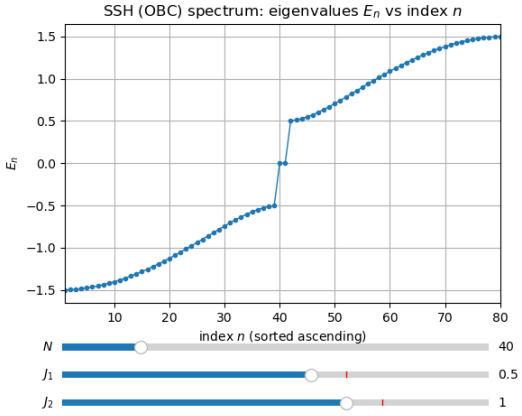

(d) $J_1 < J_2 \quad (w = 1)$. The system is gapped, with two in-gap zero-energy state.

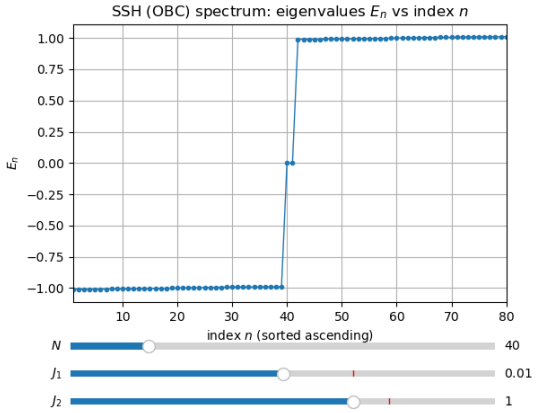

(e) $J_1 = 0$,J_2 finite. There are two degenerate energies $\pm|J_1|$, and two zero-energy states.

Figure 7: Energy Spectrum of Open Boundary SSH Model

$(N-1)$ inter-unit-cell pairs. If a particle occupies one of these boundary orbitals, every hopping term in $\hat{H}_{\text{SSH}}$ annihilates the state, so its energy is exactly zero. Meanwhile, each inter-unit-cell pair contributes eigenvalues $E = \pm|J_2|$. Hence the spectrum consists of $E_\pm = \pm|J_2|$ with $(N-1)$-fold degeneracy each, *plus* two zero-energy modes. See Fig. 7e.

In short, the presence or absence of "dangling" boundary orbitals directly corresponds to the presence or absence of zero-energy edge modes.

Next, we start from the exactly solvable point $J_1 = 0$ and adiabatically turn on J_1 while keeping $J_1 < J_2$. The system remains gapped throughout this deformation. Intuitively, the boundary zero mode cannot smoothly merge into the bulk continuum without a gap closing, so we expect it to persist [14]. See Figs. 7b, 7c, and 7d for numerical results, which confirm this analysis.

Single-particle Schrödinger equations on a bipartite lattice.

To exactly understand the zero-energy mode at $J_1 < J_2$ regime, we solve the Hamiltonian by supposing a parametrized *single-particle wavefunction*. Because $\hat{H}_{\text{SSH}}$ is quadratic, the problem reduces to single-particle eigenstates. Consider a general single-particle state

$$|\psi\rangle = \sum_{i=1}^{N} \left(\psi_{A,i}\, \hat{c}^\dagger_{A,i} + \psi_{B,i}\, \hat{c}^\dagger_{B,i} \right) |0\rangle, \tag{159}$$

[14] Although it will generally become exponentially localized rather than strictly confined to a single site

and impose the eigenequation $\hat{H}_{\mathrm{SSH}}^{(\mathrm{OBC})}|\psi\rangle = E|\psi\rangle$. Collecting coefficients of $\hat{c}_{A,i}^{\dagger}|0\rangle$ and $\hat{c}_{B,i}^{\dagger}|0\rangle$ yields the coupled difference equations

$$E\,\psi_{A,i} = -J_1\,\psi_{B,i} - J_2\,\psi_{B,i-1}, \qquad (i = 1,\ldots,N), \tag{160}$$

$$E\,\psi_{B,i} = -J_1\,\psi_{A,i} - J_2\,\psi_{A,i+1}, \qquad (i = 1,\ldots,N), \tag{161}$$

where the open boundaries are encoded by the conventions

$$\psi_{B,0} \equiv 0, \qquad \psi_{A,N+1} \equiv 0. \tag{162}$$

These boundary conditions simply express the absence of sites B_0 and A_{N+1} in the open chain.

Why a quadratic Hamiltonian reduces to a single-particle eigenproblem

The SSH Hamiltonian is *quadratic* (free-fermion), i.e. it contains only bilinears of the form $\hat{H} = \sum_{i,j} h_{ij}\,\hat{c}_i^{\dagger}\hat{c}_j$
In this case the many-body problem is completely determined by the *single-particle* matrix h. Indeed, diagonalizing h as $\sum_j h_{ij}u_{n,j} = \varepsilon_n u_{n,i}$ and defining normal-mode operators $\hat{\gamma}_n^{\dagger} = \sum_i u_{n,i}\hat{c}_i^{\dagger}$, one obtains $\hat{H} = \sum_n \varepsilon_n\,\hat{\gamma}_n^{\dagger}\hat{\gamma}_n$. Hence many-body eigenstates are Slater determinants obtained by occupying single-particle modes.

■ **Constructing the left edge mode at $E = 0$.**

We now solve Eqs. (160)–(161) at $E = 0$. Setting $E = 0$ decouples the two sublattices into independent recursion relations:

$$0 = -J_1\,\psi_{B,i} - J_2\,\psi_{B,i-1}, \tag{163}$$

$$0 = -J_1\,\psi_{A,i} - J_2\,\psi_{A,i+1}. \tag{164}$$

A *left-localized* solution is obtained by choosing support entirely on the A sublattice,

$$\psi_{B,i} = 0 \quad \forall i. \tag{165}$$

Then Eq. (163) is automatically satisfied, and Eq. (164) becomes the simple recurrence

$$J_1\,\psi_{A,i} + J_2\,\psi_{A,i+1} = 0 \quad \Longrightarrow \quad \psi_{A,i+1} = -\frac{J_1}{J_2}\,\psi_{A,i}. \tag{166}$$

Iterating,

$$\psi_{A,i} = \left(-\frac{J_1}{J_2}\right)^{i-1}\psi_{A,1}, \qquad i = 1,\ldots,N. \tag{167}$$

This wavefunction is exponentially localized near the left boundary provided

$$\left|\frac{J_1}{J_2}\right| < 1, \tag{168}$$

which, for $J_1, J_2 > 0$, is precisely the topological regime $J_2 > J_1$ (the same regime where the bulk winding is $w = 1$). A convenient normalization is

$$1 = \sum_{i=1}^{N}|\psi_{A,i}|^2 = |\psi_{A,1}|^2\sum_{i=0}^{N-1}\left|\frac{J_1}{J_2}\right|^{2i} \quad \Longrightarrow \quad |\psi_{A,1}|^2 = \left[\sum_{i=0}^{N-1}\left(\frac{J_1}{J_2}\right)^{2i}\right]^{-1}. \tag{169}$$

In the thermodynamic limit $N \to \infty$ (with $J_1 < J_2$),

$$|\psi_{A,1}|^2 \to 1 - \left(\frac{J_1}{J_2}\right)^2, \qquad |\psi_{A,i}| \sim \exp\left[-\frac{i-1}{\xi}\right], \qquad \xi^{-1} = \ln\left|\frac{J_2}{J_1}\right|. \tag{170}$$

■ **Constructing the right edge mode at $E = 0$.**

Similarly, a *right-localized* $E = 0$ solution is obtained by choosing support entirely on the B sublattice,

$$\psi_{A,i} = 0 \quad \forall i. \tag{171}$$

Then Eq. (164) is automatic, and Eq. (163) gives

$$J_1\,\psi_{B,i} + J_2\,\psi_{B,i-1} = 0 \quad \Longrightarrow \quad \psi_{B,i-1} = -\frac{J_1}{J_2}\,\psi_{B,i}. \tag{172}$$

Iterating from the right boundary,

$$\psi_{B,i} = \left(-\frac{J_1}{J_2}\right)^{N-i} \psi_{B,N}, \qquad i = 1, \ldots, N, \tag{173}$$

which is exponentially localized near $i = N$ under the same condition $|J_1/J_2| < 1$. Thus, for $J_2 > J_1$ an open chain supports *two* exponentially localized midgap states, one on each end, living on opposite sublattices.

Finite-size splitting and robustness. For a finite chain, the two edge wavefunctions have exponentially small overlap when $N \gg \xi$. Because chiral symmetry pairs nonzero energies as $\pm E$, the only way to move a single isolated boundary mode away from $E = 0$ is to hybridize it with another boundary mode. Indeed, the left and right zero modes can weakly couple through their exponentially decaying tails, producing an energy splitting[15]

$$E_{\text{split}} \sim \left(\frac{J_1}{J_2}\right)^N, \tag{174}$$

up to prefactors. In the limit $N \to \infty$ the splitting vanishes and the boundary modes are pinned at zero energy. Perturbations that preserve the sublattice (chiral) symmetry cannot generate an onsite σ_z term and therefore cannot remove the edge modes without either (i) closing the bulk gap (as at $J_1 = J_2$) or (ii) causing the two edge modes to meet and annihilate via hybridization in a finite system.

3.6 SPT viewpoint

The SSH topological distinction ,and associated robust zero-energy edge modes in an open chain, relies on symmetries that protect the effective constraint $B_z = 0$ and prevent adiabatic interpolation between the two phases without closing the gap. In this sense, SSH is a canonical 1D example of an SPT phase. Here, the protecting symmetry can be thought of as the chiral symmetry Γ, or as the inversion and time reversal symmetry, $\mathcal{P} \times \mathcal{T}$. Topology is stable only within a symmetry class.

4 Haldane Model as a Topological Band Insulator

4.1 Motivation: gapping Dirac points and realizing a Chern insulator

From Dirac semimetal to gapped topological phase. In honeycomb lattices, the nearest-neighbor model has Dirac points protected by the absence of a σ_z term. To obtain a gapped insulator at half-filling, one must generate an effective mass term $B_z(\boldsymbol{k})\sigma_z$. Depending on how this is achieved, one can obtain a trivial insulator or a topological (Chern) insulator.

[15] This splitting is exponetial with system size N. If a gap has expotential behavior with system size, we ususally say it is *degenerate* (though it is only degenerate in thermaldynamical limit).

Haldane's idea. Haldane's model realizes a quantum anomalous Hall (QAH) phase: a gapped band insulator with nonzero Chern number and chiral edge modes, achieved *without net magnetic flux per unit cell*. This is done by complex next-nearest-neighbor hoppings that break time-reversal symmetry while keeping zero average flux.

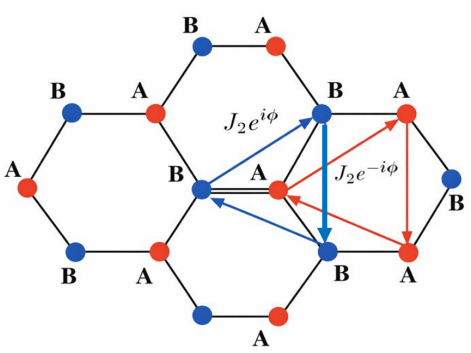

Figure 8: Haldane Model.

4.2 Model definition and momentum-space Hamiltonian

Real-space Hamiltonian. The Haldane model on a honeycomb lattice includes:

- nearest-neighbor hopping J_1 between A and B;
- next-nearest-neighbor hopping J_2 within the same sublattice, with opposite phases $\pm\phi$ on A and B;
- a staggered sublattice potential M (on-site energy difference).

Explicitly,

$$\begin{aligned}\hat{H}_{\text{Hal}} = -J_1 \sum_{\langle ij\rangle} \left(\hat{c}^\dagger_{B,j}\hat{c}_{A,i} + \text{h.c.}\right) + J_2 \sum_{\langle\langle ij\rangle\rangle} \left(e^{-i\phi}\hat{c}^\dagger_{A,j}\hat{c}_{A,i} + e^{i\phi}\hat{c}^\dagger_{B,j}\hat{c}_{B,i} + \text{h.c.}\right) \\ + M\sum_i \left(\hat{c}^\dagger_{A,i}\hat{c}_{A,i} - \hat{c}^\dagger_{B,i}\hat{c}_{B,i}\right).\end{aligned} \tag{175}$$

Momentum-space form. In (A, B) basis,

$$H(\boldsymbol{k}) = E_0(\boldsymbol{k})\, I + \boldsymbol{B}(\boldsymbol{k}) \cdot \boldsymbol{\sigma}, \tag{176}$$

with

$$E_0(\boldsymbol{k}) = 2J_2 \cos\phi \sum_{\mu=1}^{3} \cos(\boldsymbol{k}\cdot\boldsymbol{a}_\mu), \tag{177}$$

and

$$B_z(\boldsymbol{k}) = M + 2J_2 \sin\phi \sum_{\mu=1}^{3} \sin(\boldsymbol{k}\cdot\boldsymbol{a}_\mu). \tag{178}$$

The components $B_x(\boldsymbol{k}), B_y(\boldsymbol{k})$ come from the NN term and have the same structure as in the Dirac semimetal case, see Eq. (111) and Eq. (112). The definition of $\boldsymbol{a}_\mu$ can be found in Eq. (92).

4.3 Berry connection, Berry curvature, and the Chern number

Recap: Berry connection and curvature. For an isolated Bloch band, let $|u_n(\boldsymbol{k})\rangle$ denote the cell-periodic eigenstate of the Bloch Hamiltonian $H(\boldsymbol{k})$. The freedom $|u_n(\boldsymbol{k})\rangle \mapsto e^{i\chi(\boldsymbol{k})}|u_n(\boldsymbol{k})\rangle$ defines a $U(1)$ gauge structure over the Brillouin zone (BZ). The associated Berry connection (a $\boldsymbol{k}$-space "vector potential") is

$$\boldsymbol{A}_n(\boldsymbol{k}) \equiv i\langle u_n(\boldsymbol{k})|\nabla_{\boldsymbol{k}} u_n(\boldsymbol{k})\rangle\,, \tag{179}$$

and the Berry curvature (a $\boldsymbol{k}$-space "magnetic field") is

$$\Omega_n(\boldsymbol{k}) \equiv \partial_{k_x} A_{n,y}(\boldsymbol{k}) - \partial_{k_y} A_{n,x}(\boldsymbol{k}). \tag{180}$$

Under a gauge transformation $\chi(\boldsymbol{k})$, $\boldsymbol{A}_n \to \boldsymbol{A}_n - \nabla_{\boldsymbol{k}}\chi$ while $\Omega_n(\boldsymbol{k})$ is gauge invariant.

Chern number as the total Berry flux over the BZ. In two dimensions, the first Chern number of band n is defined by

$$C_n \equiv \frac{1}{2\pi}\int_{\mathrm{BZ}} d^2k\,\Omega_n(\boldsymbol{k}) \in \mathbb{Z}. \tag{181}$$

The structure of Eq. (181) is directly motivated by the electromagnetic analogy: $\boldsymbol{A}_n$ plays the role of a vector potential, Ω_n the role of a magnetic field, and $\int_{\mathrm{BZ}} \Omega_n\, d^2k$ the total "Berry flux" through the BZ. Since the BZ is a closed manifold (a two-torus T^2), the total Berry flux is quantized in units of 2π, hence $C_n \in \mathbb{Z}$(the detailed explanation is left in a following box).

Why the "Berry flux" is quantized?

Since the BZ is a closed manifold (topologically a two-torus T^2), the Berry connection $\boldsymbol{A}_n(\boldsymbol{k})$ cannot, in general, be chosen globally smooth over the entire BZ when the band bundle is topologically nontrivial. A concrete way to see the quantization is to cover the BZ by two overlapping patches U_1, U_2 on which smooth gauges $|u_n^{(1)}(\boldsymbol{k})\rangle$, $|u_n^{(2)}(\boldsymbol{k})\rangle$ exist. On the overlap $U_1 \cap U_2$, they differ by a $U(1)$ transition function

$$|u_n^{(2)}(\boldsymbol{k})\rangle = e^{i\chi(\boldsymbol{k})}|u_n^{(1)}(\boldsymbol{k})\rangle\,,$$

so the connections satisfy $\boldsymbol{A}^{(2)} = \boldsymbol{A}^{(1)} - \nabla_{\boldsymbol{k}}\chi$, while the curvature Ω is the same on both patches. Using Stokes' theorem on each patch and adding the results, the total Berry flux becomes a boundary integral along the patch interface $\partial U_1 = -\partial U_2$:

$$\int_{\mathrm{BZ}} d^2k\,\Omega = \int_{U_1} d^2k\,(\nabla\times\boldsymbol{A}^{(1)}) + \int_{U_2} d^2k\,(\nabla\times\boldsymbol{A}^{(2)}) = \oint_{\partial U_1} (\boldsymbol{A}^{(1)} - \boldsymbol{A}^{(2)})\cdot d\boldsymbol{\ell} = \oint_{\partial U_1} \nabla_{\boldsymbol{k}}\chi\cdot d\boldsymbol{\ell}.$$

But $\oint \nabla\chi\cdot d\boldsymbol{\ell} = \Delta\chi$ is the net winding of the $U(1)$ phase around the loop, hence it must be $2\pi m$ with $m \in \mathbb{Z}$. Therefore the total Berry flux is quantized in units of 2π, and

$$C_n = \frac{1}{2\pi}\int_{\mathrm{BZ}} d^2k\,\Omega_n(\boldsymbol{k}) \in \mathbb{Z}.$$

Physical meaning: anomalous velocity and quantized Hall response (derivation)

In semiclassical dynamics, a wavepacket built from band n obeys

$$\dot{\boldsymbol{r}} = \nabla_{\boldsymbol{k}}\epsilon_n(\boldsymbol{k}) - \dot{\boldsymbol{k}}\times\boldsymbol{\Omega}_n(\boldsymbol{k}), \qquad \hbar\dot{\boldsymbol{k}} = -e\boldsymbol{E}$$

(we neglect magnetic field and scattering). The electric current density from this filled band

is obtained by summing the wavepacket velocities over all occupied $\boldsymbol{k}$-states:

$$\boldsymbol{j} = -e \int_{\mathrm{BZ}} \frac{d^2k}{(2\pi)^2}\, f(\boldsymbol{k})\, \dot{\boldsymbol{r}},$$

where $f(\boldsymbol{k})$ is the occupation. For a completely filled band at zero temperature, $f(\boldsymbol{k}) = 1$. The "group-velocity" contribution integrates to zero in an insulator:

$$\int_{\mathrm{BZ}} \frac{d^2k}{(2\pi)^2}\, \nabla_{\boldsymbol{k}} \epsilon_n(\boldsymbol{k}) = 0,$$

because $\epsilon_n(\boldsymbol{k})$ is periodic on the torus and the integral of a total derivative over the BZ vanishes.
Thus only the anomalous term contributes. Using $\dot{\boldsymbol{k}} = -(e/\hbar)\boldsymbol{E}$,

$$\boldsymbol{j} = -e \int_{\mathrm{BZ}} \frac{d^2k}{(2\pi)^2} \left[-\dot{\boldsymbol{k}} \times \boldsymbol{\Omega}_n(\boldsymbol{k})\right] = -\frac{e^2}{\hbar} \int_{\mathrm{BZ}} \frac{d^2k}{(2\pi)^2}\, \boldsymbol{E} \times \boldsymbol{\Omega}_n(\boldsymbol{k}).$$

In 2D, $\boldsymbol{\Omega}_n(\boldsymbol{k}) = \Omega_n(\boldsymbol{k})\, \hat{\boldsymbol{z}}$. Writing out components,

$$j_x = -\frac{e^2}{\hbar} E_y \int_{\mathrm{BZ}} \frac{d^2k}{(2\pi)^2}\, \Omega_n(\boldsymbol{k}), \qquad j_y = \frac{e^2}{\hbar} E_x \int_{\mathrm{BZ}} \frac{d^2k}{(2\pi)^2}\, \Omega_n(\boldsymbol{k}).$$

Therefore the Hall conductivity of a filled band is

$$\sigma_{xy} \equiv \frac{j_x}{E_y} = -\frac{e^2}{\hbar} \int_{\mathrm{BZ}} \frac{d^2k}{(2\pi)^2}\, \Omega_n(\boldsymbol{k}) = -\frac{e^2}{h} \left(\frac{1}{2\pi} \int_{\mathrm{BZ}} d^2k\, \Omega_n(\boldsymbol{k}) \right) = -\frac{e^2}{h}\, C_n,$$

which is quantized because $C_n \in \mathbb{Z}$.

4.4 Two-band models: $\hat{B}$-formula and geometric interpretation

Two-band Hamiltonian and curvature in terms of $\hat{\boldsymbol{B}}$. Consider a generic two-band Bloch Hamiltonian

$$H(\boldsymbol{k}) = E_0(\boldsymbol{k})\, \mathbb{I} + \boldsymbol{B}(\boldsymbol{k}) \cdot \boldsymbol{\sigma}, \tag{182}$$

with eigenvalues $E_\pm(\boldsymbol{k}) = E_0(\boldsymbol{k}) \pm |\boldsymbol{B}(\boldsymbol{k})|$. The overall shift $E_0(\boldsymbol{k})$ does not affect eigenvectors and hence drops out of Berry quantities. For the lower (occupied) band, the Berry curvature can be written purely in terms of the unit Bloch vector $\hat{\boldsymbol{B}}(\boldsymbol{k}) \equiv \boldsymbol{B}(\boldsymbol{k})/|\boldsymbol{B}(\boldsymbol{k})|$:

$$\Omega_-(\boldsymbol{k}) = \frac{1}{2}\, \hat{\boldsymbol{B}}(\boldsymbol{k}) \cdot \left(\frac{\partial \hat{\boldsymbol{B}}}{\partial k_x} \times \frac{\partial \hat{\boldsymbol{B}}}{\partial k_y} \right). \tag{183}$$

The corresponding Chern number is

$$C_- = \frac{1}{2\pi} \int_{\mathrm{BZ}} d^2k\, \Omega_-(\boldsymbol{k}). \tag{184}$$

Derivation of $\Omega_-(\boldsymbol{k})$ for two-band models and its geometric meaning

■ **Preliminary: From $A(k)$ to the projector formula for $\Omega(k)$.**
For a normalized Bloch eigenstate $|u(\boldsymbol{k})\rangle$ ($\langle u|u\rangle = 1$), define

$$A_\mu(\boldsymbol{k}) \equiv i \langle u(\boldsymbol{k}) | \partial_\mu u(\boldsymbol{k}) \rangle\,, \qquad \Omega(\boldsymbol{k}) \equiv \partial_{k_x} A_y - \partial_{k_y} A_x,$$

where $\mu \in \{k_x, k_y\}$. A short algebra gives the standard gauge-invariant form

$$\Omega(\boldsymbol{k}) = i\Big(\langle \partial_{k_x} u | \partial_{k_y} u \rangle - \langle \partial_{k_y} u | \partial_{k_x} u \rangle \Big). \tag{185}$$

Indeed, using $\partial_\mu \langle u|u\rangle = 0 \Rightarrow \langle \partial_\mu u|u\rangle = -\langle u|\partial_\mu u\rangle$,

$$\partial_{k_x} A_y = i\Big(\langle \partial_{k_x} u | \partial_{k_y} u \rangle + \langle u | \partial_{k_x} \partial_{k_y} u \rangle \Big), \qquad \partial_{k_y} A_x = i\Big(\langle \partial_{k_y} u | \partial_{k_x} u \rangle + \langle u | \partial_{k_y} \partial_{k_x} u \rangle \Big),$$

and the mixed-derivative terms cancel, yielding Eq. (185).
Now introduce the rank-1 projector onto the band:

$$P(\boldsymbol{k}) \equiv |u(\boldsymbol{k})\rangle \langle u(\boldsymbol{k})| .$$

Then

$$\partial_\mu P = |\partial_\mu u\rangle \langle u| + |u\rangle \langle \partial_\mu u| .$$

Using $\mathrm{Tr}(P\,O) = \langle u|\,O\,|u\rangle$ for any operator O, we compute

$$i\,\mathrm{Tr}\Big(P[\partial_{k_x} P, \partial_{k_y} P]\Big) = i\Big(\langle u|\,\partial_{k_x} P\,\partial_{k_y} P\,|u\rangle - \langle u|\,\partial_{k_y} P\,\partial_{k_x} P\,|u\rangle \Big). \tag{186}$$

A convenient intermediate identity is

$$\partial_\mu P\ |u\rangle = |\partial_\mu u\rangle - |u\rangle \langle u|\partial_\mu u\rangle = (\mathbb{I} - P)\,|\partial_\mu u\rangle .$$

Therefore

$$\langle u|\,\partial_{k_x} P\,\partial_{k_y} P\,|u\rangle = \langle \partial_{k_x} u|(\mathbb{I} - P)|\partial_{k_y} u\rangle , \qquad \langle u|\,\partial_{k_y} P\,\partial_{k_x} P\,|u\rangle = \langle \partial_{k_y} u|(\mathbb{I} - P)|\partial_{k_x} u\rangle .$$

Expanding $(\mathbb{I} - P)$ and using $\langle \partial_\mu u|u\rangle = -\langle u|\partial_\mu u\rangle$, one finds that the P-dependent pieces cancel in the antisymmetrization, leaving precisely Eq. (185). Hence

$$\boxed{\Omega(\boldsymbol{k}) = i\,\mathrm{Tr}\Big(P(\boldsymbol{k})\,[\partial_{k_x} P(\boldsymbol{k}),\, \partial_{k_y} P(\boldsymbol{k})]\Big).} \tag{187}$$

Equation (187) is manifestly gauge invariant because $P(\boldsymbol{k})$ is unchanged under $|u(\boldsymbol{k})\rangle \mapsto e^{i\chi(\boldsymbol{k})}\,|u(\boldsymbol{k})\rangle$.

■ **Derivation of Eq.** (183)**.**
Start from :

$$\Omega(\boldsymbol{k}) = i\,\mathrm{Tr}\Big(P(\boldsymbol{k})\,[\partial_{k_x} P(\boldsymbol{k}),\, \partial_{k_y} P(\boldsymbol{k})]\Big).$$

For the two-band Hamiltonian $H(\boldsymbol{k}) = E_0(\boldsymbol{k})\mathbb{I} + \boldsymbol{B}(\boldsymbol{k}) \cdot \boldsymbol{\sigma}$, the projector onto the lower band is

$$P_-(\boldsymbol{k}) = \frac{1}{2}\Big(\mathbb{I} - \hat{\boldsymbol{B}}(\boldsymbol{k}) \cdot \boldsymbol{\sigma}\Big), \qquad \hat{\boldsymbol{B}}(\boldsymbol{k}) \equiv \frac{\boldsymbol{B}(\boldsymbol{k})}{|\boldsymbol{B}(\boldsymbol{k})|}.$$

Differentiating,

$$\partial_\mu P_- = -\frac{1}{2}(\partial_\mu \hat{\boldsymbol{B}}) \cdot \boldsymbol{\sigma}, \qquad \mu \in \{k_x, k_y\}.$$

Using the Pauli-matrix algebra $(\boldsymbol{u} \cdot \boldsymbol{\sigma})(\boldsymbol{v} \cdot \boldsymbol{\sigma}) = (\boldsymbol{u} \cdot \boldsymbol{v})\mathbb{I} + i(\boldsymbol{u} \times \boldsymbol{v}) \cdot \boldsymbol{\sigma}$, one finds

$$[\partial_{k_x} P_-, \partial_{k_y} P_-] = \frac{i}{2}\Big(\partial_{k_x} \hat{\boldsymbol{B}} \times \partial_{k_y} \hat{\boldsymbol{B}}\Big) \cdot \boldsymbol{\sigma}.$$

Substituting into the projector formula and taking the trace,

$$\Omega_-(\boldsymbol{k}) = \frac{1}{2}\,\hat{\boldsymbol{B}}(\boldsymbol{k}) \cdot \Big(\partial_{k_x} \hat{\boldsymbol{B}}(\boldsymbol{k}) \times \partial_{k_y} \hat{\boldsymbol{B}}(\boldsymbol{k})\Big),$$

which is Eq. (183).

■ **Geometric meaning..** The map $\boldsymbol{k} \mapsto \hat{\boldsymbol{B}}(\boldsymbol{k})$ sends the BZ (a torus) to the Bloch sphere S^2. The scalar triple product above is precisely the oriented area (solid-angle) density induced on S^2 by an area element d^2k in the BZ. Consequently,

$$C_- = \frac{1}{2\pi} \int_{\mathrm{BZ}} d^2k\, \Omega_-(\boldsymbol{k})$$

counts how many times $\hat{\boldsymbol{B}}(\boldsymbol{k})$ wraps the Bloch sphere. Since the upper band corresponds to the opposite projector $P_+ = \mathbb{I} - P_-$, one obtains $\Omega_+(\boldsymbol{k}) = -\Omega_-(\boldsymbol{k})$ and hence $C_+ = -C_-$.

Why the two bands carry opposite Chern numbers. For the upper band, the eigenstate is polarized parallel to $\hat{\boldsymbol{B}}$, which reverses the orientation of the Berry curvature:

$$\Omega_+(\boldsymbol{k}) = -\Omega_-(\boldsymbol{k}), \qquad \Rightarrow \qquad C_+ = -C_-. \tag{188}$$

Equivalently, since the two-band Hilbert space is complete and the total Berry curvature of the full (two-band) bundle is trivial, the Chern numbers must sum to zero.

4.5 Topological criterion: gap closing and the mass-sign rule at K, K′

When can the Chern number change? Only at a bulk gap closing.

For a two-band Hamiltonian $H(\boldsymbol{k}) = E_0(\boldsymbol{k})\mathbb{I} + \boldsymbol{B}(\boldsymbol{k}) \cdot \boldsymbol{\sigma}$, the band energies are

$$E_\pm(\boldsymbol{k}) = E_0(\boldsymbol{k}) \pm |\boldsymbol{B}(\boldsymbol{k})|.$$

The direct gap at momentum $\boldsymbol{k}$ is therefore $E_+(\boldsymbol{k}) - E_-(\boldsymbol{k}) = 2|\boldsymbol{B}(\boldsymbol{k})|$. Hence a necessary (and in fact the relevant) condition for a bulk gap closing is

$$\exists\, \boldsymbol{k}_0 \in \mathrm{BZ} \quad \text{s.t.} \quad |\boldsymbol{B}(\boldsymbol{k}_0)| = 0 \iff B_x(\boldsymbol{k}_0) = B_y(\boldsymbol{k}_0) = B_z(\boldsymbol{k}_0) = 0. \tag{189}$$

As long as $|\boldsymbol{B}(\boldsymbol{k})| > 0$ for all $\boldsymbol{k}$, $\hat{\boldsymbol{B}}(\boldsymbol{k})$ is well-defined and varies smoothly over the entire BZ, so C cannot change under any adiabatic parameter deformation.

For the honeycomb structure, potential gap closings occur only at K and K'.

The components $B_x(\boldsymbol{k})$ and $B_y(\boldsymbol{k})$ originate solely from the nearest-neighbor term and have the same structure as in the Dirac semimetal case (see Eq. (111) and Eq. (112)). In particular, the simultaneous zeros $B_x(\boldsymbol{k}) = B_y(\boldsymbol{k}) = 0$ occur only at the two inequivalent Dirac points $\boldsymbol{K}$ and $\boldsymbol{K}'$ (corners of the hexagonal BZ). Therefore, Eq. (189) implies that a topological phase transition in the Haldane model can only happen when

$$B_z(\boldsymbol{K}) = 0 \quad \text{or} \quad B_z(\boldsymbol{K}') = 0, \tag{190}$$

i.e., when the gap closes at one Dirac point[16].

Evaluating $B_z(\boldsymbol{K})$ and $B_z(\boldsymbol{K}')$ from the gap-closing condition $|\boldsymbol{B}| = 0$

A bulk gap closing requires $|\boldsymbol{B}(\boldsymbol{k})| = 0$, i.e. $B_x(\boldsymbol{k}) = B_y(\boldsymbol{k}) = B_z(\boldsymbol{k}) = 0$. For the honeycomb structure, $B_x = B_y = 0$ occurs only at the two inequivalent Dirac points $\boldsymbol{K}, \boldsymbol{K}'$, so the phase boundaries are determined by

$$B_z(\boldsymbol{K}) = 0 \quad \text{or} \quad B_z(\boldsymbol{K}') = 0.$$

[16] Further calculation shows that the gap at $\boldsymbol{K}$ and $\boldsymbol{K}'$ cannot close simultaneously.

Now use the explicit lattice expression (from the NNN term and staggered potential)

$$B_z(\boldsymbol{k}) = M + 2J_2 \sin\phi \sum_{\mu=1}^{3} \sin(\boldsymbol{k}\cdot\boldsymbol{a}_\mu),$$

together with the standard honeycomb identities

$$\sum_{\mu=1}^{3} \sin(\boldsymbol{K}\cdot\boldsymbol{a}_\mu) = -\frac{3\sqrt{3}}{2}, \qquad \sum_{\mu=1}^{3} \sin(\boldsymbol{K}'\cdot\boldsymbol{a}_\mu) = +\frac{3\sqrt{3}}{2},$$

which follow from inserting the explicit $\boldsymbol{K}, \boldsymbol{K}'$ and $\boldsymbol{a}_\mu$ (see Eq. (92)) and using elementary trigonometry. Therefore,

$$B_z(\boldsymbol{K}) = M + 2J_2 \sin\phi \left(-\frac{3\sqrt{3}}{2}\right) = M - 3\sqrt{3}\, J_2 \sin\phi, \tag{191}$$

$$B_z(\boldsymbol{K}') = M + 2J_2 \sin\phi \left(+\frac{3\sqrt{3}}{2}\right) = M + 3\sqrt{3}\, J_2 \sin\phi. \tag{192}$$

Thus, Eq. (190) becomes $M = \pm 3\sqrt{3} J_2 \sin(\phi)$.

Low-energy Dirac theory: $B_z(\boldsymbol{K})$ and $B_z(\boldsymbol{K}')$ are valley masses.

To connect the lattice Chern number to a simple criterion, expand $H(\boldsymbol{k})$ around each Dirac point. Let

$$\boldsymbol{k} = \boldsymbol{K}_\tau + \boldsymbol{q}, \qquad \tau = \pm,$$

where $\boldsymbol{K}_+ \equiv \boldsymbol{K}$ and $\boldsymbol{K}_- \equiv \boldsymbol{K}'$ label the two valleys. Since $B_x = B_y = 0$ at $\boldsymbol{K}_\tau$, the leading expansion is linear in $\boldsymbol{q}$ for the $\sigma_{x,y}$ terms, while the σ_z term has a constant piece

$$m_\tau \equiv B_z(\boldsymbol{K}_\tau).$$

Up to an innocuous linear redefinition of momenta (a rotation/rescaling in the $\boldsymbol{q}$-plane that does not affect the Chern number), the valley Hamiltonian can always be brought to the standard massive Dirac form

$$H_\tau(\boldsymbol{q}) \approx E_0(\boldsymbol{K}_\tau)\,\mathbb{I} + v\,(q_x\sigma_x + \eta_\tau q_y \sigma_y) + m_\tau\,\sigma_z, \tag{193}$$

where $v > 0$ is the Dirac velocity set by J_1 and the lattice geometry, and $\eta_\tau = \pm 1$ encodes the opposite chirality of the two valleys (the two Dirac cones have opposite orientation). For a detailed explanation of linearization, refer to the box below.

Why the linearized valley Hamiltonian can be put into the standard Dirac form

Near a Dirac point $\boldsymbol{K}_\tau$, write $\boldsymbol{k} = \boldsymbol{K}_\tau + \boldsymbol{q}$ and expand

$$H(\boldsymbol{K}_\tau + \boldsymbol{q}) \approx E_0(\boldsymbol{K}_\tau)\mathbb{I} + \sum_{i=x,y,z} B_i(\boldsymbol{K}_\tau + \boldsymbol{q})\sigma_i.$$

Since $B_x(\boldsymbol{K}_\tau) = B_y(\boldsymbol{K}_\tau) = 0$, the leading terms in B_x, B_y are linear in $\boldsymbol{q}$:

$$B_\alpha(\boldsymbol{K}_\tau + \boldsymbol{q}) \approx \sum_{\mu=x,y} v_{\alpha\mu}^{(\tau)} q_\mu, \qquad \alpha \in \{x, y\},$$

while

$$B_z(\boldsymbol{K}_\tau + \boldsymbol{q}) \approx m_\tau + O(q), \qquad m_\tau \equiv B_z(\boldsymbol{K}_\tau).$$

Define the 2×2 real matrix V_τ by $(V_\tau)_{\alpha\mu} = v^{(\tau)}_{\alpha\mu}$, so that the in-plane part reads

$$B_x\sigma_x + B_y\sigma_y \;\approx\; \Big[(V_\tau \boldsymbol{q})_x\Big]\sigma_x + \Big[(V_\tau \boldsymbol{q})_y\Big]\sigma_y.$$

For a genuine Dirac cone the linear dispersion is non-degenerate, which is equivalent to

$$\det V_\tau \neq 0.$$

Then V_τ admits a singular-value decomposition

$$V_\tau = R_\tau \begin{pmatrix} s_1 & 0 \\ 0 & s_2 \end{pmatrix} S_\tau^{\mathsf{T}}, \qquad R_\tau, S_\tau \in SO(2), \quad s_{1,2} > 0.$$

Introduce a new momentum coordinate

$$\boldsymbol{q}' = \begin{pmatrix} s_1 & 0 \\ 0 & s_2 \end{pmatrix} S_\tau^{\mathsf{T}} \boldsymbol{q},$$

so that

$$(V_\tau \boldsymbol{q})_x\sigma_x + (V_\tau \boldsymbol{q})_y\sigma_y = (R_\tau \boldsymbol{q}')_x\sigma_x + (R_\tau \boldsymbol{q}')_y\sigma_y.$$

Finally, since R_τ is a rotation in the x-y plane, it can be absorbed by a unitary change of sublattice basis

$$U_\tau = e^{-i\frac{\theta_\tau}{2}\sigma_z}, \qquad U_\tau^\dagger(\sigma_x, \sigma_y)U_\tau = (\sigma_x, \sigma_y)R_\tau,$$

which yields

$$U_\tau^\dagger\Big[(R_\tau \boldsymbol{q}')_x\sigma_x + (R_\tau \boldsymbol{q}')_y\sigma_y\Big]U_\tau = q'_x\sigma_x + q'_y\sigma_y.$$

After a trivial rescaling of coordinates (absorbing $s_{1,2}$ into the definition of $q'_{x,y}$), the valley Hamiltonian takes the standard massive Dirac form

$$H_\tau(\boldsymbol{q}) \approx E_0(\boldsymbol{K}_\tau)\mathbb{I} + v\,(q_x\sigma_x + \eta_\tau q_y\sigma_y) + m_\tau\sigma_z,$$

where the sign $\eta_\tau = \pm 1$ keeps track of the local orientation ("chirality") of the Dirac cone. In particular, one may take $\eta_\tau = \mathrm{sgn}(\det V_\tau)$; for the honeycomb lattice the two valleys have opposite orientation, so $\eta_{K'} = -\eta_K$.

Since the $E_0(\boldsymbol{K}_\tau)$ energy shift doesn't affect Chern number, consider the two-level Hamiltonian

$$H(\boldsymbol{q}) = v(q_x\sigma_x + \eta q_y\sigma_y) + m\sigma_z, \qquad \eta = \pm 1.$$

For the lower band, use Eq. (183) with $\boldsymbol{B} = (vq_x,\ \eta v q_y,\ m)$. A direct evaluation gives

$$\Omega_-(\boldsymbol{q}) = -\frac{\eta}{2}\,\frac{mv^2}{(m^2 + v^2q^2)^{3/2}}, \qquad q^2 = q_x^2 + q_y^2. \tag{194}$$

(Notice the curvature is sharply concentrated near $\boldsymbol{q} = 0$ and its sign is controlled by $\eta\, m$.)

Now integrate over the $\boldsymbol{q}$-plane to obtain the Berry flux (a continuum approximation to the lattice integral near the Dirac point):

$$C_{\mathrm{Dirac}} \equiv \frac{1}{2\pi}\int d^2q\,\Omega_-(\boldsymbol{q}) = -\frac{\eta}{2}\,\mathrm{sgn}(m). \tag{195}$$

The "half-integer" is not a contradiction: a single Dirac cone is not a globally well-defined lattice band over the entire BZ. On the lattice, the two valleys combine to produce an *integer*

Chern number. [17] The contributions from far away from either Dirac points can be safely neglected[18].

Derivation of Eq. (195)

In polar coordinates,

$$\int d^2q\, \frac{mv^2}{(m^2+v^2q^2)^{3/2}} = 2\pi mv^2 \int_0^\infty \frac{q\,dq}{(m^2+v^2q^2)^{3/2}} = 2\pi\,\mathrm{sgn}(m),$$

so Eq. (194) yields the result above.

Mass-sign rule: the lattice Chern number is fixed by m_K and $m_{K'}$. Applying the Dirac-cone result to the two valleys in Eq. (193), we obtain

$$C = C_K + C_{K'} = -\frac{\eta_K}{2}\,\mathrm{sgn}(m_K) - \frac{\eta_{K'}}{2}\,\mathrm{sgn}(m_{K'}).$$

For the honeycomb Dirac cones, the two chiralities are opposite, $\eta_{K'} = -\eta_K$. Choosing the convention $\eta_K = +1$ and $\eta_{K'} = -1$ (this is consistent with the usual orientation of the BZ axes), we arrive at the compact and widely used formula

$$\boxed{C = \frac{1}{2}\Big(\mathrm{sgn}(m_{K'}) - \mathrm{sgn}(m_K)\Big), \qquad m_K \equiv B_z(\boldsymbol{K}),\;\; m_{K'} \equiv B_z(\boldsymbol{K}').} \tag{196}$$

Equation (196) makes the criterion transparent:

$$C \neq 0 \iff \mathrm{sgn}\Big(B_z(\boldsymbol{K})\Big) \neq \mathrm{sgn}\Big(B_z(\boldsymbol{K}')\Big) \iff B_z(\boldsymbol{K})\,B_z(\boldsymbol{K}') < 0. \tag{197}$$

Geometric picture in the $\hat{\boldsymbol{B}}$-mapping language

At $\boldsymbol{K}$ and $\boldsymbol{K}'$, one has $B_x = B_y = 0$, so $\hat{\boldsymbol{B}}$ points exactly to the north or south pole depending on the sign of B_z. If $B_z(\boldsymbol{K})$ and $B_z(\boldsymbol{K}')$ have the same sign, $\hat{\boldsymbol{B}}$ never needs to reach both poles as $\boldsymbol{k}$ ranges over the BZ, and the mapping $\boldsymbol{k} \mapsto \hat{\boldsymbol{B}}(\boldsymbol{k})$ cannot wrap the Bloch sphere: $C = 0$. If their signs are opposite, $\hat{\boldsymbol{B}}$ is forced to cover both poles, and in the Haldane model (where the only would-be singular points are precisely K and K') this is sufficient to ensure a nontrivial wrapping: $|C| = 1$.

Haldane phase boundary and topological regime.

Using the explicit evaluations above (see Eq. (191) and (192)),

$$B_z(\boldsymbol{K}) = M - 3\sqrt{3}\,J_2 \sin\phi, \qquad B_z(\boldsymbol{K}') = M + 3\sqrt{3}\,J_2 \sin\phi,$$

the criterion $B_z(\boldsymbol{K})\,B_z(\boldsymbol{K}') < 0$ gives

$$|M| < 3\sqrt{3}\,|J_2 \sin\phi|. \tag{198}$$

At the phase boundary, either $B_z(\boldsymbol{K}) = 0$ or $B_z(\boldsymbol{K}') = 0$, so the bulk gap closes at one Dirac point, enabling the Chern number to change. In the topological regime, Eq. (196) yields $C = \pm 1$; for example, at $M = 0$ and $J_2 > 0$, one finds $C = \mathrm{sgn}(\sin\phi)$, while outside the regime the insulator is trivial with $C = 0$.

[17] Although the first BZ is often drawn as a hexagon with six corner points, those corners are related by reciprocal-lattice translations. In the Bloch description, $\boldsymbol{k}$ and $\boldsymbol{k} + \boldsymbol{G}$ (with $\boldsymbol{G}$ a reciprocal lattice vector) label the *same* physical crystal momentum, so the six corners reduce to only two inequivalent points modulo $\boldsymbol{G}$: one set is $\boldsymbol{K}$ and the other is $\boldsymbol{K}'$. Equivalently, there are three copies of $\boldsymbol{K}$ and three copies of $\boldsymbol{K}'$ on the hexagon boundary, but they represent only two distinct valleys.

[18] This point is somewhat surprising. I might hope it to be a very small correction, but only considering the two Dirac points, with certain approximations, actually gives the exact Chern number.

4.6 Visualization of Haldane Model

Go to Appedix C for the visualization code, and play with it.
Here are two of the plots:

5 General Overview: Band Topology, Defects, and Bulk–Edge Correspondence

5.1 Two common features of topological band theory

■ **Internal structure beyond a $U(1)$ phase.** Topological band invariants are defined from Bloch eigenstates over momentum space, but the overall $U(1)$ phase at each $\boldsymbol{k}$ is gauge and cannot define topology by itself. Therefore the wave function must have nontrivial internal structure (minimal: at least two sites per unit cell), producing multi-component Bloch spinors.

■ **Topology changes require band touching.** For a two-band model written as $H(\boldsymbol{k}) = E_0(\boldsymbol{k})I + \boldsymbol{B}(\boldsymbol{k})\cdot\sigma$, a gapped phase means $|\boldsymbol{B}(\boldsymbol{k})| \neq 0$ for all $\boldsymbol{k}$. Then $\hat{\boldsymbol{B}}(\boldsymbol{k})$ is well-defined everywhere and deforms continuously under smooth parameter changes. Changing a topological invariant requires a singularity where $|\boldsymbol{B}| = 0$, i.e. a band touching (gap closing).

5.2 Semimetal vs topological insulator: different topological characterizations

Semimetal: topology on enclosing surfaces. In d dimensions, semimetal band touchings are characterized by topology of maps from $(d-1)$-dimensional surfaces enclosing the nodal points to the eigenstate manifold. Nonzero invariants force the existence of a singularity (gap closing) inside, hence nodal points behave as topological defects.

Topological insulator: topology of the entire BZ. A gapped topological insulator is characterized by a map from the full d-dimensional BZ to the eigenstate manifold. Two insulators with different invariants must be separated by a gap closing transition.

Analogy inside physics

The Dirac point in 2D behaves like a vortex defect in momentum space (winding on loops). A 2D Chern insulator (Haldane phase) is more analogous to a nonsingular texture (skyrmion-like) in momentum space, where the wave function is defined everywhere and the invariant counts global wrapping.

5.3 Edge states and quantized Hall conductance

Bulk–edge correspondence. If two bulk insulators have different topological invariants, their interface must host gapless boundary modes: the spatial coordinate across the interface plays the role of a tuning parameter that crosses a topological transition somewhere, forcing a local gap closing and hence boundary states.

SSH edge mode logic. In the SSH model, in the strongly dimerized limit one can disconnect weak bonds. In the topological dimerization, this leaves an unpaired site at the boundary, producing a zero-energy boundary state. For finite weak hopping, the mode broadens but remains localized and pinned by symmetry.

Chern insulator edge modes and Hall response. A 2D insulator with Chern number C supports $|C|$ chiral edge modes. In electronic systems, these act as one-way 1D channels,

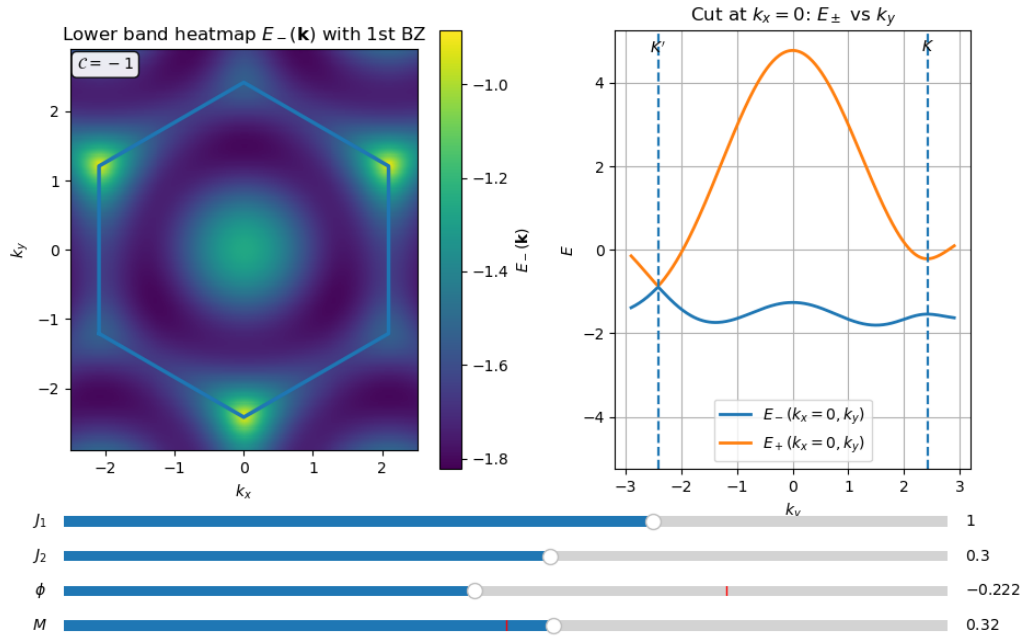

(a) $C = -1 \longrightarrow C = 0$

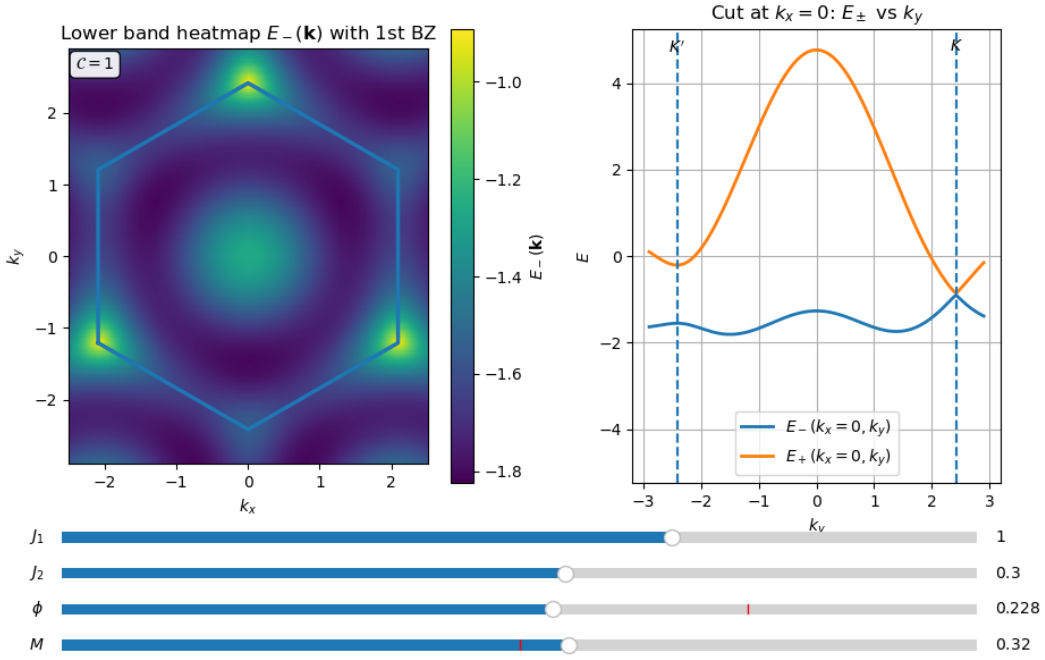

(b) $C = 1 \longrightarrow C = 0$

Figure 9: Topological phase transition of Haldane Model

leading to quantized Hall conductance

$$\sigma_{xy} = C\,\frac{e^2}{h}. \tag{199}$$

The essential theoretical point is the stability: as long as the bulk gap and the defining symmetry class are maintained, the chiral edge structure cannot be removed by smooth perturbations.

6 Three Experimental Themes (Minimal Theory-Facing Summary)

6.1 Time-of-flight momentum distribution: momentum mapping vs band mapping

Time-of-flight as a momentum-space probe (conceptual). A time-of-flight (TOF) measurement releases atoms from the trap/lattice and images the expanded cloud after a flight time. In the simplest ballistic regime, spatial density after long time reflects the initial momentum distribution (up to a known scaling).

Momentum mapping: abrupt turn-off. If both lattice and trap are turned off abruptly, the measurement projects the lattice Bloch state onto free-space plane waves. A Bloch state $\psi_{mk}(x) = e^{ikx}u_{mk}(x)$ contains plane-wave components $e^{i(k+2nk_0)x}$ with amplitudes $u_n^m(k)$. Hence the observed plane-wave momentum occupation satisfies

$$n_p = \sum_m |u_n^m(p-2nk_0)|^2\, n^m_{p-2nk_0}, \tag{200}$$

where n is chosen so that $p - 2nk_0 \in [-k_0, k_0]$. Condensation into $m = 0, k = 0$ produces peaks at reciprocal lattice vectors.

Band mapping: adiabatic lattice ramp then sudden release. If the lattice is turned off slowly first, Bloch states adiabatically connect to specific plane waves as the coupling between plane-wave sectors vanishes. Then an abrupt trap release measures populations in different Brillouin zones, approximately reflecting band populations (with known caveats near points where interband gaps become small during the ramp).

6.2 Bloch oscillation: periodic velocity in tight binding

Semiclassical equations. Under a constant force $F\hat{x}$, quasi-momentum evolves as

$$\hbar\frac{dk}{dt} = F, \qquad k(t) = k(0) + \frac{F}{\hbar}t. \tag{201}$$

The velocity in band m is

$$v(k) = \frac{1}{\hbar}\frac{\partial \mathcal{E}_m(k)}{\partial k}. \tag{202}$$

Tight-binding example and periodic motion. For a 1D tight-binding dispersion $\mathcal{E}(k) = -2J\cos(ka)$,

$$v(k) = \frac{2Ja}{\hbar}\sin(ka). \tag{203}$$

Since $k(t)$ increases linearly, $v(t)$ becomes periodic:

$$v(t) = \frac{2Ja}{\hbar}\sin\!\left(ak(0) + \frac{Fa}{\hbar}t\right). \tag{204}$$

Thus the real-space motion oscillates with Bloch period

$$T_B = \frac{2\pi\hbar}{Fa}. \tag{205}$$

6.3 Quench dynamics: Hopf map and topology (theory-centric)

Two-band quench and pseudo-spin precession. Consider a two-band Hamiltonian $\hat{H}_{\mathrm{f}}(k) = \boldsymbol{B}_{\mathrm{f}}(k) \cdot \boldsymbol{\sigma}$. After a sudden quench from an initial eigenstate $|\xi_{\mathrm{i}}(k)\rangle$, the time-evolved state is

$$|\xi(k,t)\rangle = e^{-i\,\boldsymbol{B}_{\mathrm{f}}(k)\cdot\boldsymbol{\sigma}\,t}\,|\xi_{\mathrm{i}}(k)\rangle, \tag{206}$$

and the Bloch vector is

$$\boldsymbol{s}(k,t) = \langle\xi(k,t)|\boldsymbol{\sigma}|\xi(k,t)\rangle. \tag{207}$$

If $|\xi_{\mathrm{i}}(k)\rangle$ is not aligned with $\boldsymbol{B}_{\mathrm{f}}(k)$, $\boldsymbol{s}(k,t)$ precesses around $\boldsymbol{B}_{\mathrm{f}}(k)$.

Hopf map and invariant (minimal statement). The map $(k,t) \mapsto \boldsymbol{s}(k,t)$ sends a three-dimensional periodic $\{k,t\}$ space to the Bloch sphere S^2 and is a Hopf map. Its topology is classified by $\Pi_3(S^2) = \mathbb{Z}$, with invariant called the Hopf invariant (linking number). In quenches from a topologically trivial initial Hamiltonian, this linking number equals the Chern number of the final Hamiltonian, providing a dynamical route to diagnosing band topology without relying on near-equilibrium transport logic.

A Recap:Second Quantization Procedure

The second-quantized description starts by promoting the microscopic degrees of freedom to *field operators* $\hat{\psi}(\boldsymbol{r})$ and $\hat{\psi}^\dagger(\boldsymbol{r})$, which annihilate/create a particle at position $\boldsymbol{r}$. They satisfy either bosonic or fermionic canonical (anti-)commutation relations,

$$[\hat{\psi}(\boldsymbol{r}), \hat{\psi}^\dagger(\boldsymbol{r}')]_\mp = \delta(\boldsymbol{r}-\boldsymbol{r}'), \qquad [\hat{\psi}(\boldsymbol{r}), \hat{\psi}(\boldsymbol{r}')]_\mp = 0, \qquad [\hat{\psi}^\dagger(\boldsymbol{r}), \hat{\psi}^\dagger(\boldsymbol{r}')]_\mp = 0, \tag{208}$$

where the upper (lower) sign corresponds to bosons (fermions). Importantly, the *structure* of a one-body Hamiltonian does not depend on statistics; statistics only enters through these (anti-)commutators.

■ **One-body Operator.**

Second quantization maps *single-particle* operators on the one-particle Hilbert space to *many-body* operators acting on Fock space. Concretely, given a one-body (single-particle) operator $\hat{h}_0$ with position-space kernel

$$h_0(\boldsymbol{r},\boldsymbol{r}') \equiv \langle\boldsymbol{r}|\hat{h}_0|\boldsymbol{r}'\rangle, \tag{209}$$

its second-quantized lift is

$$\hat{H}_0 = \int d^d r\, d^d r'\, \hat{\psi}^\dagger(\boldsymbol{r})\, h_0(\boldsymbol{r},\boldsymbol{r}')\, \hat{\psi}(\boldsymbol{r}'). \tag{210}$$

This operator has two key properties:

(i) it conserves particle number, $[\hat{H}_0, \hat{N}] = 0$ with $\hat{N} = \int d^d r\, \hat{\psi}^\dagger(\boldsymbol{r})\hat{\psi}(\boldsymbol{r})$;

(ii) when restricted to the N-particle sector, it coincides with the sum of single-particle operators, $\hat{H}_0\big|_N = \sum_{i=1}^N \hat{h}_0^{(i)}$. This describes N independent particles, as expected.

Example: Non-interacting atoms in an optical lattice.

For a local single-particle Hamiltonian

$$h_{\mathrm{sp}} = -\frac{\hbar^2\nabla^2}{2m} + V_{\mathrm{lat}}(\boldsymbol{r}), \tag{211}$$

the kernel is local in space,

$$h_0(\boldsymbol{r},\boldsymbol{r}') = h_{\rm sp}\,\delta(\boldsymbol{r}-\boldsymbol{r}'), \tag{212}$$

and Eq. (210) reduces to

$$\hat{H}_0 = \int d^d r\,\hat{\psi}^\dagger(\boldsymbol{r})\left(-\frac{\hbar^2\nabla^2}{2m} + V_{\rm lat}(\boldsymbol{r})\right)\hat{\psi}(\boldsymbol{r}), \tag{213}$$

■ **Two-body operators.**

In first quantization (fixed particle number N), a two-body interaction takes the form

$$\hat{V}^{(N)} = \sum_{1\le i<j\le N} \hat{U}_{ij}, \tag{214}$$

where $\hat{U}_{ij}$ acts nontrivially only on the coordinates of particles i and j. On the two-particle Hilbert space one may define the position-space kernel of $\hat{U}$ by

$$U(\boldsymbol{r},\boldsymbol{r}';\boldsymbol{s},\boldsymbol{s}') \equiv \langle \boldsymbol{r},\boldsymbol{r}'|\hat{U}|\boldsymbol{s},\boldsymbol{s}'\rangle. \tag{215}$$

The corresponding second-quantized operator is

$$\hat{H}_{\rm int} = \frac{1}{2}\int d^d r\,d^d r'\,d^d s\,d^d s'\;\hat{\psi}^\dagger(\boldsymbol{r})\hat{\psi}^\dagger(\boldsymbol{r}')\,U(\boldsymbol{r},\boldsymbol{r}';\boldsymbol{s},\boldsymbol{s}')\,\hat{\psi}(\boldsymbol{s}')\hat{\psi}(\boldsymbol{s}). \tag{216}$$

For the common case of a multiplicative potential $U(\boldsymbol{r},\boldsymbol{r}')$ (diagonal in the position basis),

$$U(\boldsymbol{r},\boldsymbol{r}';\boldsymbol{s},\boldsymbol{s}') = U(\boldsymbol{r},\boldsymbol{r}')\,\delta(\boldsymbol{r}-\boldsymbol{s})\delta(\boldsymbol{r}'-\boldsymbol{s}'), \tag{217}$$

Eq. (216) reduces to

$$\hat{H}_{\rm int} = \frac{1}{2}\int d^d r\,d^d r'\;\hat{\psi}^\dagger(\boldsymbol{r})\hat{\psi}^\dagger(\boldsymbol{r}')\,U(\boldsymbol{r},\boldsymbol{r}')\,\hat{\psi}(\boldsymbol{r}')\hat{\psi}(\boldsymbol{r}). \tag{218}$$

Example: Contact interaction in cold atoms.

For short-range s-wave dominated interactions, a widely used model is a local (contact) kernel

$$U(\boldsymbol{r},\boldsymbol{r}') = g\,\delta(\boldsymbol{r}-\boldsymbol{r}'), \tag{219}$$

which yields

$$\hat{H}_{\rm int} = \frac{g}{2}\int d^d r\;\hat{\psi}^\dagger(\boldsymbol{r})\hat{\psi}^\dagger(\boldsymbol{r})\hat{\psi}(\boldsymbol{r})\hat{\psi}(\boldsymbol{r}). \tag{220}$$

■ **Single-particle basis expansion and Discrete Hamiltonian.** Let $\{\phi_\alpha(\boldsymbol{r})\}$ be an orthonormal single-particle basis and define mode operators

$$\hat{a}_\alpha = \int d^d r\,\phi_\alpha^*(\boldsymbol{r})\hat{\psi}(\boldsymbol{r}), \qquad \hat{\psi}(\boldsymbol{r}) = \sum_\alpha \phi_\alpha(\boldsymbol{r})\hat{a}_\alpha. \tag{221}$$

Then the one-body Hamiltonian becomes

$$\hat{H}_0 = \sum_{\alpha\beta} h_{\alpha\beta}\,\hat{a}_\alpha^\dagger\hat{a}_\beta, \qquad h_{\alpha\beta} = \int d^d r\,d^d r'\,\phi_\alpha^*(\boldsymbol{r})\,h_0(\boldsymbol{r},\boldsymbol{r}')\,\phi_\beta(\boldsymbol{r}'), \tag{222}$$

and the two-body interaction reads

$$\hat{H}_{\text{int}} = \frac{1}{2}\sum_{\alpha\beta\gamma\delta} U_{\alpha\beta\gamma\delta}\,\hat{a}^\dagger_\alpha\hat{a}^\dagger_\beta\hat{a}_\gamma\hat{a}_\delta, \qquad U_{\alpha\beta\gamma\delta} = \int d^d r\, d^d r'\, \phi^*_\alpha(\boldsymbol{r})\phi^*_\beta(\boldsymbol{r}')\, U(\boldsymbol{r},\boldsymbol{r}')\,\phi_\gamma(\boldsymbol{r}')\phi_\delta(\boldsymbol{r}). \tag{223}$$

This basis form is the bridge to lattice models: choosing Bloch or Wannier functions as ϕ_α and truncating[19] to a few bands turns the continuum microscopic Hamiltonian into effective tight-binding/Hubbard-type descriptions.

Derivation of the one-body Hamiltonian

Start from the one-body operator written in terms of the field and the single-particle kernel,

$$\hat{H}_0 = \int d^d r\, d^d r'\; \hat{\psi}^\dagger(\boldsymbol{r})\, h_0(\boldsymbol{r},\boldsymbol{r}')\,\hat{\psi}(\boldsymbol{r}'). \tag{224}$$

Choose an orthonormal single-particle basis $\{\phi_\alpha(\boldsymbol{r})\}$ with

$$\int d^d r\; \phi^*_\alpha(\boldsymbol{r})\phi_\beta(\boldsymbol{r}) = \delta_{\alpha\beta}, \qquad \sum_\alpha \phi_\alpha(\boldsymbol{r})\phi^*_\alpha(\boldsymbol{r}') = \delta(\boldsymbol{r}-\boldsymbol{r}'). \tag{225}$$

Define the mode operators

$$\hat{a}_\alpha = \int d^d r\; \phi^*_\alpha(\boldsymbol{r})\hat{\psi}(\boldsymbol{r}), \qquad \hat{\psi}(\boldsymbol{r}) = \sum_\alpha \phi_\alpha(\boldsymbol{r})\hat{a}_\alpha, \qquad \hat{\psi}^\dagger(\boldsymbol{r}) = \sum_\alpha \phi^*_\alpha(\boldsymbol{r})\hat{a}^\dagger_\alpha, \tag{226}$$

where the inversion $\hat{\psi}(\boldsymbol{r}) = \sum_\alpha \phi_\alpha(\boldsymbol{r})\hat{a}_\alpha$ follows from completeness.
Insert these expansions into Eq. (224):

$$\begin{aligned}\hat{H}_0 &= \int d^d r\, d^d r' \Big(\sum_\alpha \phi^*_\alpha(\boldsymbol{r})\hat{a}^\dagger_\alpha\Big)\, h_0(\boldsymbol{r},\boldsymbol{r}')\,\Big(\sum_\beta \phi_\beta(\boldsymbol{r}')\hat{a}_\beta\Big)\\ &= \sum_{\alpha\beta}\hat{a}^\dagger_\alpha\hat{a}_\beta \int d^d r\, d^d r'\; \phi^*_\alpha(\boldsymbol{r})\, h_0(\boldsymbol{r},\boldsymbol{r}')\,\phi_\beta(\boldsymbol{r}').\end{aligned} \tag{227}$$

Define the matrix elements of the single-particle operator $\hat{h}_0$ in this basis as

$$h_{\alpha\beta} \equiv \langle\alpha|\hat{h}_0|\beta\rangle = \int d^d r\, d^d r'\; \phi^*_\alpha(\boldsymbol{r})\, h_0(\boldsymbol{r},\boldsymbol{r}')\,\phi_\beta(\boldsymbol{r}'), \tag{228}$$

which yields the desired second-quantized form

$$\hat{H}_0 = \sum_{\alpha\beta} h_{\alpha\beta}\,\hat{a}^\dagger_\alpha\hat{a}_\beta. \tag{229}$$

Derivation: two-body interaction in a basis, $\hat{H}_{\text{int}} = \frac{1}{2}\sum U_{\alpha\beta\gamma\delta}\hat{a}^\dagger_\alpha\hat{a}^\dagger_\beta\hat{a}_\gamma\hat{a}_\delta$

Start from the general number-conserving two-body interaction written in field operators. The fully general (possibly nonlocal and non-diagonal) kernel form is

$$\hat{H}_{\text{int}} = \frac{1}{2}\int d^d r\, d^d r'\, d^d s\, d^d s'\; \hat{\psi}^\dagger(\boldsymbol{r})\hat{\psi}^\dagger(\boldsymbol{r}')\, U(\boldsymbol{r},\boldsymbol{r}';\boldsymbol{s},\boldsymbol{s}')\,\hat{\psi}(\boldsymbol{s}')\hat{\psi}(\boldsymbol{s}). \tag{230}$$

(When the interaction is diagonal in the position basis, one has $U(\boldsymbol{r},\boldsymbol{r}';\boldsymbol{s},\boldsymbol{s}') = U(\boldsymbol{r},\boldsymbol{r}')\delta(\boldsymbol{r}-$

[19] Here truncating means keep only the major ingredients of $\{\phi_\alpha(\boldsymbol{r})\}$.

$s)\delta(r'-s')$, and Eq. (230) reduces to the more familiar $\frac{1}{2}\int d^d r\, d^d r'\, \hat{\psi}^\dagger(r)\hat{\psi}^\dagger(r')U(r,r')\hat{\psi}(r')\hat{\psi}(r)$.) Choose an orthonormal and complete single-particle basis $\{\phi_\alpha(r)\}$,

$$\int d^d r\, \phi_\alpha^*(r)\phi_\beta(r) = \delta_{\alpha\beta}, \qquad \sum_\alpha \phi_\alpha(r)\phi_\alpha^*(r') = \delta(r-r'). \tag{231}$$

Define mode operators

$$\hat{a}_\alpha = \int d^d r\, \phi_\alpha^*(r)\hat{\psi}(r), \qquad \hat{\psi}(r) = \sum_\alpha \phi_\alpha(r)\hat{a}_\alpha, \qquad \hat{\psi}^\dagger(r) = \sum_\alpha \phi_\alpha^*(r)\hat{a}_\alpha^\dagger. \tag{232}$$

Insert Eq. (232) into Eq. (230):

$$\begin{aligned}\hat{H}_{\text{int}} &= \frac{1}{2}\int d^d r\, d^d r'\, d^d s\, d^d s' \Big(\sum_\alpha \phi_\alpha^*(r)\hat{a}_\alpha^\dagger\Big)\Big(\sum_\beta \phi_\beta^*(r')\hat{a}_\beta^\dagger\Big)U(r,r';s,s')\Big(\sum_\gamma \phi_\gamma(s')\hat{a}_\gamma\Big)\Big(\sum_\delta \phi_\delta(s)\hat{a}_\delta\Big) \\ &= \frac{1}{2}\sum_{\alpha\beta\gamma\delta}\hat{a}_\alpha^\dagger\hat{a}_\beta^\dagger\hat{a}_\gamma\hat{a}_\delta \int d^d r\, d^d r'\, d^d s\, d^d s'\ \phi_\alpha^*(r)\phi_\beta^*(r')\, U(r,r';s,s')\, \phi_\gamma(s')\phi_\delta(s).\end{aligned} \tag{233}$$

This motivates the definition of the two-body matrix elements (interaction tensor)

$$U_{\alpha\beta\gamma\delta} \equiv \int d^d r\, d^d r'\, d^d s\, d^d s'\ \phi_\alpha^*(r)\phi_\beta^*(r')\, U(r,r';s,s')\, \phi_\gamma(s')\phi_\delta(s), \tag{234}$$

so that

$$\hat{H}_{\text{int}} = \frac{1}{2}\sum_{\alpha\beta\gamma\delta} U_{\alpha\beta\gamma\delta}\, \hat{a}_\alpha^\dagger\hat{a}_\beta^\dagger\hat{a}_\gamma\hat{a}_\delta. \tag{235}$$

Common specialization: interaction diagonal in position space. If the interaction is of multiplicative "potential" type,

$$U(r,r';s,s') = U(r,r')\,\delta(r-s)\delta(r'-s'), \tag{236}$$

then (235) still holds and Eq. (234) collapses to

$$U_{\alpha\beta\gamma\delta} = \int d^d r\, d^d r'\ \phi_\alpha^*(r)\phi_\beta^*(r')\, U(r,r')\, \phi_\gamma(r')\phi_\delta(r). \tag{237}$$

B Visualization of Bands in Weak Lattice Limit

Run the following code and try yourself!

```python
import numpy as np
import matplotlib.pyplot as plt
from matplotlib.widgets import Slider

# ----------------------
# 0) Basic configuration
# ----------------------
a = 1.0
k0 = np.pi / a
hbar2_over_2m = 1.0
ER = k0**2

```

```
def eps_free(p):
    return hbar2_over_2m * p**2

# Basis truncation
N = 7
n_vals = np.arange(-N, N + 1)
G_vals = 2.0 * n_vals * k0
dim = len(G_vals)

# k grid
nk = 401 # reduced for interactivity
k_list = np.linspace(-k0, k0, nk)

nbands_to_plot = 8

# Folded free bands
free_branches = [
    eps_free(k_list + 2*n*k0) / ER
    for n in range(-4, 5)
]

# -----------------------
# 1) Hamiltonian
# -----------------------
def make_V_fourier(V0, V1, V2, V3, V4):
    Vf = {0.0: V0}
    Vn = [0, V1, V2, V3, V4]
    for n in range(1, 5):
        Q = 2*n*k0
        Vf[+Q] = Vn[n] / 2
        Vf[-Q] = Vn[n] / 2
    return Vf

def build_Hk(k, Vf):
    H = np.zeros((dim, dim))
    p = k + G_vals
    np.fill_diagonal(H, eps_free(p))
    for i, Gi in enumerate(G_vals):
        for j, Gj in enumerate(G_vals):
            H[i, j] += Vf.get(Gi - Gj, 0.0)
    return H

def compute_bands(V0, V1, V2, V3, V4):
    Vf = make_V_fourier(V0, V1, V2, V3, V4)
    bands = np.zeros((nbands_to_plot, nk))
    for ik, k in enumerate(k_list):
        evals = np.linalg.eigvalsh(build_Hk(k, Vf))
        bands[:, ik] = evals[:nbands_to_plot] / ER
    return bands

# -----------------------
# 2) Figure + sliders
# -----------------------
fig, ax = plt.subplots(figsize=(5.2, 5.2))
plt.subplots_adjust(bottom=0.35)

# plot folded free
for fb in free_branches:
```

```
    ax.plot(k_list/k0, fb, "--", lw=1, color="gray")

# initial parameters
V0_init = 0.0 * ER
V1_init = 0.80 * ER
V2_init = 0.40 * ER
V3_init = 0.20 * ER
V4_init = 0.10 * ER

bands = compute_bands(V0_init, V1_init, V2_init, V3_init, V4_init)

band_lines = []
for n in range(nbands_to_plot):
    line, = ax.plot(k_list/k0, bands[n], lw=2)
    band_lines.append(line)

ax.set_xlim(-1, 1)
ax.set_ylim(-2, 20)
ax.set_xlabel(r"$k/k_0$")
ax.set_ylabel(r"$E/E_R$")
ax.set_title(r"$V(x)=V_0+\sum_{n=1}^4 V_n\cos(2n k_0 x)$")
ax.grid(alpha=0.3)

# ------------------------
# 3) Sliders
# ------------------------
slider_y = [0.25, 0.20, 0.15, 0.10, 0.05]
sliders = []

labels = ["V0", "V1", "V2", "V3", "V4"]
inits = [V0_init, V1_init, V2_init, V3_init, V4_init]

for y, label, init in zip(slider_y, labels, inits):
    ax_s = plt.axes([0.15, y, 0.7, 0.03])
    s = Slider(ax_s, label, 0.0, ER, valinit=init)
    sliders.append(s)

# ------------------------
# 4) Update callback
# ------------------------
def update(val):
    V0, V1, V2, V3, V4 = [s.val for s in sliders]
    new_bands = compute_bands(V0, V1, V2, V3, V4)
    for n, line in enumerate(band_lines):
        line.set_ydata(new_bands[n])
    fig.canvas.draw_idle()

for s in sliders:
    s.on_changed(update)

plt.show()
```

C Visualization of Haldane Model

Run the following code and try yourself!

```
import numpy as np
```

```
import matplotlib.pyplot as plt
from matplotlib.widgets import Slider

# ----------------------------
# Honeycomb (Haldane-like) model
# H(k) = E0(k) I + Bx(k) x + By(k) y + Bz(k) z
# E(k) = E0(k)  |B(k)|
# Plot:
# (Left) Lower band heatmap E_-(kx,ky) with 1st BZ hexagon
# (Right) Cut at kx=0: E(0,ky) vs ky with dashed lines at K and K'
# Text box (white background): Chern number via
# C = 1/2 (sgn m_{K'} - sgn m_K),
# m_K = M - 33 J2 sin, m_{K'} = M + 33 J2 sin
# ----------------------------

a = 1.0

# Nearest-neighbor vectors (A -> B)
d1 = a * np.array([-1.0, 0.0])
d2 = a * np.array([ 0.5, np.sqrt(3)/2])
d3 = a * np.array([ 0.5, -np.sqrt(3)/2])
d_vecs = np.stack([d1, d2, d3], axis=0)

# Triangular Bravais primitive vectors (also NNN directions)
a1 = d2 - d3
a2 = d3 - d1
a3 = d1 - d2
a_vecs = np.stack([a1, a2, a3], axis=0)

# Reciprocal vectors b1, b2 from a1, a2
area = a1[0]*a2[1] - a1[1]*a2[0]
b1 = 2*np.pi * np.array([ a2[1], -a2[0]]) / area
b2 = 2*np.pi * np.array([-a1[1], a1[0]]) / area

# --- 1st BZ (hexagon) as WignerSeitz cell in reciprocal space ---
G_list = [b1, b2, b1 - b2]
halfplanes = []
for G in G_list:
    c = 0.5 * (G @ G)
    halfplanes.append(( G, c))
    halfplanes.append((-G, c))

def intersect_lines(a_vec, c_val, b_vec, d_val):
    A = np.array([a_vec, b_vec], dtype=float)
    rhs = np.array([c_val, d_val], dtype=float)
    det = np.linalg.det(A)
    if abs(det) < 1e-12:
        return None
    return np.linalg.solve(A, rhs)

cands = []
for i in range(len(halfplanes)):
    ai, ci = halfplanes[i]
    for j in range(i+1, len(halfplanes)):
        aj, cj = halfplanes[j]
        p = intersect_lines(ai, ci, aj, cj)
        if p is None:
            continue
```

```
        if all(ah @ p <= ch + 1e-9 for ah, ch in halfplanes):
            cands.append(p)

# Deduplicate and sort vertices by angle
verts = []
tol = 1e-7
for p in cands:
    if not any(np.linalg.norm(p - q) < tol for q in verts):
        verts.append(p)
verts = np.array(verts)
angles = np.arctan2(verts[:, 1], verts[:, 0])
bz = verts[np.argsort(angles)]
bz = np.vstack([bz, bz[0]]) # close polygon

# Plot window: slightly larger than 1st BZ
kx_max = 1.2 * np.max(np.abs(bz[:, 0]))
ky_max = 1.2 * np.max(np.abs(bz[:, 1]))

# k-grid for heatmap
nk = 320
kx = np.linspace(-kx_max, kx_max, nk)
ky = np.linspace(-ky_max, ky_max, nk)
KX, KY = np.meshgrid(kx, ky, indexing="xy")

# Precompute dot products for heatmap
kdot_d = np.stack([KX * v[0] + KY * v[1] for v in d_vecs], axis=0)
kdot_a = np.stack([KX * v[0] + KY * v[1] for v in a_vecs], axis=0)

# Precompute dot products for the cut at kx=0
kx0 = 0.0
kdot_d_cut = np.stack([kx0 * v[0] + ky * v[1] for v in d_vecs], axis=0) # (3, nk)
kdot_a_cut = np.stack([kx0 * v[0] + ky * v[1] for v in a_vecs], axis=0) # (3, nk)

def bands_2d(J1: float, J2: float, phi: float, M: float):
    f = np.exp(1j * kdot_d).sum(axis=0)
    Bx = -J1 * np.real(f)
    By = +J1 * np.imag(f)

    sum_cos = np.cos(kdot_a).sum(axis=0)
    sum_sin = np.sin(kdot_a).sum(axis=0)
    E0 = 2.0 * J2 * np.cos(phi) * sum_cos
    Bz = M + 2.0 * J2 * np.sin(phi) * sum_sin

    Bmag = np.sqrt(Bx**2 + By**2 + Bz**2)
    Eminus = E0 - Bmag
    Eplus = E0 + Bmag
    return Eminus, Eplus

def bands_cut_kx0(J1: float, J2: float, phi: float, M: float):
    f = np.exp(1j * kdot_d_cut).sum(axis=0)
    Bx = -J1 * np.real(f)
    By = +J1 * np.imag(f)

    sum_cos = np.cos(kdot_a_cut).sum(axis=0)
    sum_sin = np.sin(kdot_a_cut).sum(axis=0)
    E0 = 2.0 * J2 * np.cos(phi) * sum_cos
    Bz = M + 2.0 * J2 * np.sin(phi) * sum_sin

```

```
    Bmag = np.sqrt(Bx**2 + By**2 + Bz**2)
    return E0 - Bmag, E0 + Bmag

# Chern number from mass signs (your formula)
def chern_from_masses(J2: float, phi: float, M: float, ztol: float = 1e-10):
    mK = M - 3.0 * np.sqrt(3.0) * J2 * np.sin(phi)
    mKp = M + 3.0 * np.sqrt(3.0) * J2 * np.sin(phi)
    if abs(mK) < ztol or abs(mKp) < ztol:
        return None # gap closing at K or K'
    C = 0.5 * (np.sign(mKp) - np.sign(mK))
    # should be -1, 0, or +1 for a gapped Haldane model in this convention
    return int(np.round(C))

# K, K' along ky-axis for this convention
kyK = 4.0 * np.pi / (3.0 * np.sqrt(3.0) * a)
kyKp = -kyK

# Initial parameters
J1_init = 1.0
J2_init = 0.3
phi_init = np.pi / 2
M_init = 0.0

Eminus2d, Eplus2d = bands_2d(J1_init, J2_init, phi_init, M_init)
Eminus_cut, Eplus_cut = bands_cut_kx0(J1_init, J2_init, phi_init, M_init)

# --- Figure with two panels ---
fig, (ax0, ax1) = plt.subplots(
    1, 2, figsize=(13.2, 5.8), gridspec_kw={"width_ratios": [1.1, 0.9]}
)
plt.subplots_adjust(bottom=0.25, wspace=0.28)

# Left: heatmap of lower band
im = ax0.imshow(
    Eminus2d,
    extent=[-kx_max, kx_max, -ky_max, ky_max],
    origin="lower",
    aspect="equal",
    interpolation="nearest",
)
ax0.plot(bz[:, 0], bz[:, 1], linewidth=2.5)
ax0.set_title(r"Lower␣band␣heatmap␣$E_-(\mathbf{k})$␣with␣1st␣BZ")
ax0.set_xlabel(r"$k_x$")
ax0.set_ylabel(r"$k_y$")
cbar = fig.colorbar(im, ax=ax0)
cbar.set_label(r"$E_-(\mathbf{k})$")

# Chern number text box (white background)
C0 = chern_from_masses(J2_init, phi_init, M_init)
chern_str0 = (rf"$\mathcal{{C}}␣=␣{C0}$" if C0 is not None else r"$\mathcal{C}$␣:␣gap␣
    closing")
chern_text = ax0.text(
    0.02, 0.98,
    chern_str0,
    transform=ax0.transAxes,
    va="top",
    bbox=dict(facecolor="white", edgecolor="black", alpha=0.9, boxstyle="round,pad
        =0.35"),
```

```
)

# Right: cut at kx=0
(line_m,) = ax1.plot(ky, Eminus_cut, linewidth=2, label=r"$E_-(k_x=0,k_y)$")
(line_p,) = ax1.plot(ky, Eplus_cut, linewidth=2, label=r"$E_+(k_x=0,k_y)$")
ax1.set_title(r"Cut at $k_x=0$: $E_\pm$ vs $k_y$")
ax1.set_xlabel(r"$k_y$")
ax1.set_ylabel(r"$E$")
ax1.grid(True)
ax1.legend(loc="best")

# Vertical dashed lines at K and K'
ax1.axvline(kyK, linestyle="--", linewidth=1.6)
ax1.axvline(kyKp, linestyle="--", linewidth=1.6)
ax1.text(kyK, 0.98, r"$K$", transform=ax1.get_xaxis_transform(), ha="center", va="top")
ax1.text(kyKp, 0.98, r"$K'$", transform=ax1.get_xaxis_transform(), ha="center", va="top")

# --- Sliders ---
axJ1 = plt.axes([0.12, 0.16, 0.76, 0.03])
axJ2 = plt.axes([0.12, 0.11, 0.76, 0.03])
axPH = plt.axes([0.12, 0.06, 0.76, 0.03])
axM = plt.axes([0.12, 0.01, 0.76, 0.03])

sJ1 = Slider(ax=axJ1, label=r"$J_1$", valmin=-3.0, valmax=3.0, valinit=J1_init, valstep=0.01)
sJ2 = Slider(ax=axJ2, label=r"$J_2$", valmin=-3.0, valmax=3.0, valinit=J2_init, valstep=0.01)
sPH = Slider(ax=axPH, label=r"$\phi$", valmin=-np.pi, valmax=np.pi, valinit=phi_init, valstep=0.01)
sM = Slider(ax=axM, label=r"$M$", valmin=-3.0, valmax=3.0, valinit=M_init, valstep=0.01)

def update(_):
    J1 = float(sJ1.val)
    J2 = float(sJ2.val)
    phi = float(sPH.val)
    M = float(sM.val)

    Eminus_new, _ = bands_2d(J1, J2, phi, M)
    im.set_data(Eminus_new)

    # Autoscale heatmap colors
    vmin, vmax = float(np.min(Eminus_new)), float(np.max(Eminus_new))
    pad = 0.02 * (vmax - vmin + 1e-12)
    im.set_clim(vmin - pad, vmax + pad)
    cbar.update_normal(im)

    # Update Chern number box
    C = chern_from_masses(J2, phi, M)
    chern_text.set_text(rf"$\mathcal{{C}} = {C}$" if C is not None else r"$\mathcal{C} : gap closing")

    # Update cut lines
    Em_cut, Ep_cut = bands_cut_kx0(J1, J2, phi, M)
    line_m.set_ydata(Em_cut)
    line_p.set_ydata(Ep_cut)
```

```
225
226     # y-limits for the cut panel
227     ymax = float(np.max(np.abs(np.r_[Em_cut, Ep_cut])))
228     ax1.set_ylim(-1.1*ymax, 1.1*ymax)
229
230     fig.canvas.draw_idle()
231
232 sJ1.on_changed(update)
233 sJ2.on_changed(update)
234 sPH.on_changed(update)
235 sM.on_changed(update)
236
237 plt.show()
```